PDGFRα signaling in cardiac stem and stromal cells modulates quiescence, metabolism and self-renewal, and promotes anatomical and functional repair

Naisana S. Asli[1,2,3,4,#], Munira Xaymardan[1,3,5,#], Elvira Forte[1,2,5], Ashley J. Waardenberg[1], James Cornwell[1,5], Vaibhao Janbandhu[1,2], Scott Kesteven[1], Vashe Chandrakanthan[1], Helena Malinowska[1], Henrik Reinhard[1], Sile F. Yang[7], Hilda A Pickett[7], Peter Schofield[8], Daniel Christ[2,8], Ishtiaq Ahmed[1], James Chong[1], Corey Heffernan[1], Joan Li[1], Mary Simonian[3], Romaric Bouveret[1,2], Surabhi Srivastava[9], Rakesh K. Mishra[9], Jyotsna Dhawan[9,10], Robert Nordon[6], Peter Macdonald[1,2], Robert M. Graham[1,2], Michael Feneley[1,2], Richard P. Harvey[1,2,5,11*]

[1] Victor Chang Cardiac Research Institute, Darlinghurst, NSW 2010, Australia

[2] St. Vincent's Clinical School, University of New South Wales, Kensington, NSW 2052, Australia

[3] Faculty of Dentistry, University of Sydney, Westmead Hospital, Westmead, NSW 2145, Australia

[4] Sydney Medical School, University of Sydney, Westmead Hospital, Westmead, NSW 2145, Australia

[5] Stem Cells Australia, Melbourne Brain Centre, The University of Melbourne, Victoria 3010, Australia

[6] Graduate School of Biomedical Engineering, University of New South Wales, Kensington, NSW 2052, Australia

[7] Telomere Length Regulation Unit, Children's Medical Research Institute, University of Sydney, Westmead, NSW 2145, Australia

[8] Garvan Institute of Medical Research, 384 Victoria Street, Darlinghurst, Sydney, NSW 2010, Australia

[9] Centre for Cellular and Molecular Biology, Uppal Rd. Hyderabad 500 007, India

[10] Institute for Stem Cell Biology and Regenerative Medicine, Bengaluru 560 065, India

[11] School of Biotechnology and Biomolecular Science, University of New South Wales, Kensington, NSW 2052, Australia

# These authors have equally contributed to this manuscript.

* Correspondence: r.harvey@victorchang.edu.au

SUMMARY

The interstitial and perivascular spaces of the heart contain stem-like cells including cardiac colony forming units - fibroblast (cCFU-F), a sub-fraction of $SCA1^{+}PDGFR\alpha^{+}CD31^{-}$ ($S^{+}P^{+}$) immature stromal cells with the qualities of mesenchymal stem cells, that we have characterized previously. Here we explore the role of platelet-derived growth factor receptor α (PDGFRα) in cCFU-F and $S^{+}P^{+}$ cell niche regulation in homeostasis and repair. PDGFRα signaling modulated quiescence, metabolic state, mitogenic propensity and colony formation, as well as the rate and stability of self-renewal. Exogenously administered PDGF-AB ligand had anti-aging effects on cCFU-F, akin to those seen in heterochronic parabiotic mice. Post-myocardial infarction (MI), exogenous PDGF-AB stimulated $S^{+}P^{+}$ cell proliferation and conversion to myofibroblasts through a metabolic priming effect, yet significantly enhanced anatomical and functional repair via multiple cellular processes. Our study provides a rationale for a novel therapeutic approach to cardiac injury involving stimulating endogenous repair mechanisms via activation of cardiac stem and stromal cells.

Keywords: cardiac, heart, CFU-F, mesenchymal stem cell, stem cells, platelet-derived growth factor, PDGF, metabolism, myocardial infarction, heart regeneration.

INTRODUCTION

Stimulation of tissue regeneration after injury is an appealing therapeutic option for many organ systems, including the heart. In humans, myocardial infarction (MI) is the most common form of acute cardiac injury leading to the death of millions of cardiomyocytes (CM), reduced heart function and high mortality. The adult hearts of zebrafish and some urodele amphibia show spectacular regeneration after injury via dedifferentiation and proliferation of spared CMs (Kikuchi et al., 2010). In mouse, a similar capacity is present in neonates but diminishes after birth as blood pressure rises and CMs lose proliferative ability (Porrello et al., 2011).

CMs interact with a variety of interstitial cell types in health and disease, including stromal and vascular cells, lymphatic vessels, epicardium, endocardium, conduction cells, adipocytes, nerves and immune cells, as well as stem and progenitor cells, although a holistic understanding of this complex cell cross-talk is lacking. Cardiac stromal cells (generically fibroblasts) are highly changeable cells that represent major sensing and signaling hubs by virtue of their stem cell, paracrine, mechanical and electrical functions (Gourdie et al., 2016; Santini et al., 2016). Importantly, they are conspicuously linked to heart disease through the processes of inflammation, fibrosis and perturbations to conduction system activity. In regenerating tissues, timely resolution of inflammation is critical for limiting fibrosis and for facilitating tissue regeneration (Mescher, 2017). In the mammalian heart, genetic manipulations that reduce myofibrosis after MI lead to reduced scar formation and better functional recovery (Furtado et al., 2014; Kaur et al., 2016; Kramann et al., 2015), albeit that hearts may be prone to rupture (Oka et al., 2007).

Numerous stem-like cells have been described in the adult mammalian heart, although their origins, lineage descendants, niche regulation and paracrine functions are poorly understood (Santini et al., 2016). We have previously defined a population of cardiac clonogenic colony-forming cells (colony forming units - fibroblast; cCFU-F) that express characteristic cell surface markers and have stem cell qualities, including lineage plasticity and the ability to self-renew, akin to bone

marrow (BM) mesenchymal stem cells (MSCs) (Chong et al., 2011; Cornwell et al., 2016; Noseda et al., 2015). Compelling evidence in the BM system shows that fractions enriched for CFU-F serve as lineage progenitors for both parenchymal and stromal elements of bone, the latter contributing to the hematopoietic stem cell vascular niche (Chan et al., 2013; Worthley et al., 2015). We hypothesize that cCFU-F cells represent one type of endogenous cardiac stem cell involved in homeostasis and repair. Cardiac stromal and vascular elements in healthy hearts undergo significant homeostatic turnover (~4%/yr and ~14%/yr, respectively) (Bergmann et al., 2015), although how this turnover relates to cardiac stem cells is unknown. Cardiac CFU-F are contained within a $SCA1^{+}PDGFR\alpha^{+}CD31^{-}$ sub-fraction of immature stromal cells ($S^{+}P^{+}$ cells), and express cardiac transcription factors (Chong et al., 2011; Noseda et al., 2015). The origin of most cCFU-F can be traced to the embryonic epicardium, the outer mesothelial layer of the forming heart that provides paracrine signals for heart growth, and progenitors for stromal and vascular elements (Chong et al., 2011). A potentially analogous population in skeletal muscle (fibro-adipo progenitors) supports satellite stem cell activation during regeneration, and gives rise to fibro-adipogenic cells in pathology (Heredia et al., 2013; Joe et al., 2010).

Platelet-derived growth factor (PDGF) ligands are expressed by numerous cell types involved in cardiac injury responses (Zhao et al., 2011), and *in vitro* can stimulate activation, proliferation and migration of cardiac fibroblasts and MSCs (Zymek et al., 2006). Chronic activation of PDGFRα signaling in mice leads to systemic fibrosis (Olson and Soriano, 2009). However, no studies have addressed the impact of PDGF signaling on cardiac stem cell identity and behavior. Here we explore the niche regulation of cardiac CFU-F and stromal cells by PDGFRα, following its activation or inhibition *in vitro* and *in vivo*. We find that PDGFRα signaling stimulates exit of cCFU-F and $S^{+}P^{+}$ cells from quiescence through modulation of their metabolic and self-renewal states, even in the absence of injury. Furthermore, PDGFRα signaling reverses the decline in self-renewal seen with aging. Short-term delivery of PDGF-AB ligand to mice led to proliferation of stromal cells and their conversion to myofibroblast, but only in the context of MI. Despite this effect, treated hearts showed enhanced anatomical and function

repair. Our study highlights the pro-reparative functions of stromal cells during cardiac injury and suggests a multi-dimensional role for PDGF as a therapy for MI.

RESULTS

Niche environment of interstitial and adventitial PDGFRα^+ cells

We first sectioned hearts from *Pdgfra*$^{nGFP/+}$ knock-in mice (Hamilton et al., 2003) to visualize *Pdgfra*-GFP$^+$ cells. GFP$^+$ nuclei were seen throughout the cardiac interstitium close to isolectin$^+$ microvascular endothelial cells (ECs) and within the *tunica adventitia* of coronary arteries, but not in CMs (Fig. 1A-C) (Chong et al., 2011). GFP staining in ECs is very low or negative (data not shown). MSCs have previously been suggested to be equivalent to pericytes, albeit controversially (Guimaraes-Camboa et al., 2017). Mature pericytes lie within the EC basal lamina (Diaz-Flores et al., 2009). We scored >1500 interstitial GFP$^+$ nuclei and all lay external to the collagen IV$^+$ lamina (Fig. 1D), suggesting that PDGFRα^+ cells are not pericytes. Consistently, immunostaining and flow cytometry showed that GFP$^+$ cells were largely negative for pericyte markers CD146 and NG2 (Fig. 1E,F; Fig. S1A), and positive but dull for PDGFRβ (Fig. 1G; Fig. S1A). As for muscle satellite cells (Urciuolo et al., 2013), interstitial GFP$^+$ cells lay within a collagen VI-rich (adventitia-like) matrix, in common with peri-arterial GFP$^+$ cells (Fig. 1H).

PDGFRα signaling modulates exit from quiescence and self-renewal

We have shown that within isolated total interstitial cells, only the S$^+$P$^+$ fraction forms colonies (Chong et al., 2011; Noseda et al., 2015). The size of colonies reflects their clonal growth characteristics – cloned large colony cells can undergo long-term self-renewal *in vitro* (>300 days), while cloned small colony cells can form secondary colonies but these progressively lose self-renewal capacity during passage (Chong et al. 2011). Cloned micro-colony cells are composed of differentiated myofibroblast-like cells which do not re-plate (Chong et al., 2011 and see Fig. 1J) and rarely divide (Fig. S1B). Single cell tracking of plated S$^+$P$^+$ cells from *Pdgfra*$^{nGFP/+}$ mice confirmed that only GFP$^+$ cells are capable of self-renewal

(Cornwell et al., 2016). The proportion of GFP^+ cells diminished with *in vitro* passage, but stabilized at ~40% by P4 (Fig. S1C). However, a constant ~15% of cloned and re-plated large colony cells retained large colony forming ability from P0 to P4 (representing 37.5% of GFP^+ cells at P4) (see Fig. 1J; Fig.S1D). We also compared the probability of division of single cells in freshly plated S^+P^+ cells (P0) and re-plated P4 colony cells over 4 generations (gen), analyzing gen 0 (whose birth was not observed) and >0 separately (Fig. S1E). Around 60% of freshly plated adherent S^+P^+ cells divided in gens 0 and >0, mostly within the first 150 hrs. All re-plated P4 cells divided at least once. Thus, cCFU-F can be defined as a sub-fraction of division-competent S^+P^+ cells, with only larger colonies arising from cells capable of long-term self-renewal.

Role of PDGFRα signaling in cCFU-F self-renewal

To identify pathways responsible for self-renewal, we tested the activity of 39 receptor tyrosine kinases (RTKs) in mouse cCFU-F cultures using an anti-phospho-tyrosine antibody array (Fig. S1F). A number of known and novel RTK pathways were revealed, including those involving PDGFRα and PDGFRβ. Since PDGF ligands are expressed by numerous cell types involved in tissue injury and repair, such as platelets, ECs, myofibroblasts and inflammatory cells (Zhao et al., 2011), we explored the function of PDGFRα in cCFU-F and stromal cell biology further. S^+P^+ cells were isolated from healthy adult hearts and cultured with and without increasing doses of PDGF-AB ligand and/or AG1296, a competitive small molecule PDGFRα/β tyrosine kinase inhibitor. PDGF-AB has a preference for PDGFRα/α and PDGFRα/β receptor dimers (Heldin and Lennartsson, 2013). We first scored large, small and micro-colonies at the end of the first passage (P0; day 12). PDGF-AB increased large colony number in a dose-dependent manner up to ~2-fold and final cell number up to 1.9-fold, without effects on small or micro-colonies (Figs. 1I; S1G). AG1296 decreased large colony numbers up to ~8-fold while increasing micro-colonies (Fig. 1I), with cell yield decreasing ~2-fold and no change in cell death (Fig. S1G,H). PDGF-AB partially mitigated the effects of inhibitor (Fig 1I). A specific ligand-blocking PDGFRα monoclonal antibody (mAb)

(Takakura et al., 1997) yielded the same dose-dependent inhibition profile as AG1296 (Fig. S1I), confirming specific involvement of PDGFRα in colony growth.

In a parallel experiment, we cloned large, small and micro colonies from inhibitor and vehicle-treated P0 cultures, and re-plated clone pools without inhibitor (Fig. 1J), continuing this clonal analysis through secondary (2°), tertiary (3°) and quaternary (4°) assays (Fig. S1D). All inhibitor-treated colony types gave rise to large 2° colonies (Fig. 1J) and further clonal passage restored large colony forming capacity to that typical of vehicle-treated large colonies (Fig. S1D). Even micro-colonies from inhibitor-treated cultures formed large colonies in 2°, 3° and 4° assays, whereas vehicle-treated micro-colonies are composed of differentiated myofibroblast-like cells that do not re-plate (Fig. 1J; Chong et al., 2011). Bulk cultures could be passaged continuously in inhibitor (120 days; P13), albeit that these cultures showed lower self-renewal than vehicle-treated cultures, and PDGF-AB induced a higher rate of self-renewal (Fig. 1K). Collectively, our data show that stimulation and inhibition of PDGFRα signaling respectively increases and decreases self-renewal of cCFU-F and their clonal *in vitro* progeny.

cCFU-F represent a metabolically inactive, quiescent S^+P^+ subset regulated by PDGFRα

To determine the cell cycle status of freshly isolated S^+P^+ stromal cells we used DNA (7AAD) and RNA (Pyronin Y) dyes and flow cytometry. Total RNA content principally reflects the abundance of ribosomal RNAs and mRNAs for ribosomal proteins, a surrogate of metabolic/biosynthetic state (Kozma and Thomas, 2002). Virtually all freshly isolated S^+P^+ cells had 2n DNA content and ~50% of cells exhibited very low RNA levels typical of a quiescent (G_0) state (Fig. 1L,N), with the remainder showing a broad distribution of higher RNA levels indicative of more active metabolic states, as seen for BM S^+P^+ cells (Morikawa et al., 2009). When S^+P^+ cells were further fractionated to $CD90^+PDGFR\beta^{low}$ cells, large colony forming capacity was enriched >10-fold (data not shown). Virtually all enriched cells were in the G_0 fraction (Fig. 1M,N), suggesting that most cCFU-F are quiescent. In cCFU-F cultures at the end of P0, ~46% of cells remained in G_0 (Fig.

1O). Because ~60% of freshly plated S^+P^+ cells divide at least once in gen 0 and >0 (Fig. S1E), and total cell number increased ~5-fold during P0 (Fig. S1G), many of the cells that divide must retain or re-enter a low metabolic state. This tendency likely accounts for the slower rate of self-renewal of cCFU-F cultures up until P4 (48 days) (Chong et al., 2011) (Fig. 1K).

Cultures treated with AG1296 showed an increase in the proportion of cells in G_0 from ~46% to ~81%, and PDGF-AB ligand decreased this to ~29% (Fig. 1O), demonstrating a role for PDGFRα signaling in modulating quiescence. AG1296 inhibited EdU incorporation in freshly plated S^+P^+ cells (24hrs in culture) to ~0.6-fold, whereas ligand stimulated incorporation to ~1.6 fold (Fig. 1P). Single cell tracking of freshly plated S^+P^+ cells showed that stimulation or inhibition of PDGFRα signaling respectively increased and decreased the probability of mitosis, with the effect of ligand being more pronounced at gen 0 and that of inhibitor being more pronounced at generations >0 (Fig. 1Q).

Western blotting showed that with inhibitor there was an increased abundance of the pocket protein members Rb and p130 (Fig. 1R), involved in the G1/S restriction point (R) and adult stem cell quiescence (Rumman et al., 2015). There was a concomitant decrease in inactive phospho-Rb (p-Rb) and an increase in the level of cyclin-dependent kinase inhibitor $p27^{kip1}$. The early G1 cyclin, cyclin D1, was also decreased with little change in late G1, or S and M phase cyclins (E/A2/B1). The opposite was seen with ligand, where cyclin B1 was also increased (Fig. 1R).

By P4, virtually all vehicle-treated cells were metabolically active ($RNA^{medium\text{-}high}$) (Fig. S1J,K). However, after AG1296 treatment, ~50% were drawn into the G_0-like state and, accordingly, cell yield was reduced to ~0.4-fold (Fig. S1J-L), without changes in cell death (Fig. S1M). Virtually all ligand-treated cells were active and cell yield increased to ~2.2-fold (Fig. S1J-M). Western blotting for cell cycle regulators showed patterns similar to P0 cultures, including increased and decreased expression of pRb and cyclins D1, A2 and B1, with ligand and inhibitor, respectively (Fig. S1N). EdU incorporation increased with ligand and decreased

with inhibitor (Fig. S1O). Inhibitor had only a minor effect on probability of mitosis in re-plated P4 cells (Fig. S1P), suggesting that the major effects of ligand and inhibitor on P4 cells were on overall rate of self-renewal (Fig. 1K).

Taken together, these experiments show that S^+P^+ cells exist in a spectrum of metabolic (RNA) states, with cCFU-F in quiescence. Modulation of PDGFRα signaling alters cCFU-F metabolic state, probability of mitosis and rate of self-renewal.

Inhibition of PDGFRα signaling involves global metabolic changes through AKT and cMYC pathways

To define the alterations in metabolic state modulated by PDGF signaling we probed mitochondrial and metabolic signaling pathways. Changes in mitochondrial mass at P0 correlated with changes in RNA content - AG1296 increased the proportion of cells with lower mitochondrial mass, while PDGF-AB increased the proportion with higher mass (Fig. 2A), with accompanying changes in the expression of genes for mitochondrial polymerases POLG and POLG2, and transcription factor TFAM (Fig. 2B).

PDGFRα activation engages the PI3K/AKT/FOXO/mTOR pathway, involved in control of cell cycle and metabolism (Demoulin and Essaghir, 2014), and AKT collaborates with the proto-oncogene cMYC to control ribosomal RNA and protein synthesis, a major checkpoint in cell cycle progression (Teng et al., 2013). P0 cCFU-F cultures treated with AG1296 showed a decrease in the phosphorylated active forms of AKT (pAKT473, pAKT308) and increased total FOXO (Fig. 2C), which regulates proliferation and energy balance, and protects stem cells against reactive oxygen species (ROS). Conversely, ligand treatment increased pAKT and AKT-dependent phosphorylation of FOXO (which excludes it from the nucleus and marks it for degradation), as well as increasing cMYC levels. Thus, PDGFR signaling in cCFU-F regulates the PI3K/AKT/FOXO/mTOR pathway for metabolic control.

Exit from quiescence imposed by PDGFRα inhibition involves AKT and cMYC

If inhibitor-treated P4 cultures were released from inhibitor for a further passage (P5) there was an induction of a hyper-metabolic state with only ~1% of cells remaining in G_0 (condition P5 AG-R; Fig. 2E; S2A). Time course Western blot analysis of AG-R cultures across P5 showed increased levels of pAKT and cMYC (Fig. 2D).

Exploiting this assay, we asked if the AKT and cMYC pathways are required for exit from the G_0-like state imposed by PDGFRα inhibition. At the concentrations used, neither the AKT inhibitor (LY294002) nor cMYC inhibitor (10058-F4) had any impact on steady state growth (data not shown) or cell cycle profile of control cultures (Fig. S2B,C). However, exit from the G_0-like state imposed by PDGFRα inhibition was blocked in a dose-dependent manner by both drugs (Fig. 2E,F). Principal component analysis (PCA) of transcriptome data from cultured cCFU-F at P0 showed that inhibitor-treated cells occupied a transcriptional state distinct from that of untreated and ligand-treated cells, which clustered together (Fig. 2G). Differential gene expression analysis, comparing inhibitor-treated and ligand-treated cells to untreated cells, identified clusters that were reciprocally expressed after ligand or inhibitor treatment (Fig. S2D; Table 1). The top gene ontology (GO) terms (biological processes) for genes downregulated with inhibitor were *chromatin assembly* and *regulation of gene expression*, driven largely by down-regulation of multiple histone genes. Also down-regulated were genes associated with *cell proliferation*, *migration* and *adhesion*, *negative regulation of apoptosis*, and angiogenic and other signaling pathways. Among the many genes up-regulated with inhibitor were those associated with *cell adhesion* and *extracellular matrix*, *negative regulation of Wnt signaling*, as well as numerous tissue-relevant developmental processes.

Thus, inhibition of PDGFRα signaling in cultured cCFU-F imposes a low metabolic, biosynthetic and proliferative state resembling quiescence, release from which required AKT and cMYC. The transcriptome signature of inhibited cells

supports the ideas of a low transcriptional and proliferative state, albeit one active in unique (potentially niche) functionalities and primed for lineage differentiation.

Effects of modulating PDGFRα signaling in vivo

We next delivered the PDGFRα/β tyrosine kinase inhibitor, Imatinib, via oral gavage and/or PDGF-AB via mini-pump to healthy young adult mice for 5 days. In S^+P^+ cells isolated from Imatinib-treated animals, large colony formation decreased, while small and micro-colonies increased (Fig. 3A). In S^+P^+ cells from PDGF-AB-treated animals, large colony formation was increased and PDGF-AB partially mitigated the impact of Imatinib (Fig. 3A). These effects mirrored those obtained by treatment of S^+P^+ cells with ligand/inhibitor *in vitro* (Fig. 1I). cCFU-F cultures from vehicle and PDGF-AB-treated animals grew identically, while those from Imatinib-treated animals were severely compromised as seen by the rapid loss of self-renewal capacity (Fig. 3B). An identical outcome was seen after injection of blocking PDGFRα mAb over 8 days, with analysis at 14 days (Fig. S3A,B). Cell cycle analysis of S^+P^+ cells from vehicle-treated animals revealed the expected broad spectrum of RNA states with >50% of cells in G_0 and no significant change was observed in inhibitor-treated animals (Fig. 3C). Importantly, however, *in vivo* PDGF-AB treatment induced a ~25% reduction in the proportion of cells in G_0, indicating that exogenous PDGF-AB induces a higher metabolic state in S^+P^+ cells in the absence of injury.

Impact of PDGF-AB on committed progenitor populations in vivo

As described above, PDGF-AB modulates self-renewal of cCFU-F cultures. We asked whether PDGF-AB could restore self-renewal capacity or change lineage potential in committed stromal progenitor cells. NKX2-5 is a homeodomain transcription factor known to be expressed in cardiomyocyte progenitors and CMs. However, immunofluorescence also showed the presence of NKX2-5$^+$SCA1$^+$ and NKX2-5$^+$*Pdgfra*-GFP$^+$ cells in the cardiac interstitium (Fig. 4A). Around 6% of cardiac S^+P^+ cells isolated from hearts of sham-operated *Nkx2-5*$^{GFP/+}$ knockin mice (Biben et al., 2000) were *Nkx2-5*-GFP$^+$ and this increased to ~12% at day 5 post-

myocardial infarction (MI) (Fig. 4A,B). All colony-forming and long-term self-renewing cells lay within the GFP^- fraction in sham and MI hearts (Fig. 4C,D and not shown). GFP^+ cells lacked colony-forming ability consistent with a more committed state. However, when GFP^+ cells from sham hearts were plated in medium supplemented with PDGF-AB (until P4), they formed colonies which were able to self-renew until ~P7 (Fig. 4D).

We extended this analysis to cloned small colonies which have limited self-renewal ability (Chong et al., 2011). We discovered that the lineage potency of cloned small colonies was restricted to the cardiovascular lineages (CM, ECs, smooth muscle (SM)), in contrast to cloned large colonies which had broad mesodermal potential (Fig. 4E; Fig. S4A). Thus, small colony cells show restricted commitment. If small colonies were cultured in PDGF-AB supplemented medium until P4, long-term self-renewal was restored to that of controls until P15, indicating a profound effect of PDGF-AB not only on self-renewal but also on the memory of this cellular state (Fig. 4F). We next cultured small and large colonies until P5 and P15 (half of the small colonies were cultured in PDGF-AB until P4 then further to P15; Fig. 4G), and compared their transcriptome profiles. Upon PCA analysis, P5 small colonies clustered together irrespective of treatment and were segregated from large colonies, and the profiles of large and small colonies remained segregated after culture to P15. Differentiation assays showed that passage of small colonies to P15 after PDGF-AB treatment to P4 did not induce an expansion of lineage potency (Fig. S4B). Thus, PDGF-AB can rejuvenate colony formation and self-renewal capacity in lineage-restricted stromal cells, and these retain a memory of this effect. However, such changes are uncoupled from lineage potential.

Behavior of cCFU-F and stromal cells after myocardial infarction

We next explored the properties of cCFU-F and S^+P^+ cells in infarcted adult hearts. At day 5 post-MI, total cCFU-F per heart were only slightly reduced after MI (Fig. 5A). However, cCFU-F from MI hearts lost self-renewal ability prematurely (Fig. 5B). Around one third of S^+P^+ cells in G_0 activated their cell cycle state after MI, and this was partially reversed by Imatinib (Fig. 5C). In the $CD90^+PDGFR\beta^{low}$

S^+P^+ stromal fraction (enriched in large colony formation; Fig. 1L-N), MI induced activation of >50% of G_0 cells to a higher metabolic state, which was also inhibited by Imatinib. Thus, cCFU-F and S^+P^+ cells are metabolically activated by MI, and this involves PDGFRα signaling, but the self-renewal ability of cCFU-F is compromised by the MI environment.

After MI, inflammatory cells induce differentiation of stromal cells to myofibroblasts (Shinde and Frangogiannis, 2014). In *Pdgfra*$^{nGFP/+}$ knockin mice there was progressive accumulation of a SCA1$^+$GFP^{medium}PDGFRα$^-$CD45$^-$ stromal population across the first 5 days post-MI (Fig. 5D; Fig. S5A). The SCA1$^+$GFP^{medium} population was also seen when cardiac fibrosis was induced by aldosterone/salt or aortic banding (Fig. S5B). We identified SCA1$^+$GFP^{medium} cells as activated myofiboblasts by the following criteria: flow cytometry showed that SCA1$^+$GFP^{medium} cells were larger and had greater granularity than SCA1$^+$GFP^{high} stromal cells (data not shown); SCA1$^+$GFP^{medium} cells formed only micro-colonies (Fig. S5C); after brief culture almost all resembled myofibroblasts (GFP^{dim}α-SMA^{high}), while GFP^{high} cells remained GFP^{bright} when plated and were predominantly SMA$^-$ (Fig. S5D); qRT-PCR showed higher expression of myofibroblast markers in SCA1$^+$GFP^{medium} cells relative to SCA1$^+$GFP^{high} cells, including a ~70 fold increase in *Acta2* (encoding α-SMA) (Fig. 5E); most heart stromal cells express cardiac transcription factor genes *Isl1, Gata4* and *Tbx20*, reflecting their epicardial origins and cardiac identity (Chong et al., 2011; Furtado et al., 2014; Noseda et al., 2015); however, SCA1$^+$GFP^{medium} cells showed reduced expression of these genes and of stromal markers vimentin and DDR-2 (Fig. S5E); cell cycle analysis showed that ~90% of SCA1$^+$GFP^{medium} cells were metabolically active (RNA^{high}) (Fig. S5F).

The GFP protein expressed by the *Pdgfra*^{nGFP} allele is a fusion between eGFP and histone H2B, and its relative stability can serve as a short-term lineage marker. Accordingly, with time post-MI, SCA1$^+$PDGFRα$^-$GFP^{high} cells increased in number before the appearance of SCA1$^+$PDGFRα$^-$GFP^{medium} cells (Fig. 5D), consistent with the concept that SCA1$^+$GFP^{high} stromal cells give rise to SCA1$^+$GFP^{medium} myofibroblasts, as expected from recent lineage tracing studies (Kanisicak et al.,

2016; Moore-Morris et al., 2014). We confirmed the origin of myofibroblasts by genetic lineage tracing of PDGFRα^+ cells using tamoxifen (tam)-inducible *Pdgfra*^{merCremer} Cre driver mice (Ding et al., 2013) crossed to a *Rosa26*^{TdTomato} CRE-reporter (Fig. 5F). Fourteen days after tam treatment and 5 days post-MI, the infarcted region contained abundant lineage-tagged PDGFRα^{dim}SMA^{high} myofibroblasts, while in sham-operated hearts tagged cells were sparse and PDGFRα^{bright}SMA$^-$. We conclude that SCA1$^+$GFP^{medium} cell are activated myofibroblasts that arise from SCA1$^+$GFP^{high} stromal cells after MI. Furthermore, the impact of *in vivo* treatments on the transition of GFP^{high} stromal cells to GFP^{medium} myofibroblasts can be assessed by flow cytometry.

Therapeutic targeting of cCFU-F and stromal cell during MI

We therefore explored the impact of modulating PDGFRα signaling on GFP^{high} and GFP^{medium} cells in *Pdgfra*$^{nGFP/+}$ mice after MI. Inhibitor was given daily by oral gavage. PDGF-AB was delivered via mini-pump from the time of MI over 5 days, which led to a ~40% increase in serum PDGF-AB (Fig. S5G). PBS or water, given as respective vehicle controls, showed identical results (Fig. 5G and data not shown).

The SCA1$^+$GFP^{medium} population was absent in Sham+PDGF-AB mice (Fig. 5G). Thus, exogenous PDGF-AB does not induce myofibroblast differentiation in the absence of injury. SCA1$^+$GFP^{medium} myofibroblasts accumulated in hearts at 5 days post-MI, as described, and this was inhibited by Imatinib (Fig. 5G) or injection of blocking anti-PDGFRα antibody (Fig. S5H), showing that formation of SCA1$^+$GFP^{medium} myofibroblasts from SCA1$^+$GFP^{high} stromal cells is dependent, at least in part, on endogenous PDGFRα signaling.

Strikingly, in the context of MI, PDGF-AB induced a ~50% increase in the number of SCA1$^+$GFP^{medium} myofibroblasts at the expense of SCA1$^+$GFP^{high} stromal cells (Fig. 5G). Immunostaining showed a higher density of SMA^{high} myofibroblasts throughout the infarct region and these were GFP^{dull} (Fig. 5H), consistent with them being GFP^{medium} as defined by flow cytometry. Induced myofibroblasts

expressed higher levels of CALPONIN than those in MI+PBS hearts (Fig. S5I). PDGF-AB did not increase BrdU incorporation in SCA1^{+}GFP^{high} cells in sham hearts, indicating that PDGF-AB alone is not mitogenic for cardiac stromal cells. However, it did induce a ~2-fold increase in this population in the context of MI (Fig. 5I). Cardiac myofibroblasts undergo a period of active proliferation (Shinde and Frangogiannis, 2014). Accordingly, *Pdgfra*-GFP^{medium} myofibroblasts incorporated BrdU at higher levels than *Pdgfra*-GFP^{high} stromal cells (Fig. 5I). However, PDGF-AB did not act as a mitogen for myofibroblasts either, noting that the majority of SCA1^{+}GFP^{medium} cells at days 3-5 post-MI lacked cell surface PDGFRα (Fig. 5D).

Thus, exogenous PDGF-AB does not act as a conventional mitogen for SCA1^{+}GFP^{high} cardiac stromal cells in healthy hearts. PDGF-AB nonetheless has a priming effect on these cells, leading to an increased metabolic state and cCFU-F numbers (Fig. 3A,C), and in the context of MI increased BrdU incorporation into SCA1^{+}GFP^{high} cardiac stromal cells and their robust differentiation to SCA1^{+}GFP^{medium} myofibroblasts that occupied the infarct zone.

Enhancement of cardiac repair in MI+PDGF-AB hearts

Myofibroblasts are important mediators of the inflammatory response and matrix remodeling during MI (Shinde and Frangogiannis, 2014). We hypothesized, therefore, that the apparent pro-fibrotic effect in PDGF-AB-treated MI hearts would lead to adverse cardiac remodeling. In contrast, at 28 days post-MI, PDGF-AB-treated WT hearts showed reduced scarring (Fig. 6A,B), normalized heart/body weight ratio (Fig. 6C), and increased total vascularity at remote as well as boarder and infarct zones (Fig. 6D), and vessel caliber within the scar (Fig. 6E). Interestingly, PDGF-AB increased BrdU incorporation in CD31^{+} vascular ECs in both sham and MI hearts (Fig. 5J). Microvascular EC cells are very low or negative for *Pdgfra*-GFP by immunofluorescence (Fig. 1C) and by flow cytometry (Chong et al., 2014), so this is likely a paracrine effect. Similarly, PDGF treatment led to a ~6-fold increase in EdU incorporation in CMs, which also lack PDGFRα/β expression (Fig. 1A,G). Positive CMs were localized around the lumen of the LV (Fig. 6F).

PDGF-AB also stimulated an increase in the Ly-6C^{low}/Ly-6C^{high} (m2/m1) monocyte ratio (Nahrendorf et al., 2007) (Fig. 6G; Fig. S6A), the result of decreased pro-inflammatory m1 monocytes (Fig. S6B), potentially reflecting a more rapid transition from a pro-inflammatory to reparative monocyte milieu (Gourdie et al., 2016).

Echocardiographic analysis revealed that ejection fraction (EF) was substantial improved at both day 5 and day 28 post-MI in PDGF-AB compared to PBS-treated hearts (Fig. 6H). Left ventricular (LV) fractional area change (FAC) was also improved at all four short axis echocardiographic planes surveyed, at both 5 and 28 days post-MI, noting that the ventricular apex in MI+PBS hearts was virtually akinetic (Fig. 6I,J; Fig. S6C). PDGF-AB-treated MI hearts also showed improvements in LV end systolic (ES) and end diastolic (ED) areas at both day 5 and 28 post-MI (Fig. 6K,L; Fig. S6D,E). Thus, increased myofibroblast formation in this MI model correlates with significantly improved anatomical and functional outcomes.

PDGF-AB can restore self-renewal of cCFU-F from aged mice

MI occurs predominantly in the aged. Therefore, we explored the effects of PDGF-AB on aging stromal cells. While there was no change in serum PDGF-AB with age, there was a catastrophic decline in large colony formation and self-renewal ability of cCFU-F (Fig. 7A-C), suggesting disruption of some aspect of niche control. We first asked whether cCFU-F growth and differentiation potential could be rejuvenated in old mice by heterochronic parabiosis, as seen for other stem cells (Conboy et al., 2013) (Fig. 7D). In old parabionts of old-young parabiotic pairings (O-y mice) at 7 weeks post-surgery, large colony formation was restored to a level intermediate between that in O-o and Y-y parabionts (Fig. 7E). Long-term self-renewal ability in S^+P^+ cultures was also restored to intermediate levels (Fig. 7F). Furthermore, the probability of *in vitro* lineage differentiation of O-y S^+P^+ cultures at P5-6, normally lower in O-o compared to Y-y and Y-o cells, was significantly restored (Fig. 7G; Fig. S7A). Telomere length in O-y cultured S^+P^+ cells was also restored to that seen in Y-y and Y-o mice (Fig. 7H), consistent with

the view that loss of stem cell self-renewal in aged mice in part involves replicative senescence and telomere dysfunction.

We then treated 2 yr old mice with PDGF-AB via mini-pump for 5 days (Fig. 7I). There was no change in the number of large colonies although long-term self-renewal was completely restored (Fig. 7J). In differentiation assays, the probability of cells undergoing lineage conversion was increased (Fig. 7K; Fig. S7B). Telomere length was also slightly increased (Fig. 7H). Thus, PDGF-AB mimics the anti-aging effects conferred on S^+P^+ cells by heterochronic parabiosis.

DISCUSSION

The reparative roles of PDGF signaling in adult mice, specifically its roles in cardiac stem cells, have not been explored. Here we investigate the function of PDGFRα in cardiac cCFU-F and S^+P^+ stromal cells in homeostasis, injury and aging. *In vivo*, S^+P^+ cells exist in a continuum of metabolic states with a sub-fraction, including cCFU-F, occupying a low metabolic/synthetic state consistent with G_0/quiescence. In cultured S^+P^+ cells, inhibition of PDGFRα induced a G_0-like state, and decreased of colony formation and rate of self-renewal. Exit from this state required AKT and cMYC, known to be involved in G_0/G_1 checkpoint control in other settings (Teng et al., 2013). Inhibition of PDGFR signaling also led to major changes in the transcriptome. In contrast, treatment of S^+P^+ cultures with PDGF-AB led to increased metabolism, propensity for mitosis, colony formation and self-renewal. PDGF-AB could rejuvenate colony formation and self-renewal in aged S^+P^+ cells and lineage-committed progenitors, although this did not affect their lineage potency. There was a memory of PDGF-stimulated self-renewal responses, including after *in vivo* treatment of aged mice as also seen in heterochronic parabiotic mice.

Inhibition of PDGFRα *in vivo* using Imatinib or blocking antibody showed that PDGFRα signaling is essential for the integrity of the cCFU-F niche *in vivo*, and, after injury, for the metabolic activation of S^+P^+ cells and conversion of $SCA1^+GFP^{high}$ cells to $SCA1^+GFP^{medium}$ myofibroblasts. Consistently, delivery of

PDGF-AB to uninjured hearts via mini-pump led to metabolic activation of S^+P^+ cells and increased colony forming ability, and also increased BrdU incorporation in coronary endothelial cells, possibly a paracrine effect from activated stromal cells. Furthermore, delivery of PDGF-AB to injured hearts accelerated myofibroblast formation and enhanced anatomical and functional repair.

PDGFs have been implicated as mitogens for mesenchymal cells and MSCs (Zymek et al., 2006) and chronic activation of PDGFR signaling has been associated with fibrosis and cancer in different settings (Kong et al., 2014; Olson and Soriano, 2009; Wang et al., 2016). Treatment of MI hearts with PDGF-AB led to a ~50% increase in the number of $SCA1^+GFP^{medium}$ myofibroblasts, which occupied the infarct area. However, we found that exogenous PDGF-AB did not act as a complete mitogen for $SCA1^+GFP^{medium}$ stromal cells in uninjured hearts. Rather, it had a metabolic priming effect on stromal cells, leading to enhanced DNA synthesis only in the context of MI. PDGF-AB did not act as a mitogen for $SCA1^+GFP^{medium}$ myofibroblasts after injury either. Priming likely accelerates the transition of stromal cells to activated states, and the impact of other injury-induced mitogens and differentiation factors, such as ROS, TGFβ and immune cytokines (Morry et al., 2017). These findings resonate with foundation work of Pledger and colleagues who showed that in BALBc 3T3 fibroblasts, PDGF can act only as a *competence* factor in the transition from G_0 to S-phases of the cell cycle (Agrawal et al., 1996). Further work has highlighted that multiple points in the G_0-S transition require distinct mitogen and/or downstream signaling inputs (Jones and Kazlauskas, 2001; Pledger et al., 1978). Stromal cell priming in the heart is also reminiscent of the mTORC-dependent priming of satellite cells in healthy skeletal muscle by remote injury, allowing more rapid regeneration if these muscles are injured directly (Rodgers et al., 2014).

Despite robust induction of myofibroblasts in PDGF-AB treated MI hearts, they showed significantly enhanced repair from 5 days post-MI, earlier than seen in other pro-regenerative models (Bassat et al., 2017; D'Uva et al., 2015). Salutary effects included 50% reduction in scar volume, normalization of heart weight/body weight ratio, increased EC proliferation and increased vascular density in the

infarct and boarder zones, 4-5-fold increased EdU incorporation into CMs, increased m2/m1 monocyte ratio and partial restoration of functional parameters. Given the severity of infarcts imposed in this mouse study (mean EF ~20%), the degree of functional improvement is noteworthy, and would be highly significant in the clinical setting.

Evolution of the cellular milieu of the injured heart involves communication between many cell types, and polarization of both monocytes and stromal cells from initially pro-inflammatory, to anti-inflammatory and pro-reparative/pro-fibrotic states (Naftali-Shani et al., 2017; Nahrendorf et al., 2007). In regenerating species, a favorable balance between these states affords the opportunity for resolution of inflammation and organ regeneration without excessive fibrosis (Mescher, 2017). Resolution of fibrosis after induction of heart failure in adult mammalian hearts has also been observed after activation of the YAP transcription factor pathway in cardiomyocytes (Leach et al., 2017). Our studies reinforce the link between metabolism, and stem and progenitor cell function in cardiac stromal cells. More specifically they suggest enhancement of the pro-regenerative phases of stromal cell activation in PDGF-AB treated MI hearts. PDGFs are normally expressed by numerous cell types associated with cardiac injury (Zhao et al., 2011), which could rapidly prime the injured stroma.

One caveat in our study is that exogenous PDGF-AB may also effect extra-cardiac cells, which could contribute to the pro-regenerative effects. While we cannot exclude this possibility, the congruence between our *in vitro* and *in vivo* studies provide a credible rationale for the predominantly local nature of the impact of exogenous PDGF. Others have delivered different PDGF ligands to injured or uninjured hearts; however, the rationale, timing and mode of delivery, and dose, varied, as did the consequence of these treatments, from improved heart repair after MI, to frank heart failure in uninjured mice (Gallini et al., 2016a; Gallini et al., 2016b; Hsieh et al., 2006a; Hsieh et al., 2006b; Medamana et al., 2017; Ponten et al., 2005; Ponten et al., 2003; Zheng et al., 2004). Only one study addressed the impact of PDGF-AB, albeit when given as a single direct myocardial injection 24 hrs before induction of MI (Zheng et al., 2004). While the cellular mechanisms

were not explored, the observed beneficial effects are consistent with stromal priming.

There remains a strong clinical and economic case for the development of new regenerative therapies including modulators of fibrosis, and indeed several existing cardiac standard-of-care drugs, including statins, act, in part, as anti-fibrotics (Gourdie et al., 2016). Our study compellingly highlights the pro-regenerative impacts of targeting cardiac stem and stromal cells during injury.

Acknowledgements

We acknowledge support from the Australian Stem Cell Centre (P082, S4M1), Australia India Strategic Research Fund (BF020084, BF050024), Australian Research Council Strategic Initiative in Stem Cell Science (SR110001002), Australian Academy of Science Visiting Scholar's Program, Foundation Leducq Transatlantic Networks of Excellence in Cardiovascular Research (13CVD01, 15CVD03), New South Wales Cardiovascular Research Network (100711), James Kirby Foundation, National Health and Medical Research Council of Australia (NHMRC; 354400, 573732, 1074386). RPH held an Australia Fellowship and Senior Principal Research Fellowship from the NHMRC (573705, 1118576).

Author Contributions

N.S.A., M.X., V.C. and R.P.H conceived of the study; All authors designed and conducted experiments, analyzed data and contributed to the paper; R.P.H, R.M.G., M.F. and R.N. provided supervision; RPH provided financial support; N.S.A., M.X. and R.P.H. wrote the paper.

References

Agrawal, D., Hauser, P., McPherson, F., Dong, F., Garcia, A., and Pledger, W.J. (1996). Repression of p27kip1 synthesis by platelet-derived growth factor in BALB/c 3T3 cells. Mol Cell Biol *16*, 4327-4336.

Bassat, E., Mutlak, Y.E., Genzelinakh, A., Shadrin, I.Y., Baruch Umansky, K., Yifa, O., Kain, D., Rajchman, D., Leach, J., Riabov Bassat, D.*, et al.* (2017). The extracellular matrix protein agrin promotes heart regeneration in mice. Nature *547*, 179-184.

Bergmann, O., Zdunek, S., Felker, A., Salehpour, M., Alkass, K., Bernard, S., Sjostrom, S.L., Szewczykowska, M., Jackowska, T., Dos Remedios, C.*, et al.* (2015). Dynamics of Cell Generation and Turnover in the Human Heart. Cell *161*, 1566-1575.

Biben, C., Weber, R., Kesteven, S., Stanley, E., McDonald, L., Elliott, D.A., Barnett, L., Koentgen, F., Robb, L., Feneley, M.*, et al.* (2000). Cardiac septal and valvular dysmorphogenesis in mice heterozygous for mutations in the homeobox gene Nkx2-5. Circ Res *87*, 888-895.

Chan, C.K., Lindau, P., Jiang, W., Chen, J.Y., Zhang, L.F., Chen, C.C., Seita, J., Sahoo, D., Kim, J.B., Lee, A.*, et al.* (2013). Clonal precursor of bone, cartilage, and hematopoietic niche stromal cells. Proc Natl Acad Sci U S A *110*, 12643-12648.

Chong, J.J., Chandrakanthan, V., Xaymardan, M., Asli, N.S., Li, J., Ahmed, I., Heffernan, C., Menon, M.K., Scarlett, C.J., Rashidianfar, A.*, et al.* (2011). Adult cardiac-resident MSC-like stem cells with a proepicardial origin. Cell stem cell *9*, 527-540.

Chong, J.J., Forte, E., and Harvey, R.P. (2014). Developmental origins and lineage descendants of endogenous adult cardiac progenitor cells. Stem Cell Res *13*, 592-614.

Conboy, M.J., Conboy, I.M., and Rando, T.A. (2013). Heterochronic parabiosis: historical perspective and methodological considerations for studies of aging and longevity. Aging Cell *12*, 525-530.

Cornwell, J.A., Hallett, R.M., der Mauer, S.A., Motazedian, A., Schroeder, T., Draper, J.S., Harvey, R.P., and Nordon, R.E. (2016). Quantifying intrinsic and extrinsic control of single-cell fates in cancer and stem/progenitor cell pedigrees with competing risks analysis. Sci Rep *6*, 27100.
D'Uva, G., Aharonov, A., Lauriola, M., Kain, D., Yahalom-Ronen, Y., Carvalho, S., Weisinger, K., Bassat, E., Rajchman, D., Yifa, O.*, et al.* (2015). ERBB2 triggers mammalian heart regeneration by promoting cardiomyocyte dedifferentiation and proliferation. Nat Cell Biol *17*, 627-638.
Demoulin, J.B., and Essaghir, A. (2014). PDGF receptor signaling networks in normal and cancer cells. Cytokine Growth Factor Rev *25*, 273-283.
Diaz-Flores, L., Gutierrez, R., Madrid, J.F., Varela, H., Valladares, F., Acosta, E., Martin-Vasallo, P., and Diaz-Flores, L., Jr. (2009). Pericytes. Morphofunction, interactions and pathology in a quiescent and activated mesenchymal cell niche. Histol Histopathol *24*, 909-969.
Ding, G., Tanaka, Y., Hayashi, M., Nishikawa, S., and Kataoka, H. (2013). PDGF receptor alpha+ mesoderm contributes to endothelial and hematopoietic cells in mice. Dev Dyn *242*, 254-268.
Furtado, M.B., Costa, M.W., Pranoto, E.A., Salimova, E., Pinto, A.R., Lam, N.T., Park, A., Snider, P., Chandran, A., Harvey, R.P.*, et al.* (2014). Cardiogenic genes expressed in cardiac fibroblasts contribute to heart development and repair. Circ Res *114*, 1422-1434.
Gallini, R., Huusko, J., Yla-Herttuala, S., Betsholtz, C., and Andrae, J. (2016a). Isoform-Specific Modulation of Inflammation Induced by Adenoviral Mediated Delivery of Platelet-Derived Growth Factors in the Adult Mouse Heart. PLoS One *11*, e0160930.
Gallini, R., Lindblom, P., Bondjers, C., Betsholtz, C., and Andrae, J. (2016b). PDGF-A and PDGF-B induces cardiac fibrosis in transgenic mice. Experimental cell research *349*, 282-290.
Gourdie, R.G., Dimmeler, S., and Kohl, P. (2016). Novel therapeutic strategies targeting fibroblasts and fibrosis in heart disease. Nat Rev Drug Discov *15*, 620-638.
Guimaraes-Camboa, N., Cattaneo, P., Sun, Y., Moore-Morris, T., Gu, Y., Dalton, N.D., Rockenstein, E., Masliah, E., Peterson, K.L., Stallcup, W.B.*, et al.* (2017). Pericytes of Multiple Organs Do Not Behave as Mesenchymal Stem Cells In Vivo. Cell stem cell *20*, 345-359 e345.
Hamilton, T.G., Klinghoffer, R.A., Corrin, P.D., and Soriano, P. (2003). Evolutionary divergence of platelet-derived growth factor alpha receptor signaling mechanisms. Mol Cell Biol *23*, 4013-4025.
Heldin, C.H., and Lennartsson, J. (2013). Structural and functional properties of platelet-derived growth factor and stem cell factor receptors. Cold Spring Harb Perspect Biol *5*, a009100.
Heredia, J.E., Mukundan, L., Chen, F.M., Mueller, A.A., Deo, R.C., Locksley, R.M., Rando, T.A., and Chawla, A. (2013). Type 2 innate signals stimulate fibro/adipogenic progenitors to facilitate muscle regeneration. Cell *153*, 376-388.
Hsieh, P.C., Davis, M.E., Gannon, J., MacGillivray, C., and Lee, R.T. (2006a). Controlled delivery of PDGF-BB for myocardial protection using injectable self-assembling peptide nanofibers. The Journal of clinical investigation *116*, 237-248.
Hsieh, P.C., MacGillivray, C., Gannon, J., Cruz, F.U., and Lee, R.T. (2006b). Local controlled intramyocardial delivery of platelet-derived growth factor improves postinfarction ventricular function without pulmonary toxicity. Circulation *114*, 637-644.
Joe, A.W., Yi, L., Natarajan, A., Le Grand, F., So, L., Wang, J., Rudnicki, M.A., and Rossi, F.M. (2010). Muscle injury activates resident fibro/adipogenic progenitors that facilitate myogenesis. Nat Cell Biol *12*, 153-163.
Jones, S.M., and Kazlauskas, A. (2001). Growth-factor-dependent mitogenesis requires two distinct phases of signalling. Nat Cell Biol *3*, 165-172.
Kanisicak, O., Khalil, H., Ivey, M.J., Karch, J., Maliken, B.D., Correll, R.N., Brody, M.J., SC, J.L., Aronow, B.J., Tallquist, M.D.*, et al.* (2016). Genetic lineage tracing defines myofibroblast origin and function in the injured heart. Nat Commun *7*, 12260.

Kaur, H., Takefuji, M., Ngai, C.Y., Carvalho, J., Bayer, J., Wietelmann, A., Poetsch, A., Hoelper, S., Conway, S.J., Mollmann, H.*, et al.* (2016). Targeted Ablation of Periostin-Expressing Activated Fibroblasts Prevents Adverse Cardiac Remodeling in Mice. Circ Res *118*, 1906-1917.
Kikuchi, K., Holdway, J.E., Werdich, A.A., Anderson, R.M., Fang, Y., Egnaczyk, G.F., Evans, T., Macrae, C.A., Stainier, D.Y., and Poss, K.D. (2010). Primary contribution to zebrafish heart regeneration by gata4(+) cardiomyocytes. Nature *464*, 601-605.
Kong, P., Christia, P., and Frangogiannis, N.G. (2014). The pathogenesis of cardiac fibrosis. Cell Mol Life Sci *71*, 549-574.
Kozma, S.C., and Thomas, G. (2002). Regulation of cell size in growth, development and human disease: PI3K, PKB and S6K. Bioessays *24*, 65-71.
Kramann, R., Schneider, R.K., DiRocco, D.P., Machado, F., Fleig, S., Bondzie, P.A., Henderson, J.M., Ebert, B.L., and Humphreys, B.D. (2015). Perivascular Gli1+ progenitors are key contributors to injury-induced organ fibrosis. Cell stem cell *16*, 51-66.
Leach, J.P., Heallen, T., Zhang, M., Rahmani, M., Morikawa, Y., Hill, M.C., Segura, A., Willerson, J.T., and Martin, J.F. (2017). Hippo pathway deficiency reverses systolic heart failure after infarction. Nature *550*, 260-264.
Medamana, J., Clark, R.A., and Butler, J. (2017). Platelet-Derived Growth Factor in Heart Failure. Handb Exp Pharmacol *243*, 355-369.
Mescher, A.L. (2017). Macrophages and fibroblasts during inflammation and tissue repair in models of organ regeneration. Regeneration (Oxf) *4*, 39-53.
Moore-Morris, T., Guimaraes-Camboa, N., Banerjee, I., Zambon, A.C., Kisseleva, T., Velayoudon, A., Stallcup, W.B., Gu, Y., Dalton, N.D., Cedenilla, M.*, et al.* (2014). Resident fibroblast lineages mediate pressure overload-induced cardiac fibrosis. The Journal of clinical investigation *124*, 2921-2934.
Morikawa, S., Mabuchi, Y., Kubota, Y., Nagai, Y., Niibe, K., Hiratsu, E., Suzuki, S., Miyauchi-Hara, C., Nagoshi, N., Sunabori, T.*, et al.* (2009). Prospective identification, isolation, and systemic transplantation of multipotent mesenchymal stem cells in murine bone marrow. The Journal of experimental medicine *206*, 2483-2496.
Morry, J., Ngamcherdtrakul, W., and Yantasee, W. (2017). Oxidative stress in cancer and fibrosis: Opportunity for therapeutic intervention with antioxidant compounds, enzymes, and nanoparticles. Redox Biol *11*, 240-253.
Naftali-Shani, N., Levin-Kotler, L.P., Palevski, D., Amit, U., Kain, D., Landa, N., Hochhauser, E., and Leor, J. (2017). Left Ventricular Dysfunction Switches Mesenchymal Stromal Cells Toward an Inflammatory Phenotype and Impairs Their Reparative Properties Via Toll-Like Receptor-4. Circulation *135*, 2271-2287.
Nahrendorf, M., Swirski, F.K., Aikawa, E., Stangenberg, L., Wurdinger, T., Figueiredo, J.L., Libby, P., Weissleder, R., and Pittet, M.J. (2007). The healing myocardium sequentially mobilizes two monocyte subsets with divergent and complementary functions. The Journal of experimental medicine *204*, 3037-3047.
Noseda, M., Harada, M., McSweeney, S., Leja, T., Belian, E., Stuckey, D.J., Abreu Paiva, M.S., Habib, J., Macaulay, I., de Smith, A.J.*, et al.* (2015). PDGFRalpha demarcates the cardiogenic clonogenic Sca1+ stem/progenitor cell in adult murine myocardium. Nat Commun *6*, 6930.
Oka, T., Xu, J., Kaiser, R.A., Melendez, J., Hambleton, M., Sargent, M.A., Lorts, A., Brunskill, E.W., Dorn, G.W., 2nd, Conway, S.J.*, et al.* (2007). Genetic manipulation of periostin expression reveals a role in cardiac hypertrophy and ventricular remodeling. Circ Res *101*, 313-321.
Olson, L.E., and Soriano, P. (2009). Increased PDGFRalpha activation disrupts connective tissue development and drives systemic fibrosis. Dev Cell *16*, 303-313.
Pledger, W.J., Stiles, C.D., Antoniades, H.N., and Scher, C.D. (1978). An ordered sequence of events is required before BALB/c-3T3 cells become committed to DNA synthesis. Proc Natl Acad Sci U S A *75*, 2839-2843.

Ponten, A., Folestad, E.B., Pietras, K., and Eriksson, U. (2005). Platelet-derived growth factor D induces cardiac fibrosis and proliferation of vascular smooth muscle cells in heart-specific transgenic mice. Circ Res *97*, 1036-1045.
Ponten, A., Li, X., Thoren, P., Aase, K., Sjoblom, T., Ostman, A., and Eriksson, U. (2003). Transgenic overexpression of platelet-derived growth factor-C in the mouse heart induces cardiac fibrosis, hypertrophy, and dilated cardiomyopathy. Am J Pathol *163*, 673-682.
Porrello, E.R., Mahmoud, A.I., Simpson, E., Hill, J.A., Richardson, J.A., Olson, E.N., and Sadek, H.A. (2011). Transient regenerative potential of the neonatal mouse heart. Science *331*, 1078-1080.
Rodgers, J.T., King, K.Y., Brett, J.O., Cromie, M.J., Charville, G.W., Maguire, K.K., Brunson, C., Mastey, N., Liu, L., Tsai, C.R.*, et al.* (2014). mTORC1 controls the adaptive transition of quiescent stem cells from G0 to G(Alert). Nature *510*, 393-396.
Rumman, M., Dhawan, J., and Kassem, M. (2015). Concise Review: Quiescence in Adult Stem Cells: Biological Significance and Relevance to Tissue Regeneration. Stem Cells *33*, 2903-2912.
Santini, M.P., Forte, E., Harvey, R.P., and Kovacic, J.C. (2016). Developmental origin and lineage plasticity of endogenous cardiac stem cells. Development *143*, 1242-1258.
Shinde, A.V., and Frangogiannis, N.G. (2014). Fibroblasts in myocardial infarction: a role in inflammation and repair. J Mol Cell Cardiol *70*, 74-82.
Takakura, N., Yoshida, H., Ogura, Y., Kataoka, H., Nishikawa, S., and Nishikawa, S. (1997). PDGFR alpha expression during mouse embryogenesis: immunolocalization analyzed by whole-mount immunohistostaining using the monoclonal anti-mouse PDGFR alpha antibody APA5. J Histochem Cytochem *45*, 883-893.
Teng, T., Thomas, G., and Mercer, C.A. (2013). Growth control and ribosomopathies. Curr Opin Genet Dev *23*, 63-71.
Urciuolo, A., Quarta, M., Morbidoni, V., Gattazzo, F., Molon, S., Grumati, P., Montemurro, F., Tedesco, F.S., Blaauw, B., Cossu, G.*, et al.* (2013). Collagen VI regulates satellite cell self-renewal and muscle regeneration. Nat Commun *4*, 1964.
Wang, Y., Appiah-Kubi, K., Wu, M., Yao, X., Qian, H., Wu, Y., and Chen, Y. (2016). The platelet-derived growth factors (PDGFs) and their receptors (PDGFRs) are major players in oncogenesis, drug resistance, and attractive oncologic targets in cancer. Growth Factors, 1-8.
Worthley, D.L., Churchill, M., Compton, J.T., Tailor, Y., Rao, M., Si, Y., Levin, D., Schwartz, M.G., Uygur, A., Hayakawa, Y.*, et al.* (2015). Gremlin 1 identifies a skeletal stem cell with bone, cartilage, and reticular stromal potential. Cell *160*, 269-284.
Zhao, W., Zhao, T., Huang, V., Chen, Y., Ahokas, R.A., and Sun, Y. (2011). Platelet-derived growth factor involvement in myocardial remodeling following infarction. J Mol Cell Cardiol *51*, 830-838.
Zheng, J., Shin, J.H., Xaymardan, M., Chin, A., Duignan, I., Hong, M.K., and Edelberg, J.M. (2004). Platelet-derived growth factor improves cardiac function in a rodent myocardial infarction model. Coronary artery disease *15*, 59-64.
Zymek, P., Bujak, M., Chatila, K., Cieslak, A., Thakker, G., Entman, M.L., and Frangogiannis, N.G. (2006). The role of platelet-derived growth factor signaling in healing myocardial infarcts. J Am Coll Cardiol *48*, 2315-2323.

Figures and Figure Legends

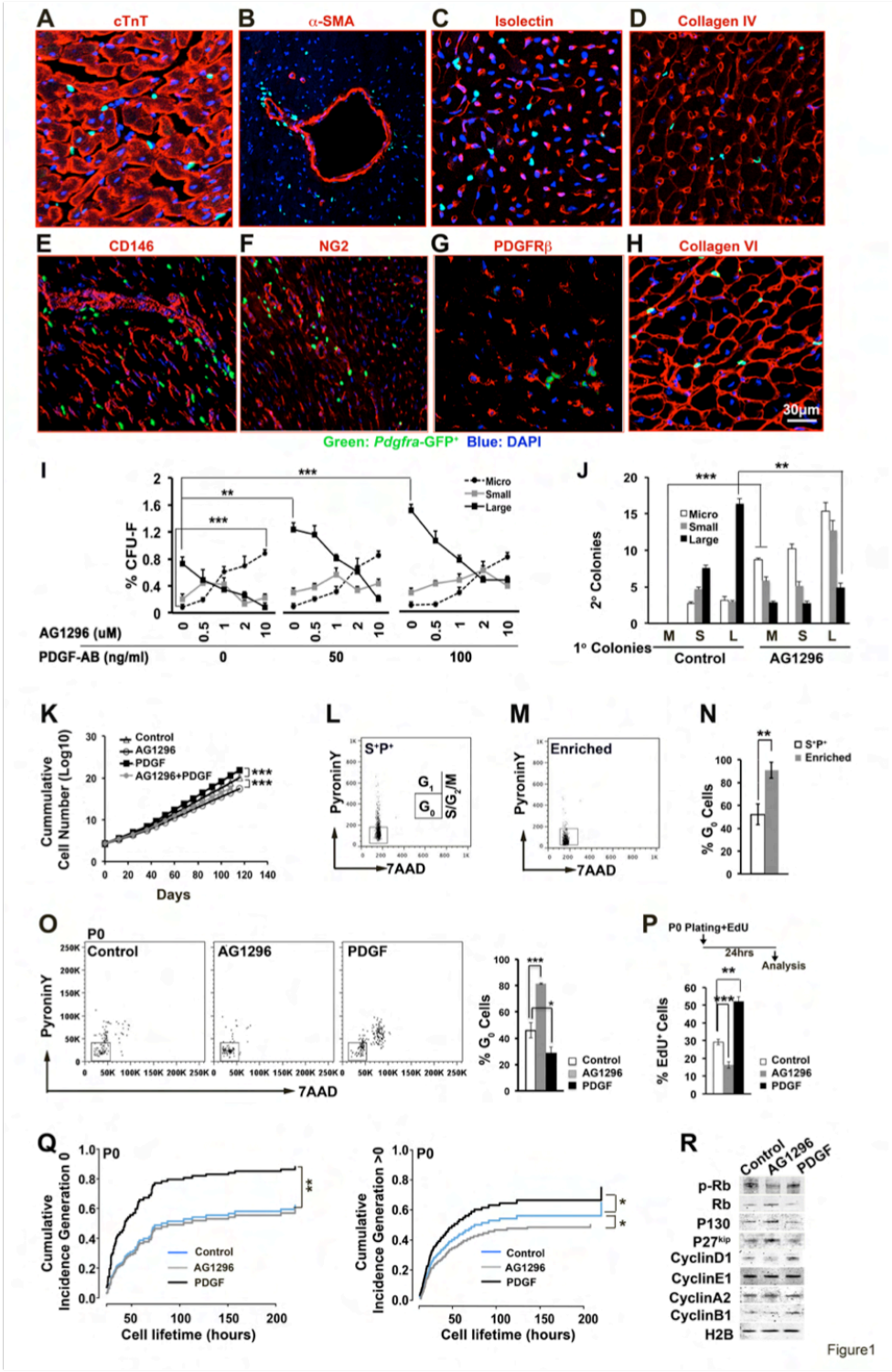

Figure 1: *In vivo* location and culture of PDGFRα$^+$ cells

(A-H) Localization of GFP^+ stromal cells in sections of hearts from *Pdgfra*$^{GFP/+}$ knock-in mice relative to indicated markers detected by immunofluorescence: cTnT: cardiac troponin T; α-SMA: α-smooth muscle actin. (I) cCFU-F analysis (large, small, micro-colonies) in S^+P^+ cells scored at passage 0 (day 12), with and without indicated concentrations of PDGF-AB ligand and PDGFR signaling inhibitor AG1296 ($p<0.001$ - untreated vs AG1296-treated (10μM) micro-colonies, and untreated vs PDGF-AB-treated (100ng/ml) large colonies; $p<0.01$ - untreated vs PDGF-AB-treated (50ng/ml) large colonies). (J). Secondary (2^0) colony formation within pooled cloned primary large, small and micro-colonies from untreated control and AG1296-inhibited (10μM) cultures as in panel I (see Fig. S1H for continuing 3^0 and 4^0 analyses) (K) Long-term cultures of S^+P^+ cells with or without PDGF-AB (100ng/ml) and AG1296 (10μM). (L,M) Cell cycle analyses of freshly isolated S^+P^+ and $S^+P^+CD90^+PDGFR\beta^{low}$ (cCFU-F enriched; Fig. 1L,M) cells at P0. Box indicates G_0 fraction. (N) Percent G_0 cells in L,M. (O) Cell cycle analyses of S^+P^+ cell cultures with and without PDGF-AB and AG1296 at P0, with percent G_0 cells indicated. (P). EdU incorporation in S^+P^+ cultures (24hr pulse, then analysis, at the end of P0). (Q). Single cell analysis of cumulative cell division in freshly plated S^+P^+ cells with and without PDGF-AB and AG1296, scored separately in generations 0 and >0. (R) Western blot analysis of indicated cell cycle regulators in S^+P^+ cultures at P0. All comparisons: * $p<0.05$; ** $p<0.01$; *** $p<0.001$.

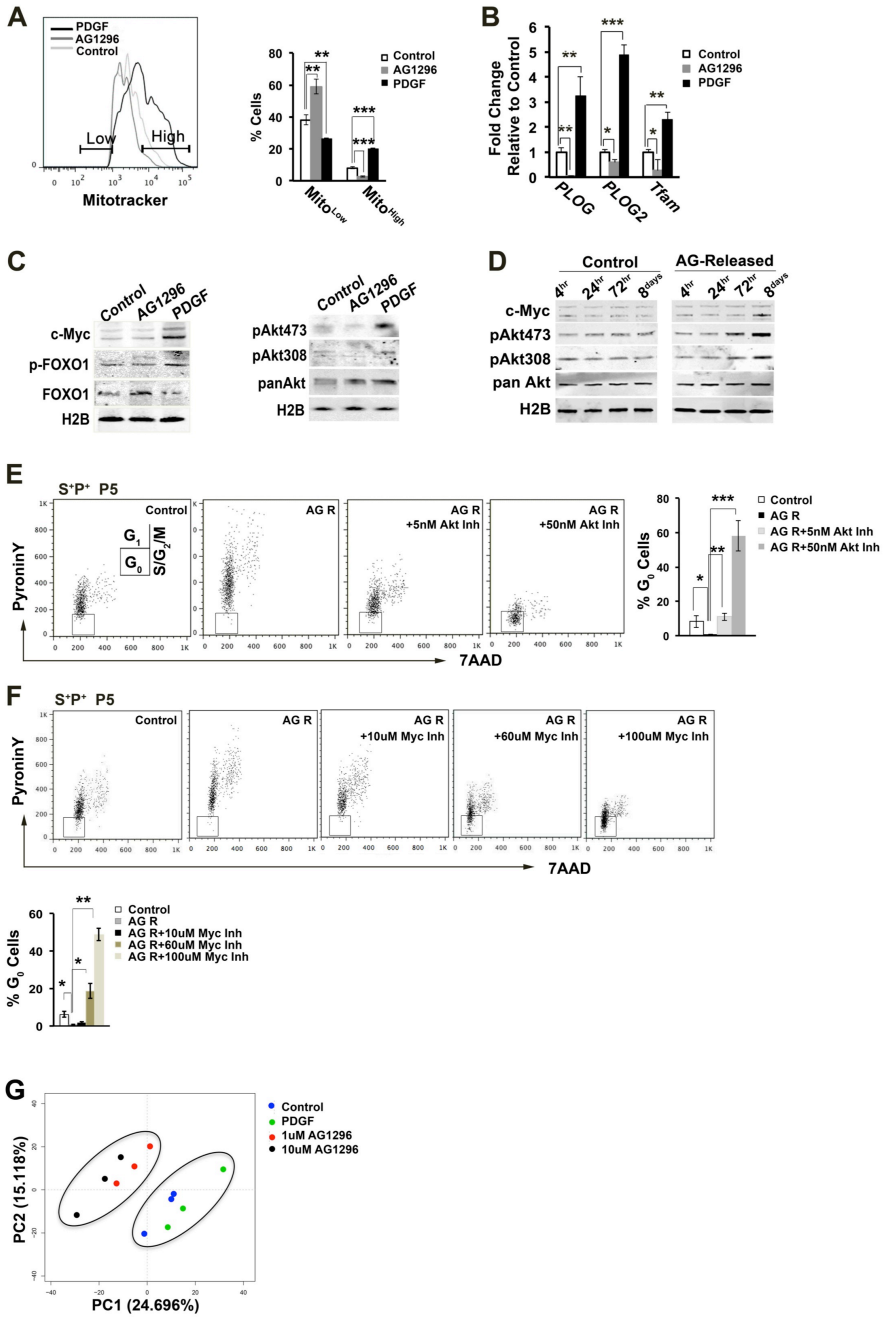

Figure 2: Metabolic, cell cycle and transcriptome analyses of S^+P^+ cultures

(A) Analysis of mitochondrial mass in S^+P^+ cells cultured to P0 by Mitotracker® Green FM (Mito) staining, with or without PDGF-AB (100ng/ml) and AG1296 (10μM), showing quantification of $Mito^{low}$ and $Mito^{high}$ fractions. (B) qRT-PCR analysis of genes for mitochondrial polymerase enzymes (POLG; POLG2) and transcription factor (TFAM). (C,D) Western blot analyses of indicated cMYC and AKT pathway proteins in PDGF-AB and AG1296-treated S^+P^+ cultures at P0 (C), and after AG1296 inhibition across P4 and release from inhibitor for a further

passage (D). (E,F) Cell cycle analysis of uninhibited cultures (P5) compared to cultures with AG1296 inhibition and release (as in panel D), with and without increasing doses of AKT and cMYC inhibitors. (G) Principal component (PC) analysis (PC1 vs PC2) of microarray transcriptome data from S^+P^+ cells cultured to P0 with and without PDGF-AB and AG1296 (1 and 10μM). All comparisons: * p<0.05; ** p<0.01; *** p<0.001.

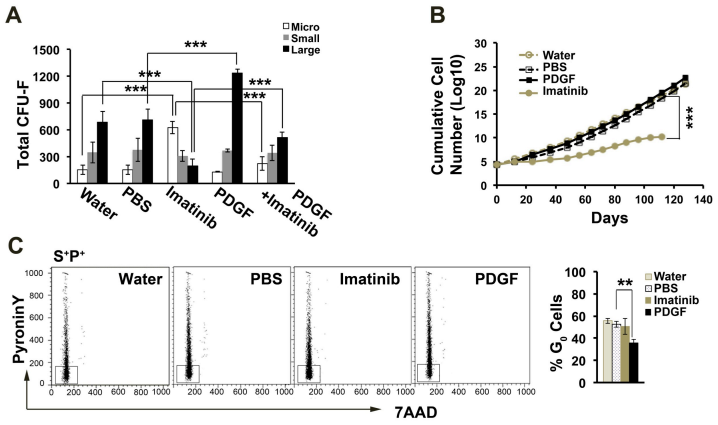

Figure3

Figure 3: Stimulation and inhibition of PDGFRα signaling *in vivo*

(A) cCFU-F analysis after *in vivo* treatment of mice with PDGF receptor inhibitor Imatinib via oral gavage and/or PDGF-AB ligand via minipump relative to vehicle controls with analysis at day 5. (B) Long-term growth curves of S^+P^+ cultures after treatments as indicated in A. (C) Cell cycle analysis of S^+P^+ cells freshly isolated from animals treated as in A, with quantification of cell in G_0. All comparisons: ** p<0.01; *** p<0.001.

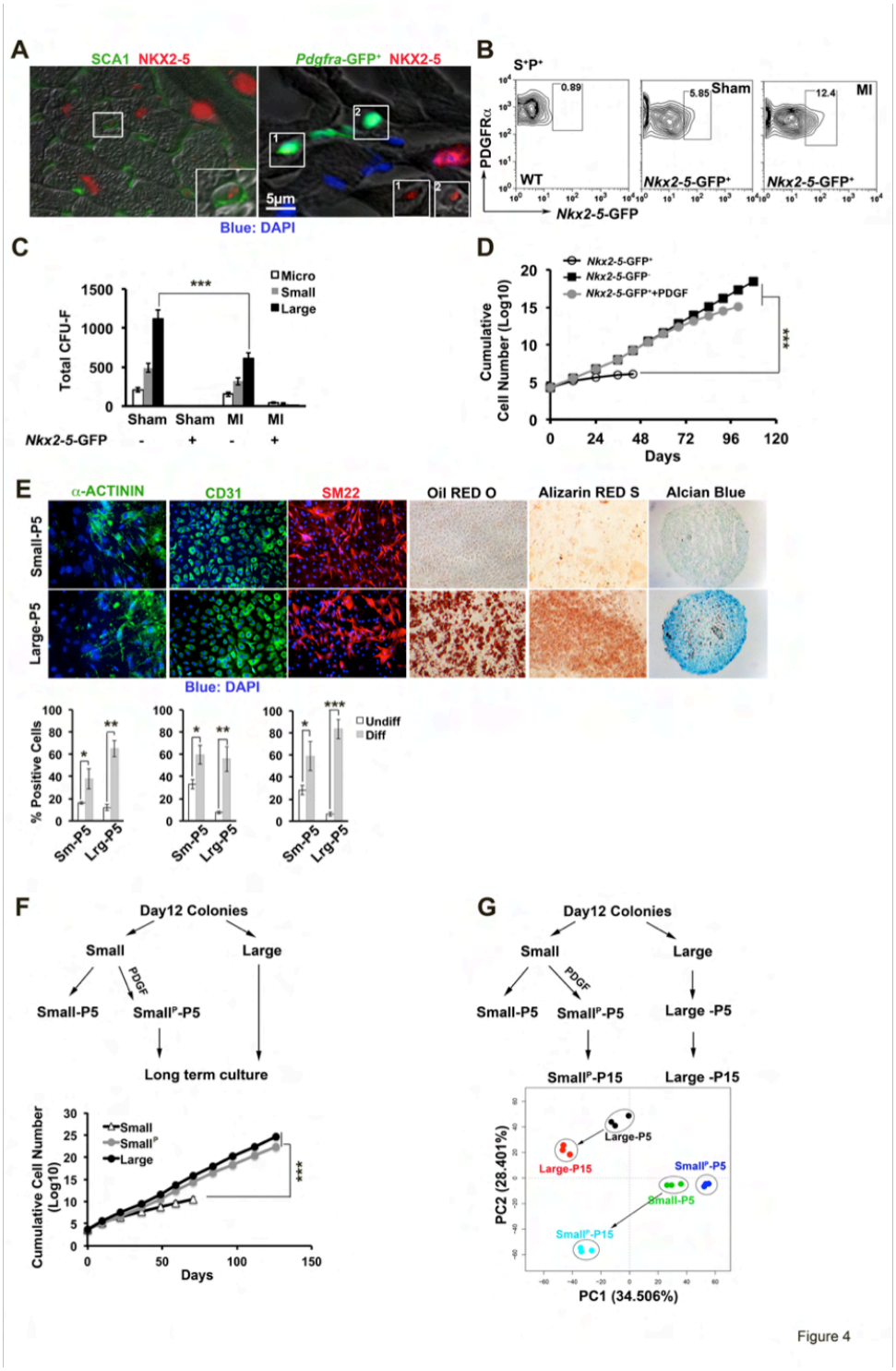

Figure 4: Restoration of long-term self-renewal in lineage-committed stromal cells

(A) Immunofluorescence analysis showing co-localization of SCA1 and NKX2-5 or *Pdgfra*-GFP and NKX2-5 in subsets of cardiac stromal cells. Arrowheads: NKX2-5^{+} cardiomyocytes; arrows: stromal cells. (B) Flow cytometry analysis of S^{+}P^{+} cells from adult *Nkx2-5*$^{GFP/+}$ mice showing PDGFRα and GFP expression. (C) cCFU-F

analysis of isolated GFP^+ and GFP^- fractions from adult *Nkx2-5*$^{GFP/+}$ hearts after sham or myocardial infarction surgery (MI). (D) Long-term growth curves of Nkx2-5-GFP^- and GFP^+ cells also showing growth of GFP^+ cells treated with PDGF-AB until P4. (E) Differentiation potential of pooled cloned P5 large and small colonies assessed *in vitro* using indicated markers (see also Fig. S4A for expanded marker profile). (F) Long-term growth curves of pooled cloned small colonies grown in the presence of PDGF-AB (100ng/ml) until P4, compared to those of untreated small and large colonies. (G) Principal component (PC) analysis (PC1 vs PC2) of RNAseq data from PDGF-AB-treated and untreated small colonies compared to large clones at P5 and P15 (see scheme). All comparisons: * $p<0.05$; ** $p<0.01$; *** $p<0.001$.

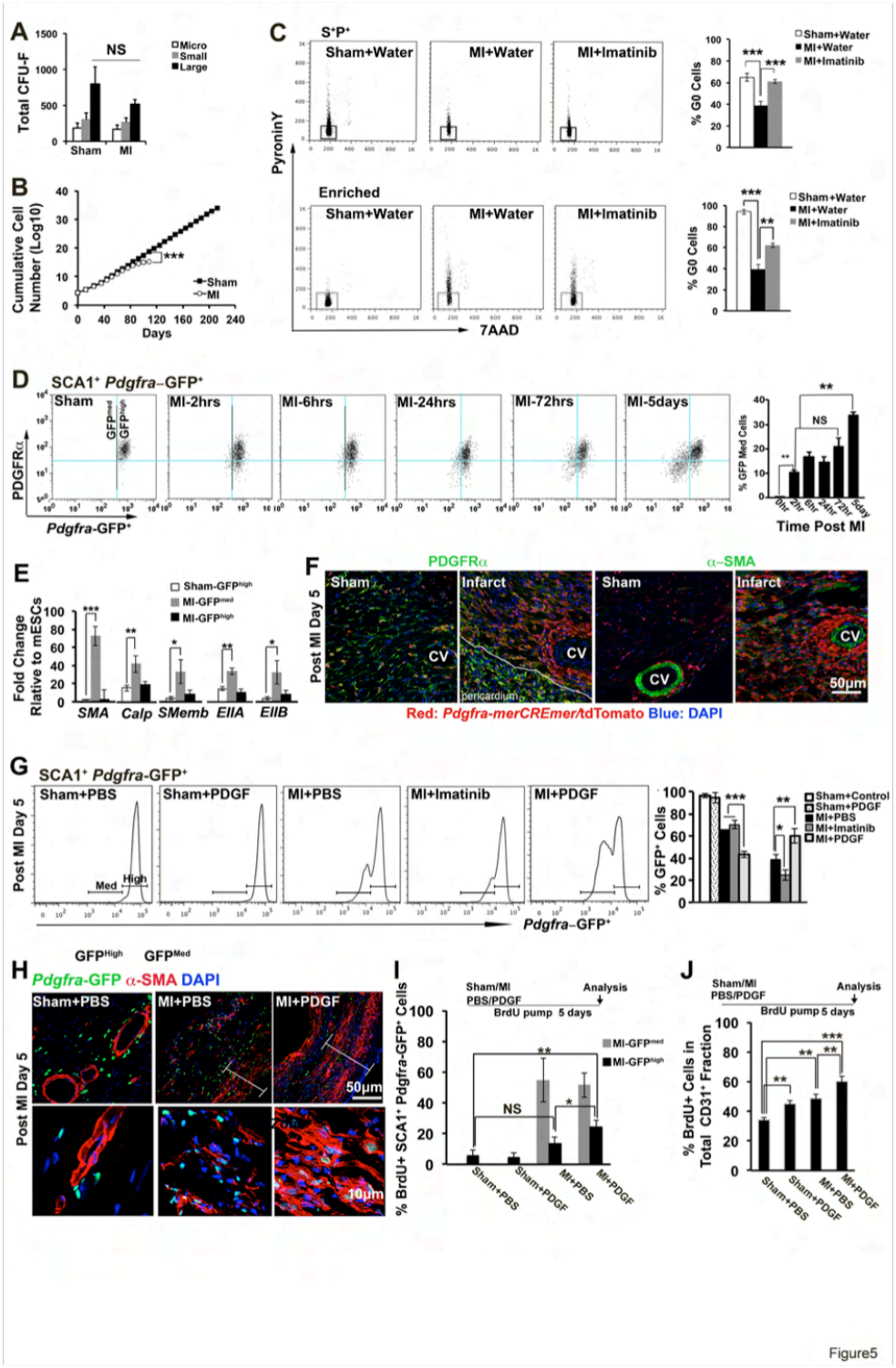

Figure 5: Impact of myocardial infarction on PDGFRα$^+$ stromal cells

(A) cCFU-F analyses of freshly isolated S$^+$P$^+$ cells at 5 days post-sham or MI surgery. (B) Long-term growth analyses of S$^+$P$^+$ cultures plated at day 5 post-sham or MI surgery. (C) Cell cycle analyses of freshly isolated S$^+$P$^+$ and colony-enriched (see Fig. 1L,M) cell at day 5 post sham or MI surgery. Cultures also shown from MI mice treated with Imatinib (daily oral gavage). Percent G_0 cells

indicated. (D) Time course flow cytometry analysis of the SCA1^{+}/*Pdgfra*-GFP^{+} stromal cell fraction displaying PDGFRα and GFP expression (GFP^{-} cells not shown), with quantification of GFP^{medium} myofibroblasts. (E) qRT-PCR analysis of myofibroblast markers in total GFP^{medium} and GFP^{high} cells at 5 days post-sham or MI. (F) Lineage tracing of PDGFRα stromal cells at 5 days post-sham or MI, using tamoxifen-treated *Pdgfra*$^{merCREmer/+}$;*Rosa26*$^{tdTomato/+}$ mice and immunofluorescence analysis for tdTomato, PDGFRα and SMA. Panels depict lineage-traced tdTomato^{+}PDGFRα^{bright} and tdTomato^{+}smooth muscle actin (SMA)-negative stromal cells in sham mice, as well as tdTomato^{+}PDGFRα^{dull} and tdTomato^{+}SMA+ myofibroblasts in the infarct region of MI mice. The *tunica media* of large coronary arteries is SMA^{bright}. First infarct panel - tdTomato^{+}PDGFRα^{bright} pericardium has adhered to the myocardium. cv: coronary vessel. (G) Flow cytometric analysis quantifying GFP^{high} stromal cells (High) and GFP^{medium} myofibroblasts (Med) from day 5 post-sham and MI hearts treated with PBS or PDGF-AB. MI mice were also treated with Imatinib (analyses of water (vehicle)-treated sham and MI mice not shown). (H) Immunofluorescence staining showing *Pdgfra*-GFP^{+} and SMA^{+} cells in sham/MI mice treated with PBS or PDGF-AB. Brackets indicate GFP^{dul}SMA^{+} myofibroblasts within the infarct zone shown at higher power in lower panels. (I) BrdU uptake in GFP^{high} and GFP^{medium} stromal fractions in 5 days post-sham/MI heart with PBS or PDGF-AB treatments. (J) BrdU uptake in CD31^{+} endothelial cells in sham/MI hearts with PBS or PDGF-AB treatments. All comparisons: * $p<0.05$; ** $p<0.01$; *** $p<0.001$.

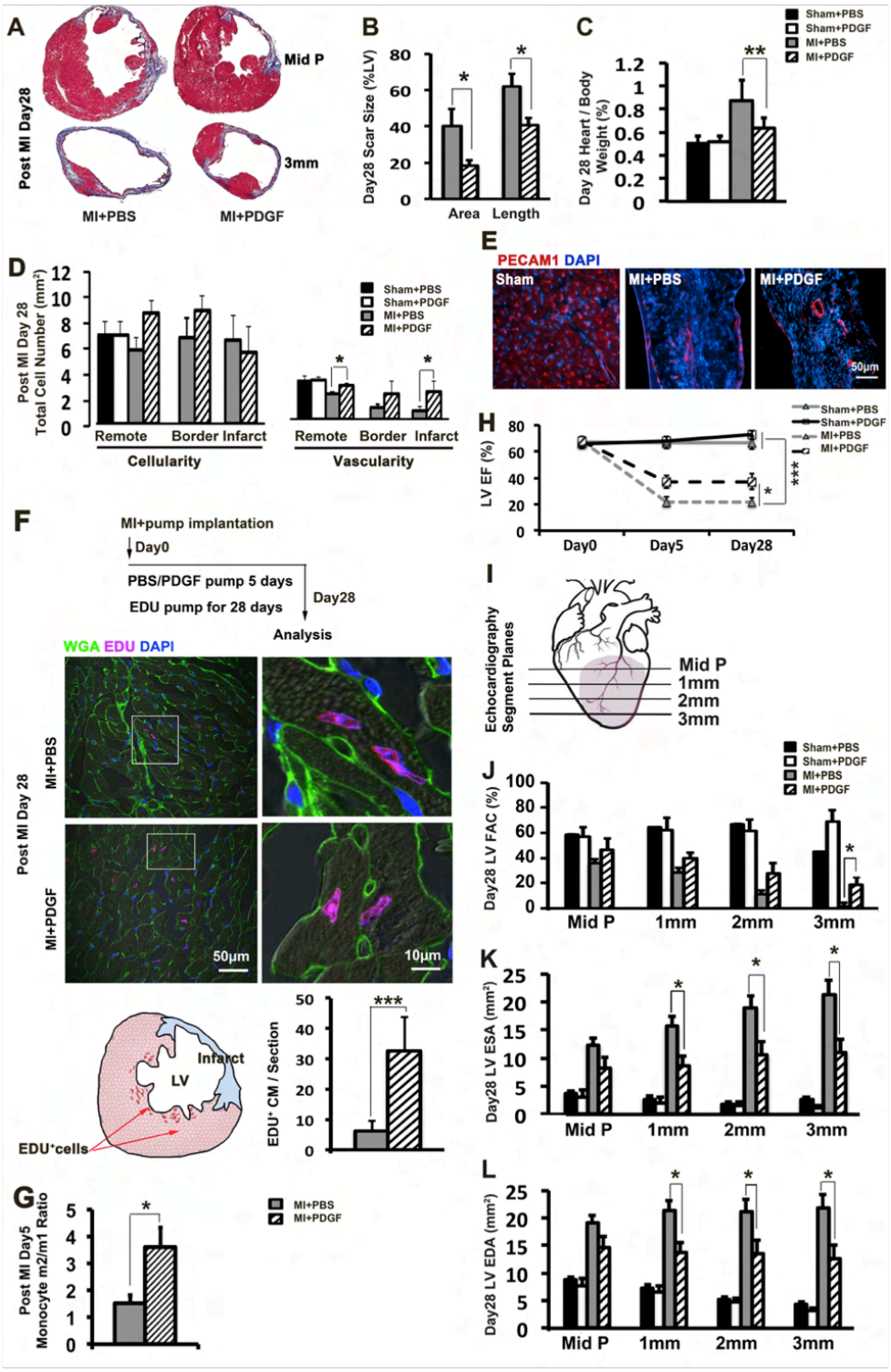

Figure 6: PDGF-AB enhancement of cardiac anatomical and function repair in MI hearts

(A) Presence of scar (Masson's Trichrome staining) in PBS and PDGF-AB-treated hearts 28 days post-MI at mid-papillary (Mid P) and 3 mm below Mid P levels (see

Fig. 6I). (B) Quantification of scar area and length in PBS and PDGF-AB MI hearts. (C) Quantification of Heart Weight/Body Weight ratio in day 28 sham/MI hearts. (D) Total cellularity (DAPI-stained nuclei/mm^3) and vascularity ($CD31^+$ micro-vessels/mm^3) in remote, boarder and infarct zones of day 28 sham/MI hearts. (E) Immunostaining showing improved caliber of $PECAM1^+$ vessels in the infarct zone of PDGF-AB-treated day 28 post-MI hearts. (F) EdU incorporation in cardiomyocytes of PBS and PDGF-AB-treated MI hearts, showing examples of nuclear uptake, location of positive cells and quantification. LV: left ventricle; WGA: wheat germ agglutinin staining. (G) Quantification of flow cytometric analysis of m2/m1 monocyte ratios in PBS and PDGF-AB-treated MI hearts at day 5. (H) LV ejection fraction (EF) in sham/MI hearts treated with PBS or PDGF-AB at 0 (baseline), 5 and 28 days. (I) Cartoon showing short axis planes for echocardiographic analyses. Mid P: mid-papillary. (J) Analysis of percent LV fractional area change (FAC) at different echocardiographic planes at day 28. (K,L) Analyses of LV end systolic area (ESA; panel K) and diastolic area (EDA; panel L) at different echocardiographic planes at day 28. All comparisons: * $p<0.05$; ** $p<0.01$; *** $p<0.001$.

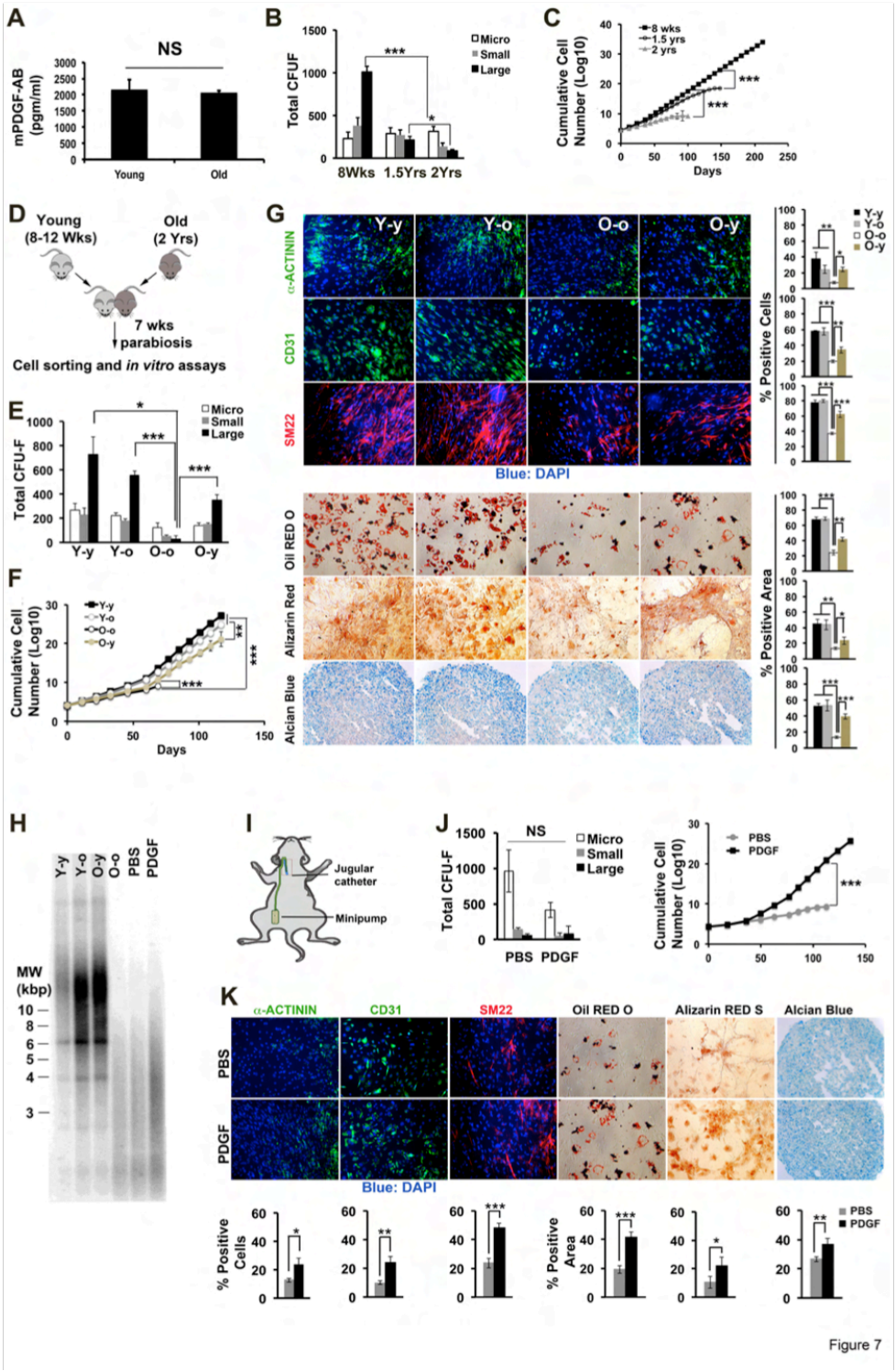

Figure 7: Role of PDGF ligand in ageing and rejuvenation

A) ELISA analysis of levels of endogenous serum PDGF-AB in 8 wks (young) and 1.5 yrs (old) mice. (B) cCFU-F analysis in S^+P^+ cells from 8 wk, 1.5 yr and 2 yr mice. (C) Long-term growth analysis of S^+P^+ cultures in young and old mice. (D) Schematic depiction of parabiotic surgery and experimental design. (E) cCFU-F

analysis of S^+P^+ cells from Young-young (Y-y), Young-old (Y-o), Old-old (O-o) and Old-young (O-y) åcultures at P5-6 from Y-y, Y-o, O-o and O-y parabionts using indicative markers for cardiomyocytes (α-actinin), enodhtelial cells (CD31), smooth muscle (SM22), adipocytes (Oil Red O), osteocytes (Alizarin Red S) and chondrocytes (Alcian Blue) (see Fig. S6B for additional markers). Percent marker activation graphed. (H) Southern blot analysis of telomere length from heterochronic parabiotic mice, as well as 2 yr old mice treated via mini-pump (see panel I) with PBS or PDGF-AB. (I) Scheme of mini-pump insertion. (J) cCFU-F and long-term growth analysis of S^+P^+ cells from 2 yr old mice treated with PBS or PDGF-AB. (K) *In vitro* lineage differentiation analysis of P5-6 S^+P^+ cultures using markers as in panel G. All comparisons: * $p<0.05$; ** $p<0.01$; *** $p<0.001$.

STAR METHODS

CONTACT FOR REAGENT AND RESOURCE SHARING

Further information and requests for resources should be directed to Munira Xaymardan (Munira.xaymardan@sydney.edu.au) or Richard Harvey (r.harvey@victorchang.edu.au).

EXPERIMENTAL MODEL AND SUBJECT DETAILS

***In vivo* animal studies:** All animal experiments were approved by the St Vincent's Hospital and Garvan Institute of Medical Research Animal Ethics Committee. Mice were bred and housed in the BioCORE facility of the Victor Chang Cardiac Institute. Rooms were temperature and light/dark cycle controlled. Standard food was provided *ad libitum*. Soggy and/or high nutrient food were provided after surgery.

Mouse strains used in experiments include C57Bl6J, *Pdgfra*-GFP, *Nkx2-5*-GFP, *Pdgfra*-merCremer and tdTomato (please see Key Resources Table for details). Both male and female mice aged 8-12 weeks (young) to 18-20 months (aged) were used. Surgical models included acute myocardial infarction (MI), catheterized minipump implantation, minipump implantation, tamoxifen treatment, oral gavage and parabiosis. Tissues were collected both from healthy and surgical mice for establishment of primary cell cultures, flow cytometry, immunohistochemistry and gene expression studies. Surgical procedures were performed in the BioCORE surgery suites between 9:30am to 3:30pm.

Primary cell culture: Primary cells were isolated from the mice and cultured at 37°C in 5% CO_2 and normoxia as described in relevant sections.

METHOD DETAILS

Cardiac CFU-F isolation and long term culture: Whole hearts were collected from mice that were either untreated, had undergone sham, MI or

parabiosis surgeries, were treated with PDGF-AB ligand or vehicle via minipump and/or PDGFRα signaling inhibitor or vehicle via oral gavage, and cCFU-F assays performed as described in relevant sections. Once collected, hearts were minced and enzymatically digested as previously described (Chong et al., 2011). The labeled cells were sorted by FACS for S^+P^+ population and plated at the density of 5000 cells/35cm^2 dish or 20,000 cells/75cm^2 flasks for long term growth assays as described (Chong et al., 2011). Colonies were scored as large, small and micro colonies according to their sizes following a crystal violet staining. For clonal analysis, the single large, small and micro-colonies were trypsinized within O-ring Cloning Cylinders (Corning), and then cells were pooled, centrifuged and plated separately. Cloned colony-derived cultures were then subjected to ligand/inhibitor treatments, differentiation assays, long-term or serial clone-based cultures as described in relevant procedures. Bulk cultured cells were split every 12 days until passage 4, then every 8 days thereafter. Cumulative growth curves were plotted on a logarithmic scale, following standard cell number calculations. In brief, cumulative cell numbers for each passage comprised the total cell number harvested, multiplied by the previous cumulative number divided by number of cells plated.

In vitro treatment of ligands, inhibitors and monoclonal antibodies

Bulk or clone cultures of flow-sorted cardiac S^+P^+ cells isolated from healthy hearts were treated with PDGF-AB (50ng/ml) ligand, PDGFRα/β chemical inhibitor AG1296 (0.5-10μM), AKT (5-50nM) or cMYC (10-100μM) inhibitors, or control or PDGFRα-blocking monoclonal IgGs (0.02-10μg/ml), adding the reagents to culture media and refreshing with each media change.

Cell cycle analysis, BrdU, EdU, TUNEL and mitochondrial assays

Cells sorted from mouse hearts with and without *in vivo* or *in vitro* treatments were used for cell cycle analysis. Staining of the cells with PyroninY and 7AAD was performed with minor modifications to the previously described method (Joun and Asli, 2017). In brief, cells were fixed in ice-cold 80% ethanol and stored at -20^{0}C at least overnight. Cells were permeabilized by

the Cytoperm Plus buffer (Becton Dickinson) for 5 mins and washed with 1x Cytoperm wash buffer before staining. Cellular DNA was stained with 7AAD (Becton Dickinson) and RNA with PyroninY (Sigma) before visualization by flow cytometry (Becton Dickinson CantoII). Data analysis was performed using FlowJo software. BrdU, EdU and TUNEL assays were performed using the APC-BrdU assay kit (Becton Dickinson), the Click-iT EdU assay kit (Thermofisher Scientific) and the DeadEnd™ Colorimetric TUNEL System (Promega), respectively, following manufacturers instructions. For mitochondrial assays, cells were harvested following standard methods, washed once with PBS and resuspended in culture medium containing 200nM of Mitotracker Green FM (Thermofisher Scientific). The staining mix was incubated for 15min at 37°C and analysed on a FACS CantoII (Becton Dickinson).

Live cell imaging and single-cell tracking of cCFU-F

Live cell imaging was performed using a Leica live cell imaging microscope (DMI6000B) equipped with x-y-z controller and hardware autofocus as described (Cornwell et al., 2016). Phase contrast images were acquired every 15 minutes for 12 days (288 hours). Raw images were exported to Matlab for removal of background noise, enhancement of contrast, and to stitch contiguous frames of view using custom-written scripts. Custom-written software implemented in Matlab (Nordon's Tracking Tool) was used to manually track cell nuclei through consecutive frames, to build trajectories and record fate outcomes (division, death, and right censored [lost or not recorded]). At least 200 cells from at least 20 individual clones per condition were tracked from two separate wells. Statistical analyses of live cell tracking data were implemented in custom-written scripts in Matlab. Kaplan-Meier analysis was used to generate empirical cumulative distribution functions for cell division. Cox regression was used to test for group differences and to estimate the relative risk of division relative to untreated controls. The relative frequency of observed fates in each treatment group was quantified by counting the number of cells with distinct fate outcomes in each group. Student's *t*-tests were used to test for significant differences in the proportion

of observed fates in each treatment group. All Matlab code will be made available upon request.

Quantitative RT-PCR, Western blots and receptor tyrosine kinase array

Quantitative RT-PCR, was performed using the SYBR master mix (Roche) following manufacturer's instructions. PCR reactions were run on LightCycler480 (Roche). Expression values were calculated using the Delta Ct method. Western blotting and immunocyto/histochemistry experiments were performed following standard protocols. For a comprehensive list of primers and antibodies used, refer to Key Resources Table. To profile active receptor tyrosine kinase pathways in cardiac CFU-F cultures, mouse phospho-RTK array kit was employed (R&D Systems) according to manufacturer's instructions. 100μg of total protein was added to each membrane.

Microarray sample preparation and analysis

For studies with inhibitor and ligand (P0) and on clonal small and large colonies (P5-P15), three independent experiments were performed for each condition. Total RNA was extracted using RNAeasy micro RNA isolation kit (Qiagen) and the quality of RNA was assessed using the Nanodrop (Thermofisher Scientific; 230/260>1.8, 260/280>1.8) and Bioanalyzer (Agilent, RIN>8.0). The RNA was further processed for microarray analysis by the Ramaciotti Center for Genomics (University of New South Wales, Sydney). Total RNA (100ng) of was labelled using the Affymetrix WT kit (Ambion). 3.52 μg of fragmented labelled ssDNA was hybridised to Mouse Gene 1.0 ST Gene Arrays for 16 hours at 45°C in the Affymetrix GeneChip Oven. Arrays were washed on the Affymetrix Fluidics 450 instrument as per manufacturer's protocol using the Affymetrix GeneChip Hybridization Wash & Stain kit for cartridge arrays. Arrays were scanned on the Affymetrix GeneChip 3000 7G Scanner instrument as per manufacturer's protocol and the Affymetrix GeneChip Command Console (AGCC) software was used to generate the CEL files from the DAT image files. RAW and normalized microarray data are

available at NCBI's Gene Expression Omnibus (GSE106778; GSE106779) (Edgar et al., 2002)

Microarray data were processed and analysed in R/Bioconductor (Gentleman et al., 2004) Heatmaps were generated using the gplots R package and where clusters were identified, were split by cutting the tree at the reported height. Gene ontology analyses were performed using DAVID (Huang da et al., 2009) against the *Mus musculus* background. Quality control was first performed using the 'affy' and 'affyPLM' R packages to assess the distribution of probe-level effects via the RLE and PLM methods as well as pseudoimage decomposition of the microarrays (Gautier et al., 2004) No artefacts or outliers were revealed. Data were then normalised at the transcript level using Robust Multichip Average (RMA) normalisation. Principle component analysis was performed using the pcaMethods R package (Stacklies et al., 2007) using singular value decomposition. For determination of differentially expressed genes, a linear model with Bayes variance shrinkage was fit using the limma R package (Smyth, 2005) to determine moderated t-statistics for all pair-wise comparisons. P-values were then corrected for multiple hypothesis testing using the Benjamini and Hochberg method (Benjamini and Hochberg, 1995). Unless reported otherwise, a corrected p-value less than or equal to 0.05 was reported as significant. Where multiple probe sets were assigned to the same annotated gene, the gene with the highest average expression was reported for further analyses.

Immunohistochemistry and confocal microscopy in tissues

Cryosections (8μm) of paraformaldehyde (PFA; 4%) perfusion fixed and sucrose treated hearts were cut and incubated with one or more primary antibodies overnight at 4°C (listed in Table S2) after incubating with a blocking solution including 1% bovine serum albumin, 3% serum (from the species that the secondary antibodies were derived), 0.03% triton X-100 in PBS for 30 minutes at room temperature. Nuclear counter-staining was performed after visualization of the markers by incubating sections with appropriate fluorochrome-conjugated secondary antibodies. EdU staining were performed on day 28 post-MI mouse hearts from animals treated with EdU+PDGF/PBS

using a Click-iT EdU assay kit (Thermofisher Scientific) following manufacturer's instructions. Images were acquired using a Zeiss upright microscope or Zeiss confocal microscope.

Immunohistochemistry and confocal microscopy on cells

Cells were fixed with 4% PFA for 5 minutes at room temperature, washed with PBS and incubated with one or more primary antibodies for 1 hour at 4°C (listed in Table S2) after incubating with a blocking solution including 1% bovine serum albumin, 3% serum (from the species that the secondary antibodies were derived), 0.03% triton X-100 in PBS for 30 minutes at room temperature. Nuclear counter-stains performed after visualization of the markers by incubating the sections with appropriate fluorochrome-conjugated secondary antibodies. Images were acquired by using a Zeiss upright microscope of Zeiss confocal microscope.

Differentiation assays

For differentiation assays, cCFU-F bulk or clonal cultures were grown in normal cCFU-F medium until 70-80% confluency and then lineage-specific differentiation medium was added for the indicated time-frame. All media contained penicillin (100μg/ml), streptomycin (250ng/ml) and L-Glutamine (2mM). Media were changed every 3-4 days and cells were fixed at the end of differentiation period. Differentiation protocols were followed as previously described (Chong et al., 2011) with modifications as follows: for cardiomyocyte differentiation, 70% confluent cCFU-F colonies were co-cultured with HL-1 cardiac muscle cells in 1:1 cCFU-F and HL-1 medium for 2 weeks (HL-1 medium: Claycomb medium (JRH Bioscences), 10% FBS, 0.1 mM Neurepinephrine, 100μg/ml Penicillin/Streptomycin, 2mM L-Glutamine). Cells were stained with antibodies against α−ACTININ, NKX2-5, TROPONIN-T and MEF2C. For endothelial differentiation, cells were cultured in plates pre-coated with 0.1% Gelatin (Sigma-Aldrich) and 0.1% Fibronectin (Sigma-Aldrich) until 70% confluent. The medium was then replaced with differentiation medium containing 1% FBS, 10ng/ml basic FGF (R&D) and 10ng/ml VEGF in Iscove's Modified Dulbecco's Medium (IMDM, Thermofisher Scientific) supplemented with penicillin/streptomycin and L-Glutamine. Cells were fixed after 1 week in

differentiation medium and stained with antibodies against CD31, CAVEOLIN, E-NOS and VE-CADHERIN (VE-CAD). For smooth muscle differentiation, cells were treated with 50ng/ml TGFB1 (R&D systems) with 2% FCS in DMEM-HG (GIBCO) for 2 weeks and stained with antibodies against Smooth muscle myosin heavy chain (MYH11), SM22, Smooth muscle actin (SMA) and CALPONIN. For differentiation to adipocytes, cells were treated with DMEM (GIBCO) medium containing 0.5µM 1 methyl-3-isobutyl methylxantine, 60µM Indomethacin, 5µg/ml Insulin and 1µM Dexamethasone plus 10% FBS, penicillin/streptomycin and L-Glutamine. After 3 weeks in differentiation medium, cells were stained with Oil RED-O as previously described (Chong et al., 2011). Differentiation to osteocytes and chondrocytes was performed and detected as previously described (Chong et al., 2011).

Systemic delivery of ligands, inhibitors and monoclonal antibodies

PDGF-AB ligand (R&D, 20µg/ml) or vehicle (PBS) was administered systemically by a subcutaneous minipump (Alzet), inserted to the right external jugular vein via 13mm of 28G catheter (Alzet) through a 1mm incision. The ligand/vehicle was continuously released at a concentration of 0.5µl/hr for 5 days. Imatinib was delivered via oral gavage once daily at a concentration of 20mg/kg daily for 5 days. To block PDGFRα *in vivo,* mice were injected with one dose of 400ug (2µg/ul) on day 1, 200µg each on days 4 and 8, before either MI or sham surgeries.

Acute myocardial infarction

Mice were anaesthetized by intraperitoneal injection of ketamine (100mg/kg) and xylazine (20mg/kg), and intratracheally intubated. The hearts were exposed via a left intercostal incision, the left anterior descending coronary arteries were ligated just before the first diagonal branching point, lungs inflated and the wounds suture closed. Sham operations were performed without the ligation of the coronary artery. The mice were given intra-muscular injection of Bupernopherine for 3 days. Hearts were collected for immunohistochemistry, FACS analysis or echocardiography 5-28 days after surgery as indicated for individual experiments.

Chronic cardiac injury models

Aldosterone mediated cardiac fibrosis: Anaesthetized mice were implanted with a 14 day mini-pump (Alzet 1002) containing either aldosterone (0.15μg/hr) or vehicle (polyethylene glycol) through a dorsal skin incision (Kageyama and Bravo, 1988). Mice were fed with water containing 1% NaCl. The osmotic pumps were replaced after 2 weeks and hearts analyzed on 28 days. Excess aldosterone generates hypervolemic hypertension and cardiac fibrosis by stimulating water and sodium reabsorption, and release of vasopressin (Brunner et al., 1972).

Aortic banding assays: The aorta was exposed through a mediastinum incision in anaesthetized and intubated mice. The aortic root was isolated and a 4-0 constrictor suture was placed by using a template wire for diameter control. The incision was then closed and the animals recovered. Hearts were analyzed at day 28 post surgery.

Echocardiography

Mice were anaesthetized using 5% isoflurane delivered by nose cone and echocardiography was performed on supine mice using a Vevo770 (Visualsonics Inc., Toronto, Canada) under 1-2% isoflurane on a warming pad set to 37°C. B-mode images were taken of the LV long axis (LAX) of the heart followed by four short axis (SAX) images, starting at the mid-papillary muscle level and at 1, 2 and 3mm towards the apex. Using Vevo770 Workstation software the following data were obtained by a blinded operator from the echocardiography images: LV length was measured from the apical dimple to the base of the aortic valve leaflets from the LAX images at end diastole (ED) and end-systole (ES) from the apical dimple to the base of the aortic valve leaflets. Endocardial areas were derived by planimetry from the four SAX planes at ED and ES. ED and ES LV volumes were derived using a modified Bullet formula; LVvol = L x (mean endocardial area) x 5/6.

Quantification of cellularity and vascularity

CD31 and DAPI stained sections of infarcted and sham-operated hearts were imaged using Zeiss 700 upright confocal microscope at 20 times magnification to cover entire left ventricle. Images were segmented as infarct, border and remote zones. The images were imported into the ImageJ to analyze total cell and vessels numbers in the respective areas.

Heart weight/body weight and infarct size measurement

Mice were weighed postmortem at post-surgical day 28, and then hearts were resected and weighed separately. Percentage heart weigh/body weight was calculated. Hearts were embedded in OCT and frozen. 10μM sections were stained using a Masson's Trichrome staining kit (Sigma) and stained slides were scanned using an Aperio ePathology scanner (Leica). The area size and length of the left ventricles were measured using ImageJ.

Flow cytometry analysis of immune cell influx and time course analysis of GFP^{medium} population

For immune influx analysis, the total interstitial population isolated by FACS was subjected to further fractionation with monocyte makers. Within the monocyte/macrophage population (CD45^{+} CD11b^{+} Ly-6G^{low}), type 1 monocytes (m1) were defined as Ly-6C^{high}[F4/80/I-A^{b}/CD11c]^{low}, and monocyte type 2 (m2) as Ly-6C^{low}[F4/80/I-A^{b}/CD11c]^{low} (see Fig. S6A,B). In time course analyses (2 hrs to 5 days), *Pdgfra*-GFP mice were used to separately quantify the *Pdgfra*-GFP^{high} stromal cells and *Pdgfra*-GFP^{medium} myofibroblasts within the S^{+}P^{+} population in sham and MI hearts (see Fig. 5G).

Terminal Restriction Fragment analysis of telomere length

Terminal telomeric restriction fragments were prepared by *Hin*fI and *Rsa*I digestion of genomic DNA and separated by 1% (w/v) agarose gel with pulsed-field electrophoresis in 0.5 × TBE. Pulsed field gels were run at 6V for 24 hrs at 14°C with an initial switch time of 1s and a final switch time of 6s. Gels were dried for 2 hrs at 60°C, denatured in 0.5M NaOH, 1.5M NaCl for 1 hr and neutralized in 0. 5M Tris-HCl (pH 8.0), 1.5M NaCl for 1 hr. Gels were rinsed in

2 × SSC and pre-hybridised in Church buffer (250 mM sodium phosphate buffer (pH 7.2), 7% (w/v) SDS, 1% (w/v) BSA fraction V grade and 1 mM EDTA) for 2 hrs at 37°C. Gels were then hybridized overnight with a [γ-^{32}P]-ATP-labelled (CCCTAA)3 oligonucleotide probe, washed three times in 0.1 × SSC for 15 min at 37°C and exposed to a PhosphorImager screen overnight.

In vivo labeling of EdU, BrdU and tamoxifen induction

BrdU (50mg/ml) and EdU (10 mg/ml) are delivered through subcutaneously implanted minipumps. 7-day pumps with a delivery rate of 0.5µl/ml were used for the 5 day assays, while 1µl/hr 2-week pumps were used for the 28 day assays with replacement pump insertions performed at the two weeks interval. For labelling of the PDGFRα lineage positive cells *in vivo*, adult *Pdgfra-merCREmer x tdTomato* mice were given tamoxifen (40mg/ml, Sigma) via oral gavage (300mg/kg) for 2 days, MI surgeries were performed 1 week after the tamoxifen treatment, and hearts were subjected to IHC or FACS analysis at day 5 and day 28 post-MI surgeries.

Heterochoronic parabiosis

Young (8-10 weeks old) and aged (18 month) syngeneic female mice were selected for heterochronic parabiosis surgeries to create three groups of paired animals: young to young, young to old and old to old. The selected pairs were caged together for one week prior to surgery for acclimatization. Each mouse received a surgical incision on the side of the body extending from the elbow joint to the knee joint, with paired mice receiving mirror-image incisions. A 4-0 silk suture was passed through the flesh and joints of each mouse and secured with knots. Skin of the paired mice was then sutured together in a ventral to ventral and dorsal to dorsal manner using a 4-0 suture. Hearts were collected after 7 weeks of parabiosis.

Production of APA5 antibody

The blocking monoclonal antibody against PDGFRα was produced in house (Centre For Targeted Therapy, Garvan Institute of Medical Research) from the APA-5 hybridoma cell line (Takakura et al., 1996; Takakura et al., 1997). IgG

was purified from the supernatant using Protein L Sepharose resin (Genscript) as previously described (Dudgeon et al., 2012)and concentrated to 2mg/mL in PBS using an Amicon Ultra-15 Centrifugal filter unit (Millipore). The purity of the antibody preparation was validated by reducing and non-reducing SDS-PAGE and endotoxin contamination was assessed using the QCL-1000™ Endpoint Chromogenic LAL Assay (Lonza) according to manufacturer's instructions. Control IgG from Rat IgG2a isotype control clone 2A3 was sourced from BioXcell.

ELIZA assay

Serum was collected from 24mo and 8wk old healthy mice, as well as 8wk old PDGF-AB-treated mice. Briefly, blood was collected via cardiac puncture after euthanasia and let clot at room temperature for 30mins before centrifugation at 1500rpm for 10mins. Serum concentration of mouse PDGF-AB and human PDGF-AB was measured using a Mouse/Rat PDGF-AB Quantikine ELISA Kit and a Human PDGF-AB Quantikine ELISA Kit (R&D Systems), respectively, following manufacturer's instructions and analysis using the ELISA Centro Luminescence Microplate Reader (Bio-Rad).

QUANTIFICATION AND STATISTICAL ANALYSIS

Statistical analyses of live cell tracking data were implemented in custom-written scripts in Matlab. Kaplan-Meier (KM) analysis was used to generate empirical cumulative distribution functions for cell division. Cox regression was used to test for group differences and to estimate the relative risk of division (relative to untreated controls). The relative frequency of observed fates in each treatment group was quantified by counting the number of cells with distinct fate outcomes in each group. Student's *t*-tests were used to test for significant differences in the proportion of observed fates in each treatment group. All Matlab code will be made available upon request. For all other data, Student's *t*-tests were used to determine significance between triplicate experiments.

DATA AND SOFTWARE AVAILABILITY

RAW and normalized microarray data are available at NCBI's Gene Expression Omnibus (GSE106778; GSE106779) (Edgar et al., 2002).

KEY RESOURCES TABLE

REAGENT or RESOURCE	SOURCE	IDENTIFIER
Antibodies		
Rb	Abcam	ab6075-1
PhosphoRb (Ser780)	Cell Signaling	D59B7
P130	Abcam	76234
$P27^{kip}$	BD Biosciences	610242
H2B	Abcam	Ab18977
CyclinA2	Cell Signaling	4656P
CyclinB1	Cell Signaling	4138P
CyclinE1	Cell Signaling	4129P
CyclinD1	Cell Signaling	2978P
c-Myc	Santa Cruz	sc-788
Akt (pan-Akt)	Cell Signaling	4691
p-Akt308	Cell Signaling	2965
p-Akt473	Cell Signaling	4060
p-FOXO1	Cell Signaling	9461
FOXO1	Cell Signaling	2880
α- actinin	Sigma-Aldrich	A7811
NKX2-5	Santa Cruz	Sc-8697
WGA	Thermo Fisher Scientific	W11261
SMA	Sigma-Aldrich	A2547
eNOS	Abcam	ab66127
SM22	Abcam	ab14106
Calponin	Abcam	ab46794
Caveolin1	BD Biosciences	610059
CD31	BD Biosciences	553370
MyH11	Santa Cruz	6956)
MEF2C	Cell Signaling	5030S
pH3	Upstate	06-570
Ki67	Abcam	ab15580
BrdU	Abcam	ab6326
PDGFRα	Cell Signaling	3164
PDGFRβ	Santa Cruz	Sc-432
Lectin	Sigma-Aldrich	L3759
Isolectin	Thermo Fisher Scientific	I21411
Collagen IV	Abcam	ab19808
Collagen VI	Abcam	ab6588
cTnT	Thermo Fisher Scientific	MS-295-P1
Ly-6C PE	eBioscience	12-5932-80
F4/80 FITC	eBioscience	11-4801
CD11c FITC	BD Biosciences	553953
$I\text{-}A^b$ FITC	BD Biosciences	553456
PE Sca1 (Ly6A/E)	BD Biosciences	5531108
CD45- APCCy7	BD Biosciences	557659

CD31-PECy7	eBioscience	25-0311-82
PDGFRa (CD140a)-APC	eBioscience	17-1401-81
Ly-6G (Gr-1)-PerCPCy5	BD Biosciences	45-5931-80
CD11b-APC	BD Biosciences	553312
mPDGFRa	R&D System	AF1042
mPDGFRb	R&D System	AF1062
CD146	Abcam	Ab75769
NG2	EMD Millipore	AB5320
Bacterial and Virus Strains		
Biological Samples		
Chemicals, Peptides, and Recombinant Proteins		
PDGF-AB	R&D System	222-AB
AG1296	Cayman Chemical	146535-11-7
Imatinib	LC Laboratories	I-5508
cMyc inhibitor (10058-F4)	Sigma-Aldrich	F3680
Akt inhibitor (LY294002)	Cell Signaling	9901
PyroninY	Polysciences	18614-5
7AAD	BD Biosciences	51-68981E
Mitotracker Green FM	Thermo Fisher Scientific	M7514
Hoechst	Invitrogen	H369
DAPI	Thermo Fisher Scientific	62247
Aldosterone	Sigma-Aldrich	234362
Tamoxifen	Sigma-Aldrich	T5648
BrdU	Sigma-Aldrich	B5002
Alizarin Red S	Sigma-Aldrich	A5533
Oil Red O	Sigma-Aldrich	O0625
Alcian Blue	Sigma-Aldrich	A5268
Critical Commercial Assays		
Mouse Phospho-Receptor Tyrosine Kinase Array Kit	R&D Systems	ARY014
Click-iT EdU assay kit	Thermo Fisher Scientific	C10337
DeadEnd™ Colorimetric TUNEL System	Promega	G736
Masson Trichrome Staining kit	Sigma-Aldrich	HT-15
Mouse/Rat PDGF-AB Quantikine ELISA Kit	R&D Systems	MHD00
Human PDGF-AB Quantikine ELISA Kit	R&D Systems	DHD00C
Deposited Data		
https://www.ncbi.nlm.nih.gov/geo/query/acc.cgi?acc=GSE106779- reviewer token: ifczsmwwhzkfxwb	This paper	N/A
Experimental Models: Cell Lines		
Experimental Models: Organisms/Strains		
Mouse, Pdgfra-GFP, KI GFP, KO	Jackson Laboratory	*Pdgfra* $^{tm11(EGFP)Sor}$
Mouse, Nkx2-5 GFP, KI GFP, KO	Harvey laboratory	*B6.129S1(C)-Nkx2-5tm4Rph/J*
Mouse, β-Actin-GFP, TG	Jackson Laboratory	*Tg(CAG-EGFP)1Osb*

Mouse, PdRa-MCM, KI	RIKEN Center for Developmental Biology, Kobe, Japan	*Pdgfra-merCremer*
Mouse, tdTomato Red, TG	Jackson Laboratory (Imported from ARMI)	*B6.Cg-Gt(ROSA)26Sor*$^{tm14(CAG\text{-}tdTomato)Hze}$*/J*
Oligonucleotides		
Primer: PolG F:CACGGACCTCCTGCCTAAG R:TCATCTAGTCGAGGGGCAGAG	This paper	N/A
Primer: PolG2 F:AGCCAATAGAAACCCTGTGG R:CACTTACAGACAGAACGCAACG	This paper	N/A
Primer: Tfam F:TCAGGAGGCAGTTATTG R:CAGGAAGTCTTCACGTTGACC	This paper	N/A
Primer: Smooth Muscle Actin F:GCTGACAGAGGCACCACTGA R:CATCTCCAGAGTCCAGCACA	This paper	N/A
Primer: Calponin F:GAACCCTGTGGACCTGTTTGA R:GCGTCGTCAAAGTTCCTCTC	This paper	N/A
Primer: Embryonic Smooth Muscle F:CGCTTTGGCAAGTTTATCCG R:CAGCACTGAAGACACGACTT	This paper	N/A
Primer: Fibronectin (EIIA) F:CCCACTGTGGAGTACGTGG R:GAGTCCTGACACAATCACCG	This paper	N/A
Primer: Fibronectin (EIIB) F:GGGGACCTCTCTGGAAGAAGTGG R:GTCCCAGGCAGGAGATTTG	This paper	N/A
Primer: Nkx2-5 F:CCCAAGTGCTCTCCTGCTTTC R:TCCAGCTCCACTGCCTTCTG	This paper	N/A
Primer: Islet-1 *Primer:* F:TCATCCGAGTGTGGTTTCAA R:CCATCATGTCTCTCCGGACT	This paper	N/A
Primer: Tbx-5 *Primer:* F:ATGGTCCGTAACTGGCAAAG R:TTTCGTCTGCTTTCACGATG	This paper	N/A
Primer: Gata-4 F:GCCCGGGCTGTCATCTCACTATG R:GCTGGCCTGCGATGTCTGAGTG	This paper	N/A
Primer: Tbx-20 F:GCAGCAGAGAACACCATCAA R:CAGAGCTCCTTCGTTTCCAG	This paper	N/A
Primer: DDR-2 F:CTGTCGGATGAGCAGGTTAT R:CTCGGCTCCTTGCTGAAGAA	This paper	N/A
Primer: Vimentin F:TACCAGGACACTATTGGCCG *Primer:* R:CTGTTGCACCAAGTGTGTGC	This paper	N/A
Primer: Desmin F:GCTATCAGGACAACATTGCG R:GTTGTTGCTGTGTAGCCTCG	This paper	N/A
Primer: mTR F:GCTGTGGGTTCTGGTCTTTT R:CGTTTGTTTTTGAGGCTCGG	This paper	N/A
Primer: mTERT	This paper	N/A

F:CCAACACTGTTATTGAGACCCTG R:GGCCTGTAACTAGCGGACACA		
Primer: GusB *Primer:* F:CCTTCTAGCTTCAATGACATC R:GATCCTCAACACCACTCTC	This paper	N/A
Primer: 18S rRNA F:AGGGGAGAGCGGGTAAGAGA R:GGACAGGACTAGGCGGAACA	This paper	N/A
Primer: GAPDH F:GGTCCTCAGTGTAGCCCAAG R:AATGTGTCCGTCGTGGATCT	This paper	N/A
Primer: HPRT F:AGTGTTGGATACAGGCCAGAC R:CGTGATTCAAATCCCTGAAGT	This paper	N/A
Recombinant DNA		
Software and Algorithms		
Other		

Refrences for the methods

Benjamini, Y., and Hochberg, Y. (1995). Controlling the false discovery rate: a practical and powerful approach to multiple testing. Journal of the Royal Statistical Society, Series B *57*, 289-300.

Brunner, H.R., Laragh, J.H., Baer, L., Newton, M.A., Goodwin, F.T., Krakoff, L.R., Bard, R.H., and Buhler, F.R. (1972). Essential hypertension: renin and aldosterone, heart attack and stroke. N Engl J Med *286*, 441-449.

Chong, J.J., Chandrakanthan, V., Xaymardan, M., Asli, N.S., Li, J., Ahmed, I., Heffernan, C., Menon, M.K., Scarlett, C.J., Rashidianfar, A.*, et al.* (2011). Adult cardiac-resident MSC-like stem cells with a proepicardial origin. Cell stem cell *9*, 527-540.

Cornwell, J.A., Hallett, R.M., der Mauer, S.A., Motazedian, A., Schroeder, T., Draper, J.S., Harvey, R.P., and Nordon, R.E. (2016). Quantifying intrinsic and extrinsic control of single-cell fates in cancer and stem/progenitor cell pedigrees with competing risks analysis. Sci Rep *6*, 27100.

Dudgeon, K., Rouet, R., Kokmeijer, I., Schofield, P., Stolp, J., Langley, D., Stock, D., and Christ, D. (2012). General strategy for the generation of human antibody variable domains with increased aggregation resistance. Proc Natl Acad Sci U S A *109*, 10879-10884.

Edgar, R., Domrachev, M., and Lash, A.E. (2002). Gene Expression Omnibus: NCBI gene expression and hybridization array data repository. Nucleic Acids Res *30*, 207-210.

Gautier, L., Cope, L., Bolstad, B.M., and Irizarry, R.A. (2004). affy--analysis of Affymetrix GeneChip data at the probe level. Bioinformatics *20*, 307-315.

Gentleman, R.C., Carey, V.J., Bates, D.M., Bolstad, B., Dettling, M., Dudoit, S., Ellis, B., Gautier, L., Ge, Y., Gentry, J.*, et al.* (2004). Bioconductor: open software development for computational biology and bioinformatics. Genome Biol *5*, R80.

Huang da, W., Sherman, B.T., and Lempicki, R.A. (2009). Systematic and integrative analysis of large gene lists using DAVID bioinformatics resources. Nat Protoc *4*, 44-57.

Joun, G., and Asli, N.S. (2017). Cancer Cell Properties Shape Along Metabolic Activity in Human Epithelial Carcinoma. Journal of Stem Cell: Advanced Research and Therapy *4*, 1-5.

Kageyama, Y., and Bravo, E.L. (1988). Hypertensive mechanisms associated with centrally administered aldosterone in dogs. Hypertension *11*, 750-753.

Smyth, G.K. (2005). limma: Linear Models for Microarray Data. In Bioinformatics and Computational Biology Solutions Using R and Bioconductor Statistics for Biology and Health, R. Gentleman, V.J. Carey, W. Huber, I. R.A., and S. Dudoit, eds. (New York, NY: Springer).

Stacklies, W., Redestig, H., Scholz, M., Walther, D., and Selbig, J. (2007). pcaMethods--a bioconductor package providing PCA methods for incomplete data. Bioinformatics *23*, 1164-1167.

Takakura, N., Yoshida, H., Kunisada, T., Nishikawa, S., and Nishikawa, S.I. (1996). Involvement of platelet-derived growth factor receptor-alpha in hair canal formation. J Invest Dermatol *107*, 770-777.

Takakura, N., Yoshida, H., Ogura, Y., Kataoka, H., Nishikawa, S., and Nishikawa, S. (1997). PDGFR alpha expression during mouse embryogenesis: immunolocalization analyzed by whole-mount immunohistostaining using the monoclonal anti-mouse PDGFR alpha antibody APA5. J Histochem Cytochem *45*, 883-893.

Inventory of Supplementary Information

Fig. S1 relates to Fig. 1. This contains the analysis of pericyte markers on SCA1^{+}*Pdgfra*-GFP^{+} cells; *in vitro* growth and marker characterisitcs of these cells; survey of active tyrosine kinase receptor signalling in serum-cultured cells; effect of PDGFRα inhibitor and bocking antibody, and PDGF-AB ligand, on the growth and expression of cell cycle regulators in cCFU-F cultures.

Fig. S2 relates to Fig. 2. Contains the effect of the PDGFRα inhibitor AG1296 on the cell cycle profile of passage 4 cCFU-F cultures; analysis of the involvement of cMYC and AKT on steady state growth of cCFU-F cultures in serum; and the results of microarray transcriptome analysis of cCFU-F cultures treated with PDGFRα inhibitor or PDGF-AB ligand.

Fig. S3 relates to Fig. 3. Contains colony formation and long-term growth assays on cCFU-F cultures established in the presence of PDGFRα blocking antibody or control IgG.

Fig. S4 relates to Fig. 4. Contains immunofluorescence and histochemical staining analyses of lineage markers after *in vitro* differentiation of cloned large and small colonies from cCFU-F cultures.

Fig. S5 relates to Fig. 5. Contains flow cytometric analysis of the influx of CD45^{+} cells into hearts after myocardial infarction (MI); definition of *Pdgfra*-GFP^{medium} myofibroblasts and analysis of myofibroblast formation in several animal models of fibrosis including after treatment of MI mice with PDGFRα blocking antibody; analysis

of colony-formation, gene expression and cell cycle profile in *Pdgfra*-GFP^{medium} myofibroblasts formed after MI; analysis of serum levels of endogenous and exogenous PDGF-AB in a mice perfused with human recombinant PDGF-AB via mini-osmotic pump.

Fig. S6 relates to Fig 6. Contains flow cytometic data used to define m1 and m2 monocytes and their proportion after treatment of MI hearts with PBS or PDGF-AB ligand via mini-osmotic pump; Quanticaiton of left ventricular fractional shortening, end systolic areas and end diastolic areas in sham and MI hearts treated with PBS or PDGF-AB ligand.

Fig. S7 related to Fig 7. Contains immunofluorescence images of the expression of lineage markers in cCFU-F cultures established from heterochronic parabiotic mice and aged mice treated for 5 days with PBS or PDGF-AB ligand via mini-osmotic pump.

Table 1 is related to Biological process GO Terms presented in Figure S1

Supplementary Figures and Figure Legends:

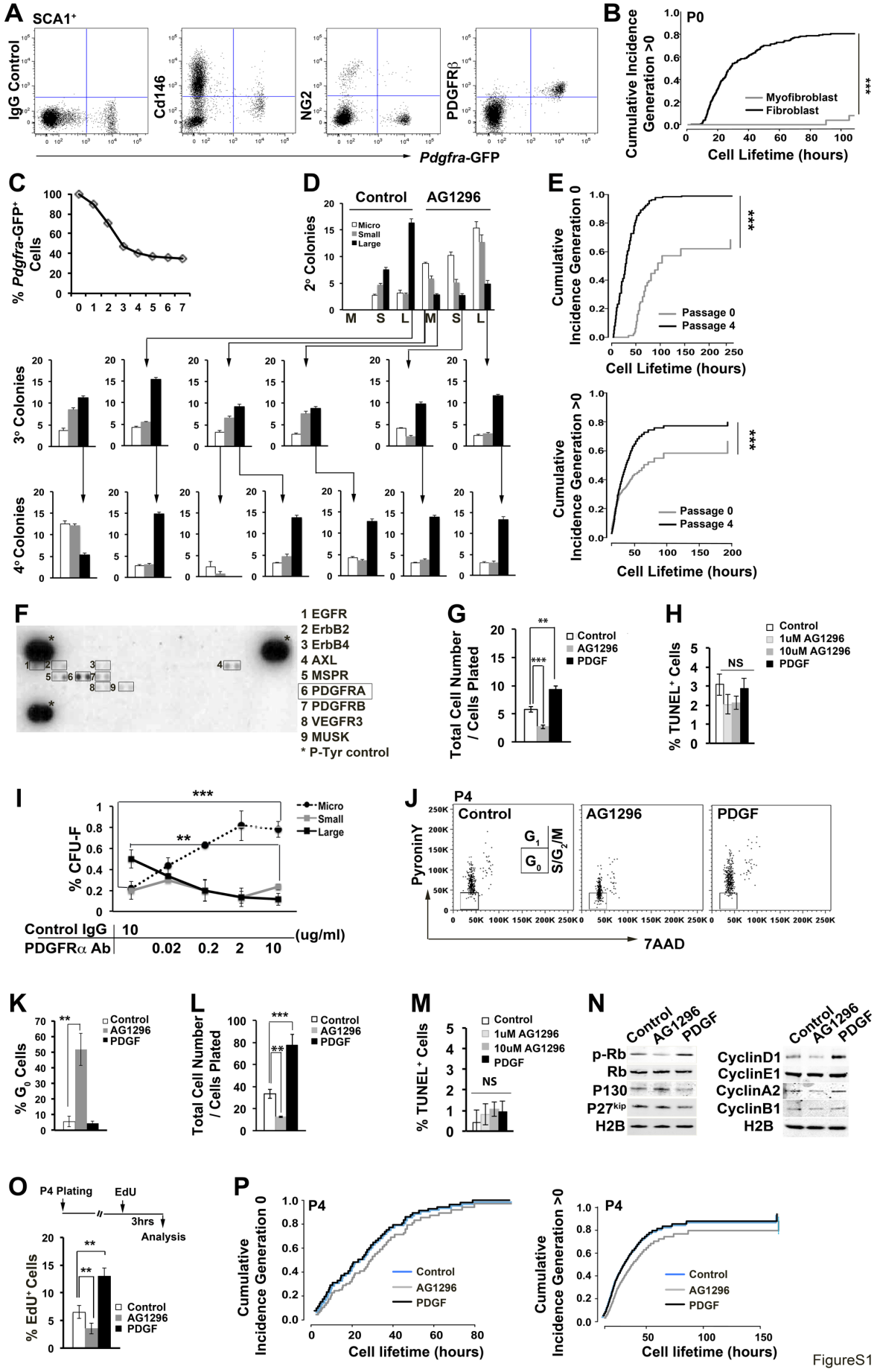
A
SCA1+
IgG Control
Cd146
NG2
PDGFRβ
Pdgfra-GFP
B
P0
Cumulative Incidence Generation >0
Myofibroblast
Fibroblast
Cell Lifetime (hours)
C
% Pdgfra-GFP+ Cells
D
Control
AG1296
2° Colonies
Micro
Small
Large
3° Colonies
4° Colonies
E
Cumulative Incidence Generation 0
Passage 0
Passage 4
Cell Lifetime (hours)
F
1 EGFR
2 ErbB2
3 ErbB4
4 AXL
5 MSPR
6 PDGFRA
7 PDGFRB
8 VEGFR3
9 MUSK
* P-Tyr control
G
Total Cell Number / Cells Plated
Control
AG1296
PDGF
H
% TUNEL+ Cells
Control
1uM AG1296
10uM AG1296
PDGF
NS
I
% CFU-F
Micro
Small
Large
Control IgG
PDGFRα Ab
(ug/ml)
J
P4
Control
AG1296
PDGF
PyroninY
7AAD
K
% G0 Cells
L
Total Cell Number / Cells Plated
M
% TUNEL+ Cells
N
p-Rb
Rb
P130
P27kip
H2B
CyclinD1
CyclinE1
CyclinA2
CyclinB1
O
P4 Plating
EdU
3hrs
Analysis
% EdU+ Cells
P
Cumulative Incidence Generation 0
Cell lifetime (hours)

FigureS1

Figure S1: *In vivo* and *in vitro* qualities of cardiac PDGFRα^+ stromal cells and cCFU-F (A) Flow cytometric analysis of indicated pericyte markers on cardiac SCA1$^+$ *Pdgfra*-GFP$^+$ cells. PDGFRβ and NG2 stainings were performed on permeabilized cells. (B) Accumulated proportion of plated S$^+$P$^+$ cells which show fibroblastic or myofibroblastic morphologies and undergoing cell division (generations >0)(see STAR Methods). (C) Graph of the decline in percent *Pdgfra*-GFP$^+$ cells with passage in cultures of freshly plated cardiac SCA1$^+$ *Pdgfra*-GFP$^+$ interstitial cells. (D) Selected data from a serial clonal cCFU-F analysis of large (L), small (S) and micro-colonies (M) initially arising from freshly plated S$^+$P$^+$ cells cultured in vehicle (control) or PDGFRα inhibitor AG1296 until the end of passage (P) 0. Graphs show secondary (2^0), tertiary (3^0) and quaternary (4^0) colony assays after cloned primary colonies were passaged until the end of P1, P2 and P3 in the absence of inhibitor. (E) Accumulated proportion of cells undergoing division over time in freshly plated S$^+$P$^+$ cells across P0, or cCFU-F cultures replated at the end of P4, scored separately in generation 0 (whose birth was not observed) and generations >0. (F) Results of membrane-based tyrosine kinase receptor activity assay detecting tyrosine phosphorylation of specific receptors within extracts of S$^+$P$^+$ cultures at P0. Boxes – activity above background. (G,H) Total cell number and percent TUNEL-positive cells, respectively, in cCFU-F cultures treated throughout passage 0 with vehicle (control), AG1296 or PDGF-AB (see Fig. 1I). (I) cCFU-F analysis of S$^+$P$^+$ cells incubated in the presence of control IgG antibody or blocking anti-PDGFRα antibody, scored at the end of P0. (J) Cell cycle analysis of cCFU-F cultures after culture across P4 in the presence of vehicle (control), AG1296 or PDGF-AB. (K) Graph of percent G_0 cells, as boxed in panel J. (L) Graph of total number of cells arising from treatments of cCFU-F cultures across P4 with AG1296 or PDGF-AB, as shown in

panel J. (M) TUNEL assay showing percent cell death arising from treatment of cCFU-F cultures across P4 with AG1296 or PDGF-AB, as shown in panel J. (N). Western blot analysis of cell cycle-associated proteins after treatment of cCFU-F cultures across P4 with AG1296 or PDGF-AB, as shown in panel J. (O) EdU incorporation in cCFU-F cultures treated with vehicle, AG1296 or PDGF-AB, measured from a pulse 3hrs before analysis, as indicated. (P) Live cell tracking analysis of the accumulated proportion of cells undergoing division over time across P4 cells treated with vehicle, AG1296 or PDGF-AB, scored separately in generation 0 and generations >0. All comparisons: * $p<0.05$; ** $p<0.01$; *** $p<0.001$. NS: non-significant.

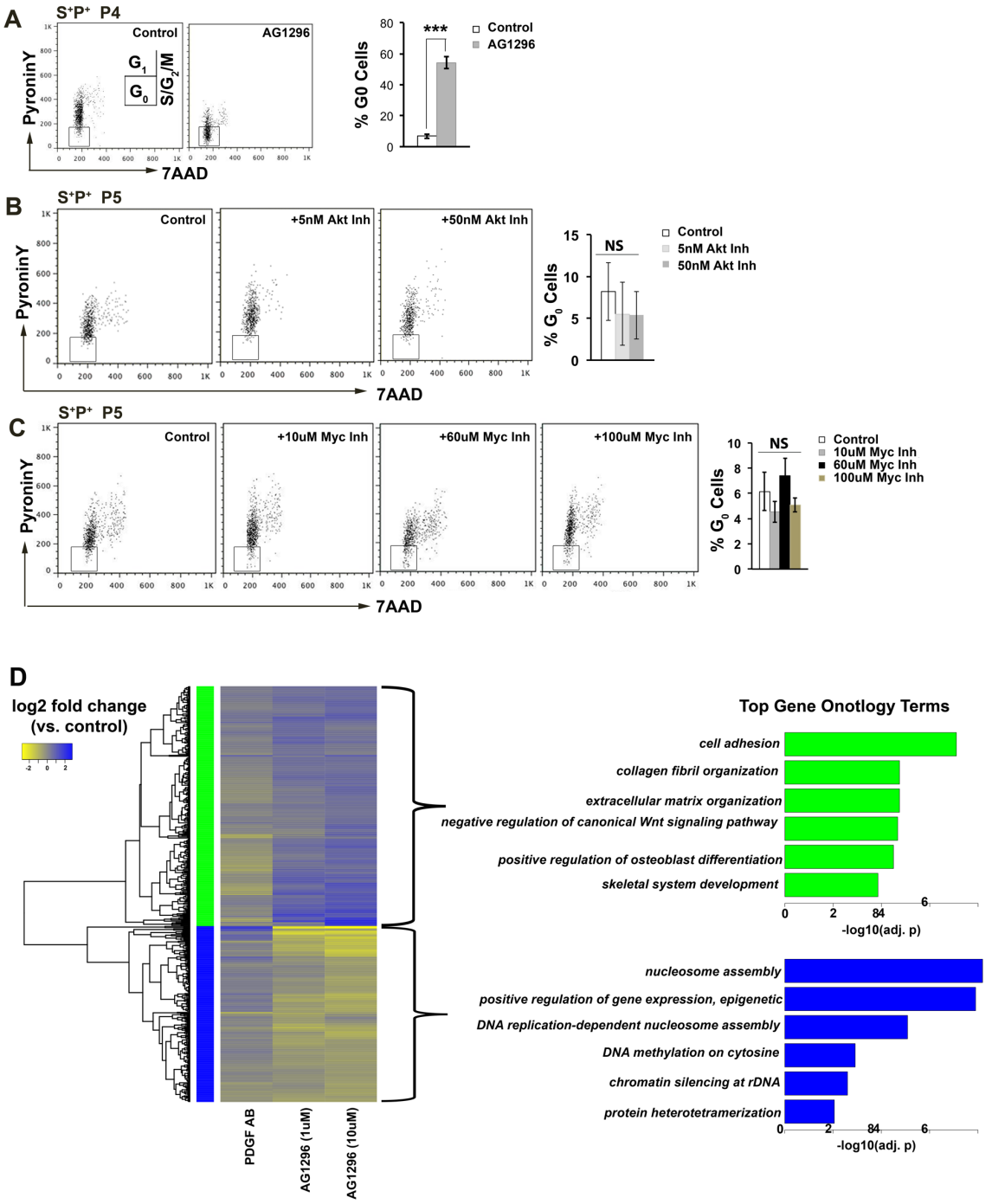

Figure S2: Signaling requirements and transcriptome analysis of cCFU-F cultures

(A) Cell cycle analysis of cCFU-F cultures treated with vehicle (control) or PDGFRα inhibitor AG1296 over passage (P) 4 (see Fig. 2E,F). Graph shows percent cells in G_0 (boxed in cell cycle analysis). (B,C) Cell cycle analysis and graph of percent cells

in G_0 of cCFU-F cultures treated across P5 with 5nM and 50nM AKT inhibitor (LY294002) or 10μM, 60μM, and 100μM MYC inhibitor 10058-F4, respectively, compared to vehicle (control). (D) Heatmap of differentially expressed genes (log2 ratio) between AG1296 (1μM), AG1296 (10μM), or PDGF-AB-treated cells versus untreated controls (adjusted p value <0.05); and top gene ontology terms for biological processes (benjamini adjusted p values) of the two clusters (green and blue bars beside heatmap (see Fig. 2G). *** p<0.001. NS: non-significant.

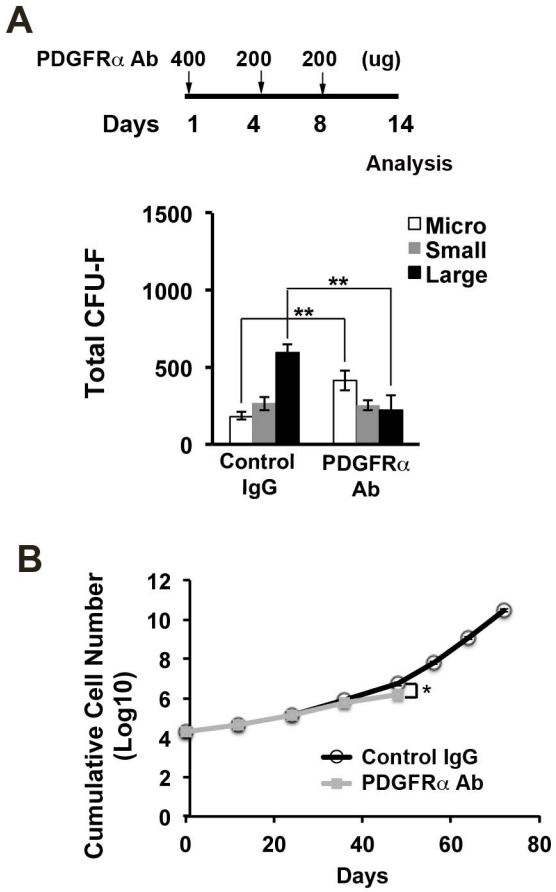

FigureS3

Figure S3: Inhibition of PDGFRα *in vivo* using blocking anti-PDGFRα antibody

(A) Treatment regime applicable to both control IgG or blocking PDGFRα (APA5) antibody, and graph of colony formation (cCFU-F) analysis at day 14. (B) Long-term growth of cCFU-F cultures from control IgG and APA5-treated animals initiated at day 14. * $p<0.05$; ** $p<0.01$.

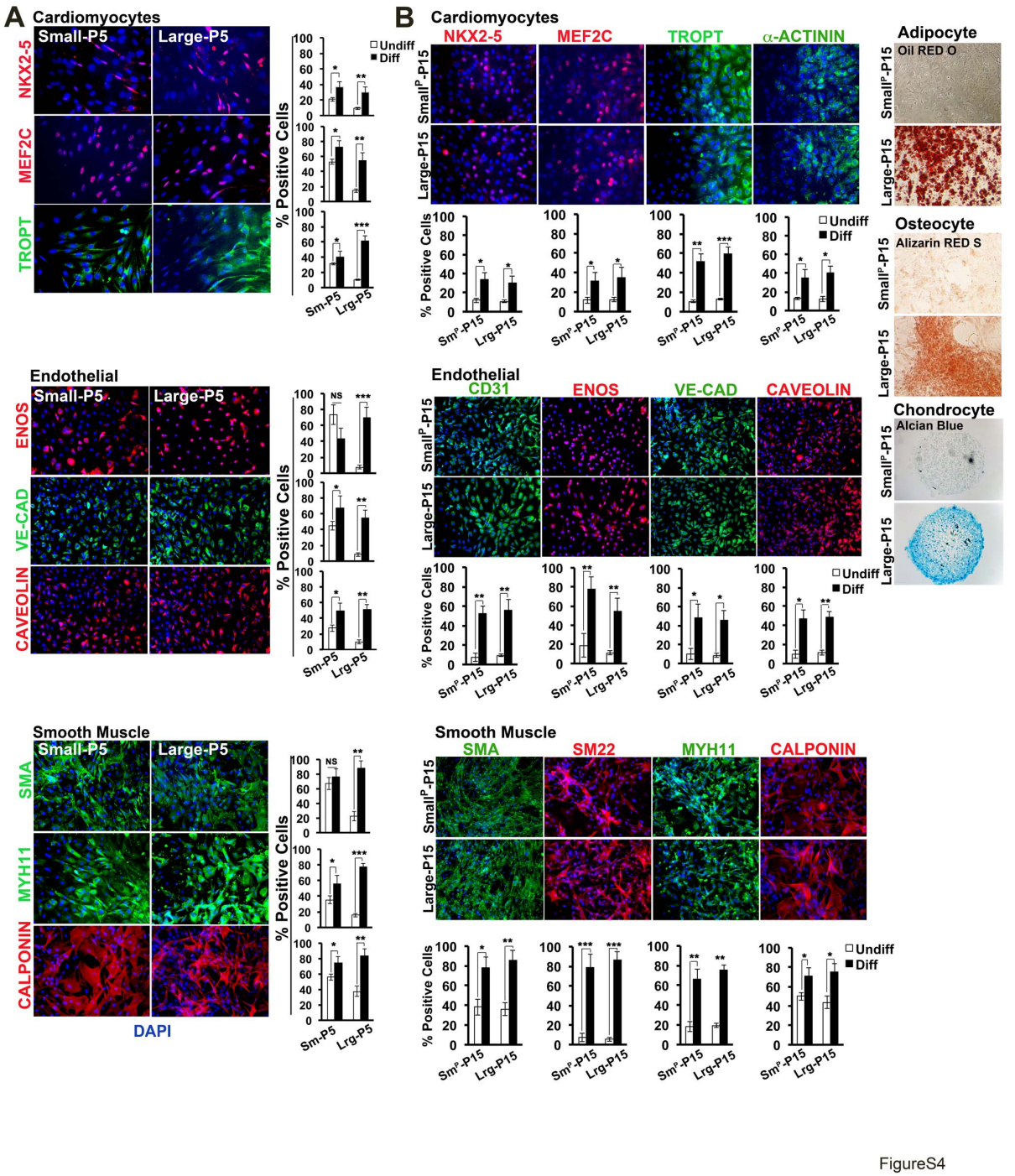

Figure S4: *In vitro* differentiation analysis of cCFU-F cultures from cloned small and large colonies

(A) Immunofluorescence micrographs showing expression of indicated lineage markers in cultures of cloned small and large colonies differentiated *in vitro* into cardiomyocytes, endothelial cells and smooth muscle cells at passage (P) 5. Graphs

indicate percent marker-positive cells in differentiated compared to undifferentiated cultures. See also Figure 4E. (B) Micrographs showing immunofluorescence or histochemical staining of indicated lineage markers after *in vitro* differentiation of cloned small and large colonies into cardiomyocytes, endothelial cells, smooth muscle cells, adipocytes, osteocytes and chondrocytes, at P15 (see Fig. 4G). Graphs show percent marker expression in differentiated compared to undifferentiated cultures. Cloned small colonies were cultured in PDGF-AB until P4 before further passage without PDGF until P15 ($Small^{P}$-P15; Sm^{P}-P15). Large colonies were cultured without PDGF-AB until P15 (Large-P15/Lrg-P15). In all immunofluorescence micrographs, DAPI staining highlights cell nuclei. TROPT: TROPONIN T; VE-CAD: VE-CADHERIN; CAVEOLIN: CAVEOLIN 3; SMA; SMOOTH MUSCLE ACTIN. All comparisons: * $p<0.05$; ** $p<0.01$; *** $p<0.001$. NS: non-significant.

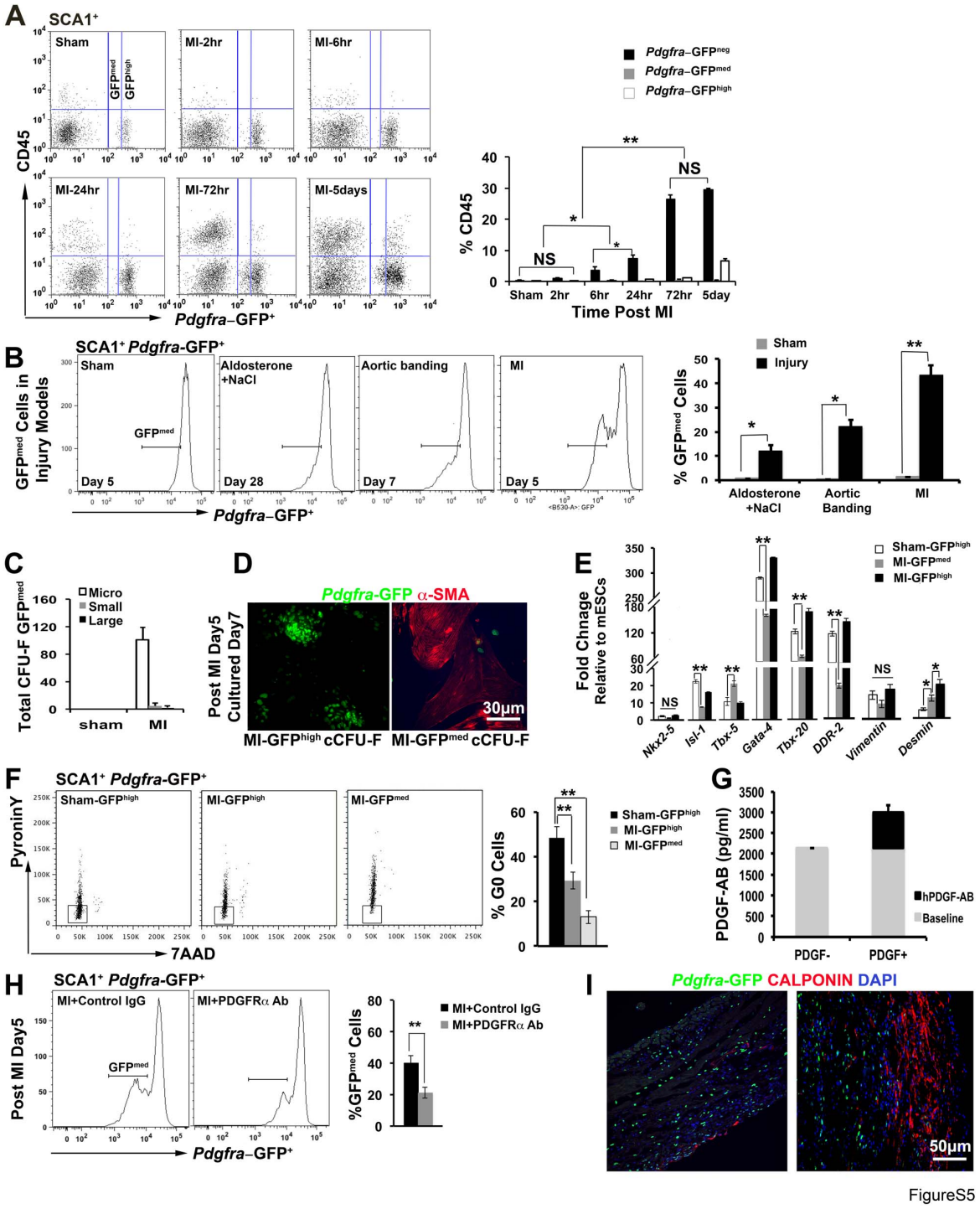

Figure S5: Characterization of the *Pdgfra*-GFP^{medium} myofibroblast population

(A) Flow cytometric analysis of CD45 and GFP expression in freshly isolated SCA1^{+} cardiac interstitial cells from *Pdgfra*$^{GFP/+}$ mice with time after induction of myocardial infarction (MI), compared to cells from sham-operated mice. Graph indicates percent CD45^{+} cells in GFP^{negative}, GFP^{medium} and GFP^{high} cardiac interstitial populations. (B)

Flow cytometric analysis plots showing only the SCA1^{+}*Pdgfra*-GFP^{+} cell population of cardiac interstitial cells from *Pdgfra*$^{GFP/+}$ mice subjected to sham operation or MI, aldosterone/high salt treatment and aortic banding to induce cardiac fibrosis, highlighting GFP^{medium} sub-population (bar) (see Fig. 5G). (C) cCFU-F analysis of GFP^{medium} population from sham-operated and MI mice as defined in panel B. (D) Micrographs showing GFP fluorescence and α-SMOOTH MUSCLE ACTIN (α-SMA) immunofluorescence staining in 2 day cCFU-F cultures of flow-purified GFP^{medium} and GFP^{high} cells from *Pdgfra*$^{GFP/+}$ mice subject to MI (cells harvested at day 5 post-MI). (E) Quantitative RT-PCR analysis of indicated cardiac transcription factor and fibroblast markers in flow-purified GFP^{medium} and GFP^{high} cells from *Pdgfra*$^{GFP/+}$ mice subject to sham operation or MI. Fold change is relative to expression in undifferentiated mouse embryonic stem cells (mESCs). (F) Cell cycle analysis of SCA1^{+}*Pdgfra*-GFP^{+} cells (flow-purified GFP^{high} and GFP^{medium} fractions) from *Pdgfra*$^{GFP/+}$ mice subject to sham operation or MI. Graph indicates percent G_0 cells (boxed in cell cycle analysis). (G) Graph of levels of mouse (baseline) and human (h) PDGF-AB detected in mice untreated and treated with exogenous human recombinant PDGF-AB, analyzed by ELISA. (H) Flow cytometric analysis of SCA1^{+}*Pdgfra*-GFP^{+} cardiac interstitial cells at day 5 post-MI after treatment with control IgG antibody or blocking PDGFRα antibody (Ab), highlighting the GFP^{medium} population (bar). Graph indicates percent GFP^{medium} cells. (I) Micrographs showing GFP fluorescence and CALPONIN immunofluorescence in the infarct zone of *Pdgfra*$^{GFP/+}$ mice subject to MI. DAPI staining indicated nuclei. All comparisons: * $p<0.05$; ** $p<0.01$; NS: non-significant.

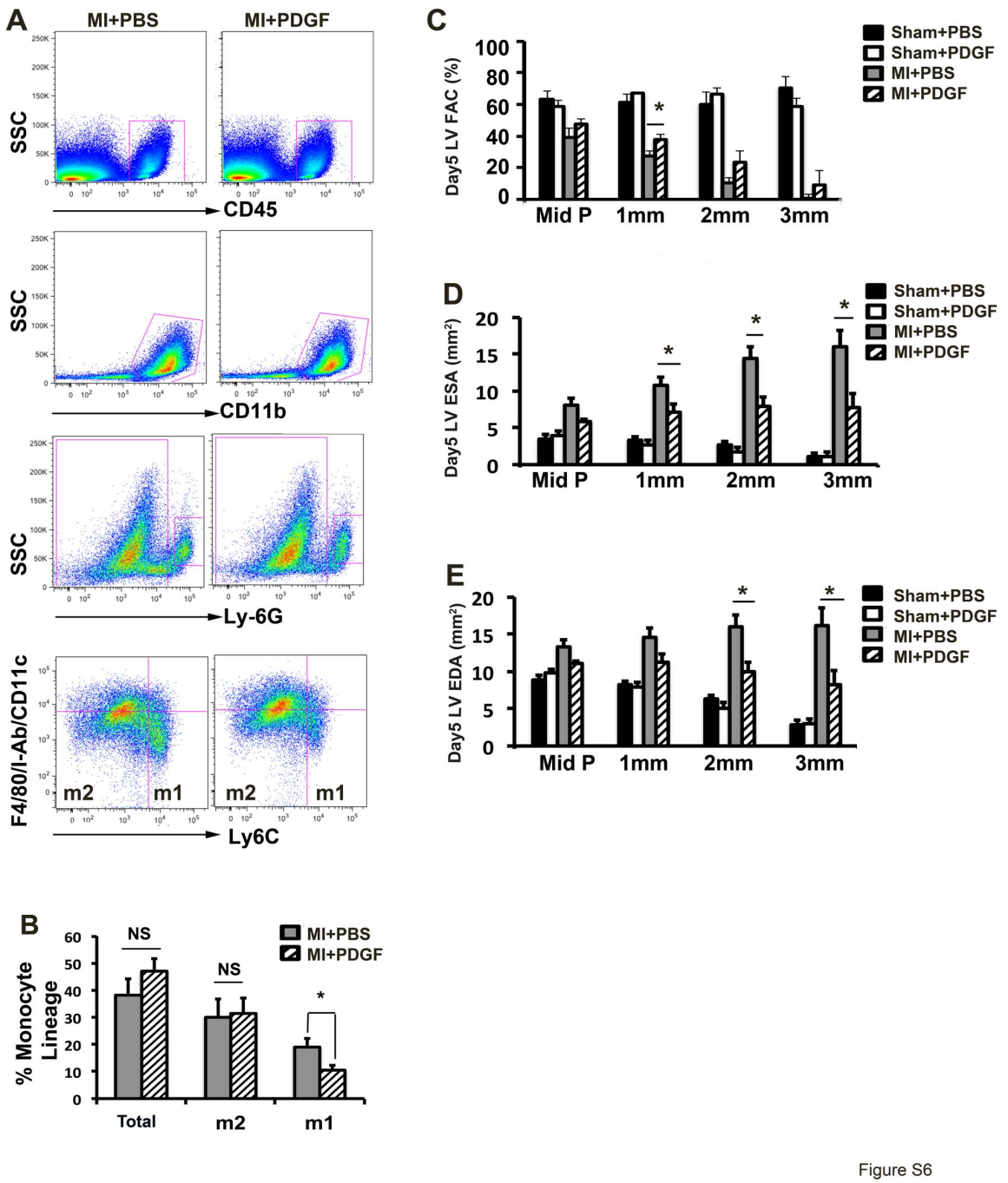

Figure S6: Flow cytometry and functional analysis of PDGF-AB-treated hearts

(A) Flow cytometric analysis strategy using side scatter (SSC) and indicated antibodies applied to total interstitial cells from MI+PBS control and MI+PDGF-AB hearts used to define m1 and m2 monocyte fractions. (B) Quantification of total monocyte lineage population and specifically m1 and m2 monocytes from MI+PBS control and MI+PDGF-AB hearts (see Fig. 6G). (C-E) Quantification of functional

parameters in MI+PDGF-AB hearts at day 5 post-surgery, compared to MI+PBS, sham+PBS and sham+PDGF-AB controls – fractional area change (FAC), left ventricular end systolic area (LV ESA), and left ventricular end diastolic area (LV EDA), respectively, at different echocardiographic planes (1-3mm below papillary level), as shown in Fig. 6I-L. All comparisons: * p<0.05; NS: non-significant.

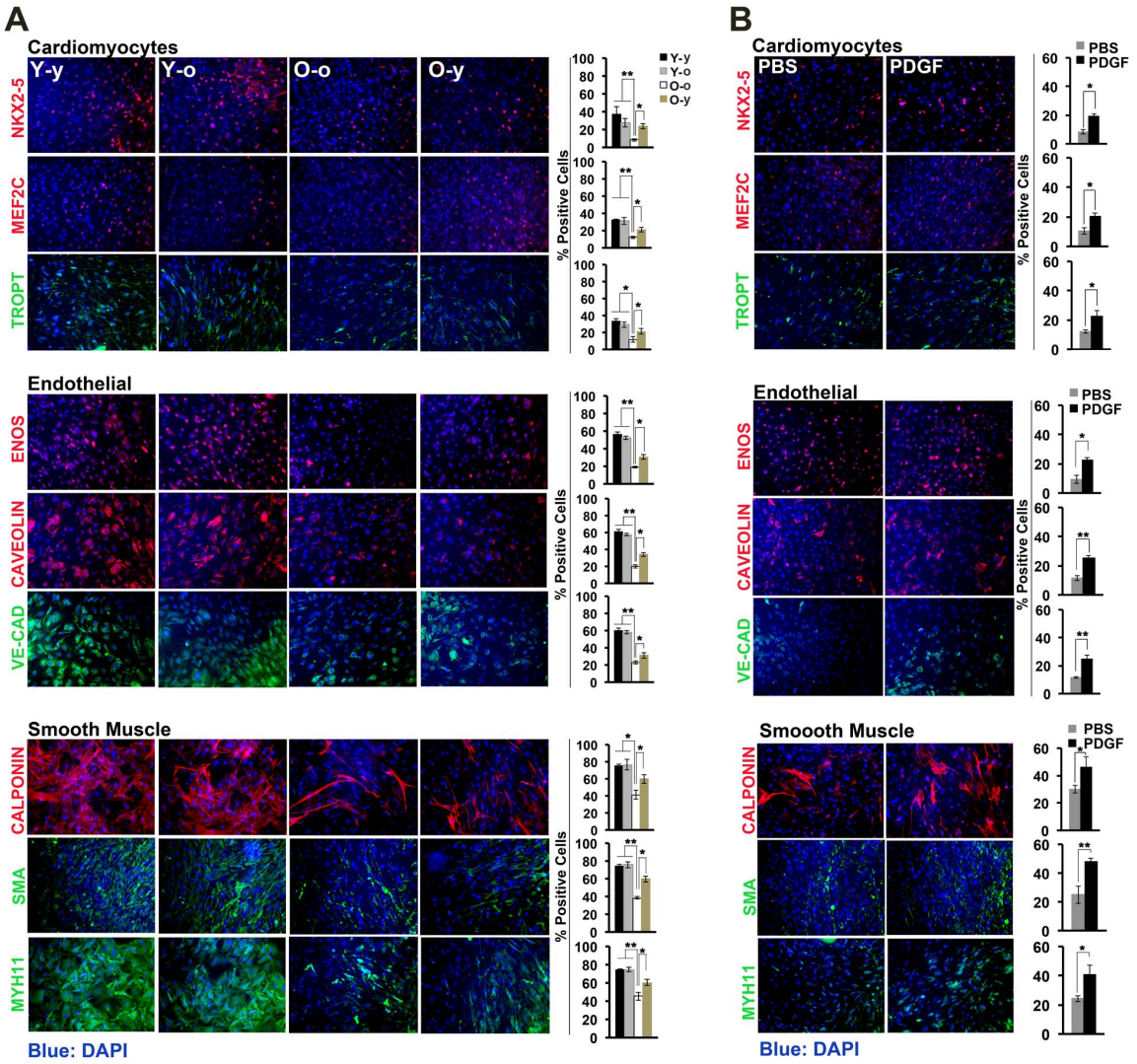

FigureS7

Figure S7: Analysis of differentiation potential in cCFU-F cultures from aged mice

(A) Immunofluorescence analysis using antibodies against indicated cardiomyocyte, endothelial cell and smooth muscle lineage markers in differentiation assays of cultures of cCFU-F at P0 from heterochronic parabiotic mice. Nuclei labelled with DAPI. Graphs show quantification of marker-positive cells. (B) Like analysis of differentiation assays of cultures of cCFU-F at P0 from aged mice treated for 5 days via mini-osmotic pump with PDGF-AB or PBS. CAVEOLIN: CAVEOLIN 3; SMA: smooth muscle actin; TROPT: Cardiac TROPONIN T; VE-CAD: VE-CADHERIN. All comparisons: * $p<0.05$; ** $p<0.01$.

Table 1 Biological process GO Terms

Term	Genes	Benjamini	GeneID	NA10_ratio	NA1_ratio	NAAB_ratio	cluster
GO:0006334~nucleosome assembly	HIST1H4N, HIST1H4M, HIST1H2BB, HIST1H1D, HIST1H4K, HIST2H3C2, HIST2H3C1, HIST2H4, HIST2H2BB, HIST1H2BN, HIST1H2BK, HIST1H4A, HIST2H2BE, HIST1H4D	7.85E-08	HIST1H4N	-0.621169979	-0.188708644	0.159653836	1
GO:0006334~nucleosome assembly	HIST1H4N, HIST1H4M, HIST1H2BB, HIST1H1D, HIST1H4K, HIST2H3C2, HIST2H3C1, HIST2H4, HIST2H2BB, HIST1H2BN, HIST1H2BK, HIST1H4A, HIST2H2BE, HIST1H4D	7.85E-08	HIST1H4M	-0.565809662	-0.194100272	0.137729182	1
GO:0006334~nu	HIST1H4N,	7.85E-	HIST1	-	-	0.0773	1

cleosome assembly	HIST1H4M, HIST1H2BB, HIST1H1D, HIST1H4K, HIST2H3C2, HIST2H3C1, HIST2H4, HIST2H2BB, HIST1H2BN, HIST1H2BK, HIST1H4A, HIST2H2BE, HIST1H4D	08	H2BB	0.644359525	0.283103368	19952	
GO:0006334~nucleosome assembly	HIST1H4N, HIST1H4M, HIST1H2BB, HIST1H1D, HIST1H4K, HIST2H3C2, HIST2H3C1, HIST2H4, HIST2H2BB, HIST1H2BN, HIST1H2BK, HIST1H4A, HIST2H2BE, HIST1H4D	7.85E-08	HIST1H1D	-0.797623968	-0.770888956	-0.416405143	1
GO:0006334~nucleosome assembly	HIST1H4N, HIST1H4M, HIST1H2BB, HIST1H1D, HIST1H4K, HIST2H3C2, HIST2H3C1, HIST2H4, HIST2H2BB, HIST1H2BN, HIST1H2BK, HIST1H4A, HIST2H2BE, HIST1H4D	7.85E-08	HIST1H4K	-0.613928276	-0.170731403	0.166247266	1
GO:0006334~nucleosome assembly	HIST1H4N, HIST1H4M, HIST1H2BB, HIST1H1D, HIST1H4K, HIST2H3C2, HIST2H3C1, HIST2H4, HIST2H2BB, HIST1H2BN, HIST1H2BK, HIST1H4A, HIST2H2BE, HIST1H4D	7.85E-08	HIST2H3C2	-0.46085736	-0.104496009	0.150091546	1

GO:0006334~nucleosome assembly	HIST1H4N, HIST1H4M, HIST1H2BB, HIST1H1D, HIST1H4K, HIST2H3C2, HIST2H3C1, HIST2H4, HIST2H2BB, HIST1H2BN, HIST1H2BK, HIST1H4A, HIST2H2BE, HIST1H4D	7.85E-08	HIST2H3C1	-0.448130003	-0.10990776	0.133832752	1
GO:0006334~nucleosome assembly	HIST1H4N, HIST1H4M, HIST1H2BB, HIST1H1D, HIST1H4K, HIST2H3C2, HIST2H3C1, HIST2H4, HIST2H2BB, HIST1H2BN, HIST1H2BK, HIST1H4A, HIST2H2BE, HIST1H4D	7.85E-08	HIST2H4	-0.425142597	-0.143745074	0.129408846	1
GO:0006334~nucleosome assembly	HIST1H4N, HIST1H4M, HIST1H2BB, HIST1H1D, HIST1H4K, HIST2H3C2, HIST2H3C1, HIST2H4, HIST2H2BB, HIST1H2BN, HIST1H2BK, HIST1H4A, HIST2H2BE, HIST1H4D	7.85E-08	HIST2H2BB	-0.699687867	-0.233237906	0.205675198	1
GO:0006334~nucleosome assembly	HIST1H4N, HIST1H4M, HIST1H2BB, HIST1H1D, HIST1H4K, HIST2H3C2, HIST2H3C1, HIST2H4, HIST2H2BB, HIST1H2BN, HIST1H2BK, HIST1H4A, HIST2H2BE,	7.85E-08	HIST1H2BN	-0.645313402	-0.203264947	0.181669073	1

	HIST1H4D						
GO:0006334~nucleosome assembly	HIST1H4N, HIST1H4M, HIST1H2BB, HIST1H1D, HIST1H4K, HIST2H3C2, HIST2H3C1, HIST2H4, HIST2H2BB, HIST1H2BN, HIST1H2BK, HIST1H4A, HIST2H2BE, HIST1H4D	7.85E-08	HIST1H2BK	-0.509820734	-0.204682195	0.133836776	1
GO:0006334~nucleosome assembly	HIST1H4N, HIST1H4M, HIST1H2BB, HIST1H1D, HIST1H4K, HIST2H3C2, HIST2H3C1, HIST2H4, HIST2H2BB, HIST1H2BN, HIST1H2BK, HIST1H4A, HIST2H2BE, HIST1H4D	7.85E-08	HIST1H4A	-0.597593432	-0.183356772	0.159101748	1
GO:0006334~nucleosome assembly	HIST1H4N, HIST1H4M, HIST1H2BB, HIST1H1D, HIST1H4K, HIST2H3C2, HIST2H3C1, HIST2H4, HIST2H2BB, HIST1H2BN, HIST1H2BK, HIST1H4A, HIST2H2BE, HIST1H4D	7.85E-08	HIST2H2BE	-0.526938534	-0.323547959	-0.192197457	1
GO:0006334~nucleosome assembly	HIST1H4N, HIST1H4M, HIST1H2BB, HIST1H1D, HIST1H4K, HIST2H3C2, HIST2H3C1, HIST2H4, HIST2H2BB, HIST1H2BN, HIST1H2BK,	7.85E-08	HIST1H4D	-0.46986279	-0.226814425	-0.067355592	1

	HIST1H4A, HIST2H2BE, HIST1H4D						
GO:0006335~DNA replication-dependent nucleosome assembly	HIST1H4N, HIST1H4M, HIST1H4K, HIST1H4A, HIST2H3C2, HIST2H3C1, HIST1H4D, HIST2H4	1.78E-05	HIST1H4N	-0.621169979	-0.188708644	0.159653836	1
GO:0006335~DNA replication-dependent nucleosome assembly	HIST1H4N, HIST1H4M, HIST1H4K, HIST1H4A, HIST2H3C2, HIST2H3C1, HIST1H4D, HIST2H4	1.78E-05	HIST1H4M	-0.565809662	-0.194100272	0.137729182	1
GO:0006335~DNA replication-dependent nucleosome assembly	HIST1H4N, HIST1H4M, HIST1H4K, HIST1H4A, HIST2H3C2, HIST2H3C1, HIST1H4D, HIST2H4	1.78E-05	HIST1H4K	-0.613928276	-0.170731403	0.166247266	1
GO:0006335~DNA replication-dependent nucleosome assembly	HIST1H4N, HIST1H4M, HIST1H4K, HIST1H4A, HIST2H3C2, HIST2H3C1, HIST1H4D, HIST2H4	1.78E-05	HIST1H4A	-0.597593432	-0.183356772	0.159101748	1
GO:0006335~DNA replication-dependent nucleosome assembly	HIST1H4N, HIST1H4M, HIST1H4K, HIST1H4A, HIST2H3C2, HIST2H3C1, HIST1H4D, HIST2H4	1.78E-05	HIST2H3C2	-0.46085736	-0.104496009	0.150091546	1
GO:0006335~DNA replication-dependent nucleosome assembly	HIST1H4N, HIST1H4M, HIST1H4K, HIST1H4A, HIST2H3C2, HIST2H3C1, HIST1H4D, HIST2H4	1.78E-05	HIST2H3C1	-0.448130003	-0.10990776	0.133832752	1
GO:0006335~DNA replication-dependent nucleosome assembly	HIST1H4N, HIST1H4M, HIST1H4K, HIST1H4A, HIST2H3C2, HIST2H3C1, HIST1H4D, HIST2H4	1.78E-05	HIST1H4D	-0.46986279	-0.226814425	-0.067355592	1
GO:0006335~DNA replication-	HIST1H4N, HIST1H4M,	1.78E-05	HIST2H4	-0.4251	-0.1437	0.129408846	1

dependent nucleosome assembly	HIST1H4K, HIST1H4A, HIST2H3C2, HIST2H3C1, HIST1H4D, HIST2H4			42597	45074		
GO:0045815~positive regulation of gene expression, epigenetic	HIST1H4N, HIST1H4M, HIST1H4K, HIST1H4A, HIST2H3C2, HIST2H3C1, HIST1H4D, HIST2H4	1.78E-05	HIST1H4N	-0.621169979	-0.188708644	0.159653836	1
GO:0045815~positive regulation of gene expression, epigenetic	HIST1H4N, HIST1H4M, HIST1H4K, HIST1H4A, HIST2H3C2, HIST2H3C1, HIST1H4D, HIST2H4	1.78E-05	HIST1H4M	-0.565809662	-0.194100272	0.137729182	1
GO:0045815~positive regulation of gene expression, epigenetic	HIST1H4N, HIST1H4M, HIST1H4K, HIST1H4A, HIST2H3C2, HIST2H3C1, HIST1H4D, HIST2H4	1.78E-05	HIST1H4K	-0.613928276	-0.170731403	0.166247266	1
GO:0045815~positive regulation of gene expression, epigenetic	HIST1H4N, HIST1H4M, HIST1H4K, HIST1H4A, HIST2H3C2, HIST2H3C1, HIST1H4D, HIST2H4	1.78E-05	HIST1H4A	-0.597593432	-0.183356772	0.159101748	1
GO:0045815~positive regulation of gene expression, epigenetic	HIST1H4N, HIST1H4M, HIST1H4K, HIST1H4A, HIST2H3C2, HIST2H3C1, HIST1H4D, HIST2H4	1.78E-05	HIST2H3C2	-0.46085736	-0.104496009	0.150091546	1
GO:0045815~positive regulation of gene expression, epigenetic	HIST1H4N, HIST1H4M, HIST1H4K, HIST1H4A, HIST2H3C2, HIST2H3C1, HIST1H4D, HIST2H4	1.78E-05	HIST2H3C1	-0.448130003	-0.10990776	0.133832752	1
GO:0045815~positive regulation of gene expression, epigenetic	HIST1H4N, HIST1H4M, HIST1H4K, HIST1H4A, HIST2H3C2, HIST2H3C1, HIST1H4D, HIST2H4	1.78E-05	HIST1H4D	-0.46986279	-0.226814425	-0.067355592	1

GO:0045815~positive regulation of gene expression, epigenetic	HIST1H4N, HIST1H4M, HIST1H4K, HIST1H4A, HIST2H3C2, HIST2H3C1, HIST1H4D, HIST2H4	1.78E-05	HIST2H4	-0.425142597	-0.143745074	0.129408846	1
GO:0032776~DNA methylation on cytosine	HIST1H4N, HIST1H4M, HIST1H4K, HIST1H4A, HIST2H3C2, HIST2H3C1, HIST1H4D, HIST2H4	2.13E-05	HIST1H4N	-0.621169979	-0.188708644	0.159653836	1
GO:0032776~DNA methylation on cytosine	HIST1H4N, HIST1H4M, HIST1H4K, HIST1H4A, HIST2H3C2, HIST2H3C1, HIST1H4D, HIST2H4	2.13E-05	HIST1H4M	-0.565809662	-0.194100272	0.137729182	1
GO:0032776~DNA methylation on cytosine	HIST1H4N, HIST1H4M, HIST1H4K, HIST1H4A, HIST2H3C2, HIST2H3C1, HIST1H4D, HIST2H4	2.13E-05	HIST1H4K	-0.613928276	-0.170731403	0.166247266	1
GO:0032776~DNA methylation on cytosine	HIST1H4N, HIST1H4M, HIST1H4K, HIST1H4A, HIST2H3C2, HIST2H3C1, HIST1H4D, HIST2H4	2.13E-05	HIST1H4A	-0.597593432	-0.183356772	0.159101748	1
GO:0032776~DNA methylation on cytosine	HIST1H4N, HIST1H4M, HIST1H4K, HIST1H4A, HIST2H3C2, HIST2H3C1, HIST1H4D, HIST2H4	2.13E-05	HIST2H3C2	-0.46085736	-0.104496009	0.150091546	1
GO:0032776~DNA methylation on cytosine	HIST1H4N, HIST1H4M, HIST1H4K, HIST1H4A, HIST2H3C2, HIST2H3C1, HIST1H4D, HIST2H4	2.13E-05	HIST2H3C1	-0.448130003	-0.10990776	0.133832752	1
GO:0032776~DNA methylation on cytosine	HIST1H4N, HIST1H4M, HIST1H4K, HIST1H4A, HIST2H3C2,	2.13E-05	HIST1H4D	-0.46986279	-0.226814425	-0.067355592	1

	HIST2H3C1, HIST1H4D, HIST2H4						
GO:0032776~DNA methylation on cytosine	HIST1H4N, HIST1H4M, HIST1H4K, HIST1H4A, HIST2H3C2, HIST2H3C1, HIST1H4D, HIST2H4	2.13E-05	HIST2H4	-0.425142597	-0.143745074	0.129408846	1
GO:0000183~chromatin silencing at rDNA	HIST1H4N, HIST1H4M, HIST1H4K, HIST1H4A, TAF1D, HIST2H3C2, HIST2H3C1, HIST1H4D, HIST2H4	3.16E-05	HIST1H4N	-0.621169979	-0.188708644	0.159653836	1
GO:0000183~chromatin silencing at rDNA	HIST1H4N, HIST1H4M, HIST1H4K, HIST1H4A, TAF1D, HIST2H3C2, HIST2H3C1, HIST1H4D, HIST2H4	3.16E-05	HIST1H4M	-0.565809662	-0.194100272	0.137729182	1
GO:0000183~chromatin silencing at rDNA	HIST1H4N, HIST1H4M, HIST1H4K, HIST1H4A, TAF1D, HIST2H3C2, HIST2H3C1, HIST1H4D, HIST2H4	3.16E-05	HIST1H4K	-0.613928276	-0.170731403	0.166247266	1
GO:0000183~chromatin silencing at rDNA	HIST1H4N, HIST1H4M, HIST1H4K, HIST1H4A, TAF1D, HIST2H3C2, HIST2H3C1, HIST1H4D, HIST2H4	3.16E-05	HIST1H4A	-0.597593432	-0.183356772	0.159101748	1
GO:0000183~chromatin silencing at rDNA	HIST1H4N, HIST1H4M, HIST1H4K, HIST1H4A, TAF1D, HIST2H3C2, HIST2H3C1, HIST1H4D, HIST2H4	3.16E-05	TAF1D	-0.215151381	-0.646659596	-0.091162893	1
GO:0000183~chromatin silencing at rDNA	HIST1H4N, HIST1H4M, HIST1H4K, HIST1H4A, TAF1D, HIST2H3C2, HIST2H3C1, HIST1H4D, HIST2H4	3.16E-05	HIST2H3C2	-0.46085736	-0.104496009	0.150091546	1
GO:0000183~chromatin silencing at rDNA	HIST1H4N, HIST1H4M, HIST1H4K,	3.16E-05	HIST2H3C1	-0.448130003	-0.10990776	0.133832752	1

	HIST1H4A, TAF1D, HIST2H3C2, HIST2H3C1, HIST1H4D, HIST2H4						
GO:0000183~chromatin silencing at rDNA	HIST1H4N, HIST1H4M, HIST1H4K, HIST1H4A, TAF1D, HIST2H3C2, HIST2H3C1, HIST1H4D, HIST2H4	3.16E-05	HIST1H4D	-0.46986279	-0.226814425	-0.067355592	1
GO:0000183~chromatin silencing at rDNA	HIST1H4N, HIST1H4M, HIST1H4K, HIST1H4A, TAF1D, HIST2H3C2, HIST2H3C1, HIST1H4D, HIST2H4	3.16E-05	HIST2H4	-0.425142597	-0.143745074	0.129408846	1
GO:0051290~protein heterotetramerization	HIST1H4N, HIST1H4M, HIST1H4K, HIST1H4A, HIST2H3C2, HIST2H3C1, HIST1H4D, HIST2H4	0.000139283	HIST1H4N	-0.621169979	-0.188708644	0.159653836	1
GO:0051290~protein heterotetramerization	HIST1H4N, HIST1H4M, HIST1H4K, HIST1H4A, HIST2H3C2, HIST2H3C1, HIST1H4D, HIST2H4	0.000139283	HIST1H4M	-0.565809662	-0.194100272	0.137729182	1
GO:0051290~protein heterotetramerization	HIST1H4N, HIST1H4M, HIST1H4K, HIST1H4A, HIST2H3C2, HIST2H3C1, HIST1H4D, HIST2H4	0.000139283	HIST1H4K	-0.613928276	-0.170731403	0.166247266	1
GO:0051290~protein heterotetramerization	HIST1H4N, HIST1H4M, HIST1H4K, HIST1H4A, HIST2H3C2, HIST2H3C1, HIST1H4D, HIST2H4	0.000139283	HIST1H4A	-0.597593432	-0.183356772	0.159101748	1
GO:0051290~protein heterotetramerization	HIST1H4N, HIST1H4M, HIST1H4K, HIST1H4A, HIST2H3C2, HIST2H3C1, HIST1H4D, HIST2H4	0.000139283	HIST2H3C2	-0.46085736	-0.104496009	0.150091546	1
GO:0051290~pr	HIST1H4N,	0.0001	HIST2	-	-	0.1338	1

otein heterotetramerization	HIST1H4M, HIST1H4K, HIST1H4A, HIST2H3C2, HIST2H3C1, HIST1H4D, HIST2H4	39283	H3C1	0.448130003	0.10990776	32752	
GO:0051290~protein heterotetramerization	HIST1H4N, HIST1H4M, HIST1H4K, HIST1H4A, HIST2H3C2, HIST2H3C1, HIST1H4D, HIST2H4	0.000139283	HIST1H4D	-0.46986279	-0.226814425	-0.067355592	1
GO:0051290~protein heterotetramerization	HIST1H4N, HIST1H4M, HIST1H4K, HIST1H4A, HIST2H3C2, HIST2H3C1, HIST1H4D, HIST2H4	0.000139283	HIST2H4	-0.425142597	-0.143745074	0.129408846	1
GO:0045653~negative regulation of megakaryocyte differentiation	HIST1H4N, HIST1H4M, HIST1H4K, HIST1H4A, HIST1H4D, HIST2H4	0.00014384	HIST1H4N	-0.621169979	-0.188708644	0.159653836	1
GO:0045653~negative regulation of megakaryocyte differentiation	HIST1H4N, HIST1H4M, HIST1H4K, HIST1H4A, HIST1H4D, HIST2H4	0.00014384	HIST1H4M	-0.565809662	-0.194100272	0.137729182	1
GO:0045653~negative regulation of megakaryocyte differentiation	HIST1H4N, HIST1H4M, HIST1H4K, HIST1H4A, HIST1H4D, HIST2H4	0.00014384	HIST1H4K	-0.613928276	-0.170731403	0.166247266	1
GO:0045653~negative regulation of megakaryocyte differentiation	HIST1H4N, HIST1H4M, HIST1H4K, HIST1H4A, HIST1H4D, HIST2H4	0.00014384	HIST1H4A	-0.597593432	-0.183356772	0.159101748	1
GO:0045653~negative regulation of megakaryocyte differentiation	HIST1H4N, HIST1H4M, HIST1H4K, HIST1H4A, HIST1H4D, HIST2H4	0.00014384	HIST1H4D	-0.46986279	-0.226814425	-0.067355592	1
GO:0045653~negative regulation of megakaryocyte differentiation	HIST1H4N, HIST1H4M, HIST1H4K, HIST1H4A, HIST1H4D, HIST2H4	0.00014384	HIST2H4	-0.425142597	-0.143745074	0.129408846	1
GO:0001525~angiogenesis	PTPRB, NRP2, CYP1B1, PTGS2, EFNB2, ESM1, MCAM, EREG,	0.000260287	PTPRB	-1.272295565	-0.682530654	0.079615522	1

	HMOX1, SEMA3E, ECSCR, FGF2, TNFAIP2, PLAU						
GO:0001525~angiogenesis	PTPRB, NRP2, CYP1B1, PTGS2, EFNB2, ESM1, MCAM, EREG, HMOX1, SEMA3E, ECSCR, FGF2, TNFAIP2, PLAU	0.000260287	NRP2	-0.519742916	-0.247671189	0.177469955	1
GO:0001525~angiogenesis	PTPRB, NRP2, CYP1B1, PTGS2, EFNB2, ESM1, MCAM, EREG, HMOX1, SEMA3E, ECSCR, FGF2, TNFAIP2, PLAU	0.000260287	CYP1B1	-1.010712986	-0.507932985	0.214850664	1
GO:0001525~angiogenesis	PTPRB, NRP2, CYP1B1, PTGS2, EFNB2, ESM1, MCAM, EREG, HMOX1, SEMA3E, ECSCR, FGF2, TNFAIP2, PLAU	0.000260287	PTGS2	-1.484870085	-1.695190956	0.286626058	1
GO:0001525~angiogenesis	PTPRB, NRP2, CYP1B1, PTGS2, EFNB2, ESM1, MCAM, EREG, HMOX1, SEMA3E, ECSCR, FGF2, TNFAIP2, PLAU	0.000260287	EFNB2	-0.493942633	-0.527684043	0.158722493	1
GO:0001525~angiogenesis	PTPRB, NRP2, CYP1B1, PTGS2, EFNB2, ESM1, MCAM, EREG, HMOX1, SEMA3E, ECSCR, FGF2, TNFAIP2, PLAU	0.000260287	ESM1	-1.676901661	-1.962004842	0.232764535	1
GO:0001525~angiogenesis	PTPRB, NRP2, CYP1B1, PTGS2, EFNB2, ESM1, MCAM, EREG, HMOX1, SEMA3E, ECSCR, FGF2, TNFAIP2, PLAU	0.000260287	MCAM	-1.417441084	-0.587348783	-0.299371592	1
GO:0001525~angiogenesis	PTPRB, NRP2, CYP1B1, PTGS2, EFNB2, ESM1, MCAM, EREG, HMOX1, SEMA3E, ECSCR, FGF2, TNFAIP2, PLAU	0.000260287	EREG	-0.021918492	-0.496740145	-0.086555927	1
GO:0001525~angiogenesis	PTPRB, NRP2, CYP1B1, PTGS2,	0.000260287	HMOX1	-0.3768	-0.9874	-0.0031	1

	EFNB2, ESM1, MCAM, EREG, HMOX1, SEMA3E, ECSCR, FGF2, TNFAIP2, PLAU			62598	11621	74755	
GO:0001525~angiogenesis	PTPRB, NRP2, CYP1B1, PTGS2, EFNB2, ESM1, MCAM, EREG, HMOX1, SEMA3E, ECSCR, FGF2, TNFAIP2, PLAU	0.000260287	SEMA3E	-0.742357249	-0.665614674	-0.167255282	1
GO:0001525~angiogenesis	PTPRB, NRP2, CYP1B1, PTGS2, EFNB2, ESM1, MCAM, EREG, HMOX1, SEMA3E, ECSCR, FGF2, TNFAIP2, PLAU	0.000260287	ECSCR	-0.485332782	-0.215438307	-0.274351718	1
GO:0001525~angiogenesis	PTPRB, NRP2, CYP1B1, PTGS2, EFNB2, ESM1, MCAM, EREG, HMOX1, SEMA3E, ECSCR, FGF2, TNFAIP2, PLAU	0.000260287	FGF2	0.118448677	-0.492964607	0.272034532	1
GO:0001525~angiogenesis	PTPRB, NRP2, CYP1B1, PTGS2, EFNB2, ESM1, MCAM, EREG, HMOX1, SEMA3E, ECSCR, FGF2, TNFAIP2, PLAU	0.000260287	TNFAIP2	-0.881017093	-0.692657286	0.21556035	1
GO:0001525~angiogenesis	PTPRB, NRP2, CYP1B1, PTGS2, EFNB2, ESM1, MCAM, EREG, HMOX1, SEMA3E, ECSCR, FGF2, TNFAIP2, PLAU	0.000260287	PLAU	-1.028169119	-0.534422078	0.207035543	1
GO:0008284~positive regulation of cell proliferation	ADORA2B, PTGS2, LGALS3, CD248, EFNB2, ESM1, HGF, HMGA2, CXCL12, PLAC8, PLA2G4A, CCND1, EREG, CLCF1, PDGFRA, PTN, FGF2, PLAU, NGF, HTR2A	0.000662371	ADORA2B	-0.776534953	-0.553049483	0.262234282	1
GO:0008284~positive regulation of cell proliferation	ADORA2B, PTGS2, LGALS3, CD248, EFNB2, ESM1, HGF, HMGA2, CXCL12, PLAC8, PLA2G4A,	0.000662371	PTGS2	-1.484870085	-1.695190956	0.286626058	1

	CCND1, EREG, CLCF1, PDGFRA, PTN, FGF2, PLAU, NGF, HTR2A						
GO:0008284~positive regulation of cell proliferation	ADORA2B, PTGS2, LGALS3, CD248, EFNB2, ESM1, HGF, HMGA2, CXCL12, PLAC8, PLA2G4A, CCND1, EREG, CLCF1, PDGFRA, PTN, FGF2, PLAU, NGF, HTR2A	0.000662371	LGALS3	-0.69840726	-0.41083659	0.108258074	1
GO:0008284~positive regulation of cell proliferation	ADORA2B, PTGS2, LGALS3, CD248, EFNB2, ESM1, HGF, HMGA2, CXCL12, PLAC8, PLA2G4A, CCND1, EREG, CLCF1, PDGFRA, PTN, FGF2, PLAU, NGF, HTR2A	0.000662371	CD248	-0.631469209	0.028469536	0.333592521	1
GO:0008284~positive regulation of cell proliferation	ADORA2B, PTGS2, LGALS3, CD248, EFNB2, ESM1, HGF, HMGA2, CXCL12, PLAC8, PLA2G4A, CCND1, EREG, CLCF1, PDGFRA, PTN, FGF2, PLAU, NGF, HTR2A	0.000662371	EFNB2	-0.493942633	-0.527684043	0.158722493	1
GO:0008284~positive regulation of cell proliferation	ADORA2B, PTGS2, LGALS3, CD248, EFNB2, ESM1, HGF, HMGA2, CXCL12, PLAC8, PLA2G4A, CCND1, EREG, CLCF1, PDGFRA, PTN, FGF2, PLAU, NGF, HTR2A	0.000662371	ESM1	-1.676901661	-1.962004842	0.232764535	1
GO:0008284~positive regulation of cell proliferation	ADORA2B, PTGS2, LGALS3, CD248, EFNB2, ESM1, HGF, HMGA2, CXCL12, PLAC8, PLA2G4A, CCND1, EREG, CLCF1, PDGFRA, PTN, FGF2, PLAU, NGF, HTR2A	0.000662371	HGF	-0.316537949	-0.409370915	1.200569685	1
GO:0008284~positive regulation of cell proliferation	ADORA2B, PTGS2, LGALS3, CD248, EFNB2, ESM1, HGF, HMGA2, CXCL12, PLAC8, PLA2G4A,	0.000662371	HMGA2	-1.388611605	-0.995973927	0.422206229	1

	CCND1, EREG, CLCF1, PDGFRA, PTN, FGF2, PLAU, NGF, HTR2A						
GO:0008284~positive regulation of cell proliferation	ADORA2B, PTGS2, LGALS3, CD248, EFNB2, ESM1, HGF, HMGA2, CXCL12, PLAC8, PLA2G4A, CCND1, EREG, CLCF1, PDGFRA, PTN, FGF2, PLAU, NGF, HTR2A	0.000662371	CXCL12	-1.096137743	-0.485286992	0.577416667	1
GO:0008284~positive regulation of cell proliferation	ADORA2B, PTGS2, LGALS3, CD248, EFNB2, ESM1, HGF, HMGA2, CXCL12, PLAC8, PLA2G4A, CCND1, EREG, CLCF1, PDGFRA, PTN, FGF2, PLAU, NGF, HTR2A	0.000662371	PLAC8	-1.68715324	-0.811324009	-0.105281737	1
GO:0008284~positive regulation of cell proliferation	ADORA2B, PTGS2, LGALS3, CD248, EFNB2, ESM1, HGF, HMGA2, CXCL12, PLAC8, PLA2G4A, CCND1, EREG, CLCF1, PDGFRA, PTN, FGF2, PLAU, NGF, HTR2A	0.000662371	PLA2G4A	-1.176823388	-1.093747275	0.162418202	1
GO:0008284~positive regulation of cell proliferation	ADORA2B, PTGS2, LGALS3, CD248, EFNB2, ESM1, HGF, HMGA2, CXCL12, PLAC8, PLA2G4A, CCND1, EREG, CLCF1, PDGFRA, PTN, FGF2, PLAU, NGF, HTR2A	0.000662371	CCND1	-0.629935652	-0.102976531	0.210531411	1
GO:0008284~positive regulation of cell proliferation	ADORA2B, PTGS2, LGALS3, CD248, EFNB2, ESM1, HGF, HMGA2, CXCL12, PLAC8, PLA2G4A, CCND1, EREG, CLCF1, PDGFRA, PTN, FGF2, PLAU, NGF, HTR2A	0.000662371	EREG	-0.021918492	-0.496740145	-0.086555927	1
GO:0008284~positive regulation of cell proliferation	ADORA2B, PTGS2, LGALS3, CD248, EFNB2, ESM1, HGF, HMGA2, CXCL12, PLAC8, PLA2G4A,	0.000662371	CLCF1	-0.44127015	-0.24742057	-0.046635788	1

	CCND1, EREG, CLCF1, PDGFRA, PTN, FGF2, PLAU, NGF, HTR2A						
GO:0008284~positive regulation of cell proliferation	ADORA2B, PTGS2, LGALS3, CD248, EFNB2, ESM1, HGF, HMGA2, CXCL12, PLAC8, PLA2G4A, CCND1, EREG, CLCF1, PDGFRA, PTN, FGF2, PLAU, NGF, HTR2A	0.000662371	PDGFRA	-0.907253413	-0.396614293	0.1338055	1
GO:0008284~positive regulation of cell proliferation	ADORA2B, PTGS2, LGALS3, CD248, EFNB2, ESM1, HGF, HMGA2, CXCL12, PLAC8, PLA2G4A, CCND1, EREG, CLCF1, PDGFRA, PTN, FGF2, PLAU, NGF, HTR2A	0.000662371	PTN	-1.07403337	-0.56582526	-0.617159513	1
GO:0008284~positive regulation of cell proliferation	ADORA2B, PTGS2, LGALS3, CD248, EFNB2, ESM1, HGF, HMGA2, CXCL12, PLAC8, PLA2G4A, CCND1, EREG, CLCF1, PDGFRA, PTN, FGF2, PLAU, NGF, HTR2A	0.000662371	FGF2	0.118448677	-0.492964607	0.272034532	1
GO:0008284~positive regulation of cell proliferation	ADORA2B, PTGS2, LGALS3, CD248, EFNB2, ESM1, HGF, HMGA2, CXCL12, PLAC8, PLA2G4A, CCND1, EREG, CLCF1, PDGFRA, PTN, FGF2, PLAU, NGF, HTR2A	0.000662371	PLAU	-1.028169119	-0.534422078	0.207035543	1
GO:0008284~positive regulation of cell proliferation	ADORA2B, PTGS2, LGALS3, CD248, EFNB2, ESM1, HGF, HMGA2, CXCL12, PLAC8, PLA2G4A, CCND1, EREG, CLCF1, PDGFRA, PTN, FGF2, PLAU, NGF, HTR2A	0.000662371	NGF	-0.420443361	-0.352168505	0.059154538	1
GO:0008284~positive regulation of cell proliferation	ADORA2B, PTGS2, LGALS3, CD248, EFNB2, ESM1, HGF, HMGA2, CXCL12, PLAC8, PLA2G4A,	0.000662371	HTR2A	-1.276006418	-0.973220171	0.138210845	1

	CCND1, EREG, CLCF1, PDGFRA, PTN, FGF2, PLAU, NGF, HTR2A						
GO:0006336~DNA replication-independent nucleosome assembly	HIST1H4N, HIST1H4M, HIST1H4K, HIST1H4A, HIST1H4D, HIST2H4	0.000769306	HIST1H4N	-0.621169979	-0.188708644	0.159653836	1
GO:0006336~DNA replication-independent nucleosome assembly	HIST1H4N, HIST1H4M, HIST1H4K, HIST1H4A, HIST1H4D, HIST2H4	0.000769306	HIST1H4M	-0.565809662	-0.194100272	0.137729182	1
GO:0006336~DNA replication-independent nucleosome assembly	HIST1H4N, HIST1H4M, HIST1H4K, HIST1H4A, HIST1H4D, HIST2H4	0.000769306	HIST1H4K	-0.613928276	-0.170731403	0.166247266	1
GO:0006336~DNA replication-independent nucleosome assembly	HIST1H4N, HIST1H4M, HIST1H4K, HIST1H4A, HIST1H4D, HIST2H4	0.000769306	HIST1H4A	-0.597593432	-0.183356772	0.159101748	1
GO:0006336~DNA replication-independent nucleosome assembly	HIST1H4N, HIST1H4M, HIST1H4K, HIST1H4A, HIST1H4D, HIST2H4	0.000769306	HIST1H4D	-0.46986279	-0.226814425	-0.067355592	1
GO:0006336~DNA replication-independent nucleosome assembly	HIST1H4N, HIST1H4M, HIST1H4K, HIST1H4A, HIST1H4D, HIST2H4	0.000769306	HIST2H4	-0.425142597	-0.143745074	0.129408846	1
GO:0006352~DNA-templated transcription, initiation	HIST1H4N, HIST1H4M, HIST1H4K, HIST1H4A, HIST1H4D, HIST2H4	0.005122967	HIST1H4N	-0.621169979	-0.188708644	0.159653836	1
GO:0006352~DNA-templated transcription, initiation	HIST1H4N, HIST1H4M, HIST1H4K, HIST1H4A, HIST1H4D, HIST2H4	0.005122967	HIST1H4M	-0.565809662	-0.194100272	0.137729182	1
GO:0006352~DNA-templated transcription, initiation	HIST1H4N, HIST1H4M, HIST1H4K, HIST1H4A, HIST1H4D, HIST2H4	0.005122967	HIST1H4K	-0.613928276	-0.170731403	0.166247266	1
GO:0006352~DNA-templated transcription, initiation	HIST1H4N, HIST1H4M, HIST1H4K, HIST1H4A, HIST1H4D, HIST2H4	0.005122967	HIST1H4A	-0.597593432	-0.183356772	0.159101748	1

GO:0006352~DNA-templated transcription, initiation	HIST1H4N, HIST1H4M, HIST1H4K, HIST1H4A, HIST1H4D, HIST2H4	0.005122967	HIST1H4D	-0.46986279	-0.226814425	-0.067355592	1
GO:0006352~DNA-templated transcription, initiation	HIST1H4N, HIST1H4M, HIST1H4K, HIST1H4A, HIST1H4D, HIST2H4	0.005122967	HIST2H4	-0.425142597	-0.143745074	0.129408846	1
GO:0042493~response to drug	TXNIP, INHBA, CCND1, PTGS2, HMGCS1, PTN, ENO3, ABCC1, FOSB, AQP1, GCLM, POR, DUSP6, HTR2A	0.005851051	TXNIP	-0.488645629	-0.334661679	-0.072422834	1
GO:0042493~response to drug	TXNIP, INHBA, CCND1, PTGS2, HMGCS1, PTN, ENO3, ABCC1, FOSB, AQP1, GCLM, POR, DUSP6, HTR2A	0.005851051	INHBA	-0.165408956	-0.454744251	-0.060209691	1
GO:0042493~response to drug	TXNIP, INHBA, CCND1, PTGS2, HMGCS1, PTN, ENO3, ABCC1, FOSB, AQP1, GCLM, POR, DUSP6, HTR2A	0.005851051	CCND1	-0.629935652	-0.102976531	0.210531411	1
GO:0042493~response to drug	TXNIP, INHBA, CCND1, PTGS2, HMGCS1, PTN, ENO3, ABCC1, FOSB, AQP1, GCLM, POR, DUSP6, HTR2A	0.005851051	PTGS2	-1.484870085	-1.695190956	0.286626058	1
GO:0042493~response to drug	TXNIP, INHBA, CCND1, PTGS2, HMGCS1, PTN, ENO3, ABCC1, FOSB, AQP1, GCLM, POR, DUSP6, HTR2A	0.005851051	HMGCS1	-0.487611865	0.123735082	-0.081360753	1
GO:0042493~response to drug	TXNIP, INHBA, CCND1, PTGS2, HMGCS1, PTN, ENO3, ABCC1, FOSB, AQP1, GCLM, POR, DUSP6, HTR2A	0.005851051	PTN	-1.07403337	-0.56582526	-0.617159513	1
GO:0042493~response to drug	TXNIP, INHBA, CCND1, PTGS2,	0.005851051	ENO3	-0.8294	-0.4438	0.350274932	1

	HMGCS1, PTN, ENO3, ABCC1, FOSB, AQP1, GCLM, POR, DUSP6, HTR2A			85548	03637		
GO:0042493~response to drug	TXNIP, INHBA, CCND1, PTGS2, HMGCS1, PTN, ENO3, ABCC1, FOSB, AQP1, GCLM, POR, DUSP6, HTR2A	0.005851051	ABCC1	-0.428339319	-0.33270194	0.214136453	1
GO:0042493~response to drug	TXNIP, INHBA, CCND1, PTGS2, HMGCS1, PTN, ENO3, ABCC1, FOSB, AQP1, GCLM, POR, DUSP6, HTR2A	0.005851051	FOSB	-0.72242176	-0.839750518	-0.874927267	1
GO:0042493~response to drug	TXNIP, INHBA, CCND1, PTGS2, HMGCS1, PTN, ENO3, ABCC1, FOSB, AQP1, GCLM, POR, DUSP6, HTR2A	0.005851051	AQP1	-0.707154235	-0.600787565	0.255362055	1
GO:0042493~response to drug	TXNIP, INHBA, CCND1, PTGS2, HMGCS1, PTN, ENO3, ABCC1, FOSB, AQP1, GCLM, POR, DUSP6, HTR2A	0.005851051	GCLM	-0.377203486	-0.51565766	0.022762576	1
GO:0042493~response to drug	TXNIP, INHBA, CCND1, PTGS2, HMGCS1, PTN, ENO3, ABCC1, FOSB, AQP1, GCLM, POR, DUSP6, HTR2A	0.005851051	POR	-0.892932008	-0.465914477	0.361743915	1
GO:0042493~response to drug	TXNIP, INHBA, CCND1, PTGS2, HMGCS1, PTN, ENO3, ABCC1, FOSB, AQP1, GCLM, POR, DUSP6, HTR2A	0.005851051	DUSP6	-0.636288799	-0.782141778	0.023999833	1
GO:0042493~response to drug	TXNIP, INHBA, CCND1, PTGS2, HMGCS1, PTN, ENO3, ABCC1, FOSB, AQP1, GCLM, POR, DUSP6, HTR2A	0.005851051	HTR2A	-1.276006418	-0.973220171	0.138210845	1

GO:0030335~positive regulation of cell migration	C3AR1, ITGA5, SEMA3E, PDGFRA, ABCC1, HGF, AQP1, GPNMB, MCAM, CXCL12, PLAU	0.005962812	C3AR1	-1.22676413	-0.927252235	0.584071632	1
GO:0030335~positive regulation of cell migration	C3AR1, ITGA5, SEMA3E, PDGFRA, ABCC1, HGF, AQP1, GPNMB, MCAM, CXCL12, PLAU	0.005962812	ITGA5	-0.477172253	-0.17622396	0.050794061	1
GO:0030335~positive regulation of cell migration	C3AR1, ITGA5, SEMA3E, PDGFRA, ABCC1, HGF, AQP1, GPNMB, MCAM, CXCL12, PLAU	0.005962812	SEMA3E	-0.742357249	-0.665614674	-0.167255282	1
GO:0030335~positive regulation of cell migration	C3AR1, ITGA5, SEMA3E, PDGFRA, ABCC1, HGF, AQP1, GPNMB, MCAM, CXCL12, PLAU	0.005962812	PDGFRA	-0.907253413	-0.396614293	0.1338055	1
GO:0030335~positive regulation of cell migration	C3AR1, ITGA5, SEMA3E, PDGFRA, ABCC1, HGF, AQP1, GPNMB, MCAM, CXCL12, PLAU	0.005962812	ABCC1	-0.428339319	-0.33270194	0.214136453	1
GO:0030335~positive regulation of cell migration	C3AR1, ITGA5, SEMA3E, PDGFRA, ABCC1, HGF, AQP1, GPNMB, MCAM, CXCL12, PLAU	0.005962812	HGF	-0.316537949	-0.409370915	1.200569685	1
GO:0030335~positive regulation of cell migration	C3AR1, ITGA5, SEMA3E, PDGFRA, ABCC1, HGF, AQP1, GPNMB, MCAM, CXCL12, PLAU	0.005962812	AQP1	-0.707154235	-0.600787565	0.255362055	1
GO:0030335~positive regulation of cell migration	C3AR1, ITGA5, SEMA3E, PDGFRA, ABCC1, HGF, AQP1, GPNMB, MCAM, CXCL12, PLAU	0.005962812	GPNMB	-0.447514067	0.009257219	0.313147954	1
GO:0030335~positive regulation of cell migration	C3AR1, ITGA5, SEMA3E, PDGFRA, ABCC1, HGF, AQP1, GPNMB, MCAM, CXCL12, PLAU	0.005962812	MCAM	-1.417441084	-0.587348783	-0.299371592	1
GO:0030335~positive regulation of cell migration	C3AR1, ITGA5, SEMA3E, PDGFRA, ABCC1, HGF, AQP1, GPNMB, MCAM, CXCL12, PLAU	0.005962812	CXCL12	-1.096137743	-0.485286992	0.577416667	1
GO:0030335~positive regulation of cell migration	C3AR1, ITGA5, SEMA3E, PDGFRA, ABCC1, HGF, AQP1, GPNMB, MCAM,	0.005962812	PLAU	-1.028169119	-0.534422078	0.207035543	1

	CXCL12, PLAU						
GO:0007155~cell adhesion	FLRT2, ATP1B1, CYP1B1, NPNT, EFNB2, NID1, MCAM, TINAGL1, CD24A, CD9, PKP1, CD44, ITGA5, GPNMB, SPON2, PARVB, SPP1	0.005965103	FLRT2	-0.753165786	-0.57372512	-0.133525535	1
GO:0007155~cell adhesion	FLRT2, ATP1B1, CYP1B1, NPNT, EFNB2, NID1, MCAM, TINAGL1, CD24A, CD9, PKP1, CD44, ITGA5, GPNMB, SPON2, PARVB, SPP1	0.005965103	ATP1B1	-0.788716332	-0.460856882	0.140741545	1
GO:0007155~cell adhesion	FLRT2, ATP1B1, CYP1B1, NPNT, EFNB2, NID1, MCAM, TINAGL1, CD24A, CD9, PKP1, CD44, ITGA5, GPNMB, SPON2, PARVB, SPP1	0.005965103	CYP1B1	-1.010712986	-0.507932985	0.214850664	1
GO:0007155~cell adhesion	FLRT2, ATP1B1, CYP1B1, NPNT, EFNB2, NID1, MCAM, TINAGL1, CD24A, CD9, PKP1, CD44, ITGA5, GPNMB, SPON2, PARVB, SPP1	0.005965103	NPNT	-0.447168282	-0.651735773	0.029240619	1
GO:0007155~cell adhesion	FLRT2, ATP1B1, CYP1B1, NPNT, EFNB2, NID1, MCAM, TINAGL1, CD24A, CD9, PKP1, CD44, ITGA5, GPNMB, SPON2, PARVB, SPP1	0.005965103	EFNB2	-0.493942633	-0.527684043	0.158722493	1
GO:0007155~cell adhesion	FLRT2, ATP1B1, CYP1B1, NPNT, EFNB2, NID1, MCAM, TINAGL1, CD24A, CD9, PKP1, CD44, ITGA5, GPNMB, SPON2, PARVB, SPP1	0.005965103	NID1	-0.631400618	-0.23562376	0.21415057	1
GO:0007155~cell adhesion	FLRT2, ATP1B1, CYP1B1, NPNT, EFNB2, NID1, MCAM, TINAGL1, CD24A, CD9, PKP1,	0.005965103	MCAM	-1.417441084	-0.587348783	-0.299371592	1

	CD44, ITGA5, GPNMB, SPON2, PARVB, SPP1						
GO:0007155~cell adhesion	FLRT2, ATP1B1, CYP1B1, NPNT, EFNB2, NID1, MCAM, TINAGL1, CD24A, CD9, PKP1, CD44, ITGA5, GPNMB, SPON2, PARVB, SPP1	0.005965103	TINAGL1	-0.760318625	-0.552416214	0.27400175	1
GO:0007155~cell adhesion	FLRT2, ATP1B1, CYP1B1, NPNT, EFNB2, NID1, MCAM, TINAGL1, CD24A, CD9, PKP1, CD44, ITGA5, GPNMB, SPON2, PARVB, SPP1	0.005965103	CD24A	-2.012644425	-1.569299129	0.446804746	1
GO:0007155~cell adhesion	FLRT2, ATP1B1, CYP1B1, NPNT, EFNB2, NID1, MCAM, TINAGL1, CD24A, CD9, PKP1, CD44, ITGA5, GPNMB, SPON2, PARVB, SPP1	0.005965103	CD9	-0.354138468	0.029541306	-0.1053562	1
GO:0007155~cell adhesion	FLRT2, ATP1B1, CYP1B1, NPNT, EFNB2, NID1, MCAM, TINAGL1, CD24A, CD9, PKP1, CD44, ITGA5, GPNMB, SPON2, PARVB, SPP1	0.005965103	PKP1	-0.55624597	-0.436155459	-0.049553974	1
GO:0007155~cell adhesion	FLRT2, ATP1B1, CYP1B1, NPNT, EFNB2, NID1, MCAM, TINAGL1, CD24A, CD9, PKP1, CD44, ITGA5, GPNMB, SPON2, PARVB, SPP1	0.005965103	CD44	-0.423537378	-0.583789719	-0.019520047	1
GO:0007155~cell adhesion	FLRT2, ATP1B1, CYP1B1, NPNT, EFNB2, NID1, MCAM, TINAGL1, CD24A, CD9, PKP1, CD44, ITGA5, GPNMB, SPON2, PARVB, SPP1	0.005965103	ITGA5	-0.477172253	-0.17622396	0.050794061	1
GO:0007155~cell adhesion	FLRT2, ATP1B1, CYP1B1, NPNT, EFNB2, NID1,	0.005965103	GPNMB	-0.447514067	0.009257219	0.313147954	1

	MCAM, TINAGL1, CD24A, CD9, PKP1, CD44, ITGA5, GPNMB, SPON2, PARVB, SPP1						
GO:0007155~cell adhesion	FLRT2, ATP1B1, CYP1B1, NPNT, EFNB2, NID1, MCAM, TINAGL1, CD24A, CD9, PKP1, CD44, ITGA5, GPNMB, SPON2, PARVB, SPP1	0.005965103	SPON2	-0.776785837	-0.829808688	0.416122816	1
GO:0007155~cell adhesion	FLRT2, ATP1B1, CYP1B1, NPNT, EFNB2, NID1, MCAM, TINAGL1, CD24A, CD9, PKP1, CD44, ITGA5, GPNMB, SPON2, PARVB, SPP1	0.005965103	PARVB	-0.697241124	-0.627770276	0.317466879	1
GO:0007155~cell adhesion	FLRT2, ATP1B1, CYP1B1, NPNT, EFNB2, NID1, MCAM, TINAGL1, CD24A, CD9, PKP1, CD44, ITGA5, GPNMB, SPON2, PARVB, SPP1	0.005965103	SPP1	-0.868611397	-0.831046522	1.004219144	1
GO:0010811~positive regulation of cell-substrate adhesion	ITGA5, NPNT, PTN, NID1, VIT, SPP1	0.006841217	ITGA5	-0.477172253	-0.17622396	0.050794061	1
GO:0010811~positive regulation of cell-substrate adhesion	ITGA5, NPNT, PTN, NID1, VIT, SPP1	0.006841217	NPNT	-0.447168282	-0.651735773	0.029240619	1
GO:0010811~positive regulation of cell-substrate adhesion	ITGA5, NPNT, PTN, NID1, VIT, SPP1	0.006841217	PTN	-1.07403337	-0.56582526	-0.617159513	1
GO:0010811~positive regulation of cell-substrate adhesion	ITGA5, NPNT, PTN, NID1, VIT, SPP1	0.006841217	NID1	-0.631400618	-0.23562376	0.21415057	1
GO:0010811~positive regulation of cell-substrate adhesion	ITGA5, NPNT, PTN, NID1, VIT, SPP1	0.006841217	VIT	-0.620399314	-0.471265041	-0.283586966	1
GO:0010811~positive regulation of cell-substrate adhesion	ITGA5, NPNT, PTN, NID1, VIT, SPP1	0.006841217	SPP1	-0.868611397	-0.831046522	1.004219144	1
GO:0045766~po	C3AR1, CYP1B1,	0.0241	C3AR	-	-	0.5840	1

sitive regulation of angiogenesis	LGALS3, HMOX1, HGF, AQP1, FGF2, VASH2	3581	1	1.2267 6413	0.9272 52235	71632	
GO:0045766~positive regulation of angiogenesis	C3AR1, CYP1B1, LGALS3, HMOX1, HGF, AQP1, FGF2, VASH2	0.0241 3581	CYP1 B1	-1.0107 12986	-0.5079 32985	0.2148 50664	1
GO:0045766~positive regulation of angiogenesis	C3AR1, CYP1B1, LGALS3, HMOX1, HGF, AQP1, FGF2, VASH2	0.0241 3581	LGAL S3	-0.6984 0726	-0.4108 3659	0.1082 58074	1
GO:0045766~positive regulation of angiogenesis	C3AR1, CYP1B1, LGALS3, HMOX1, HGF, AQP1, FGF2, VASH2	0.0241 3581	HMO X1	-0.3768 62598	-0.9874 11621	-0.0031 74755	1
GO:0045766~positive regulation of angiogenesis	C3AR1, CYP1B1, LGALS3, HMOX1, HGF, AQP1, FGF2, VASH2	0.0241 3581	HGF	-0.3165 37949	-0.4093 70915	1.2005 69685	1
GO:0045766~positive regulation of angiogenesis	C3AR1, CYP1B1, LGALS3, HMOX1, HGF, AQP1, FGF2, VASH2	0.0241 3581	AQP1	-0.7071 54235	-0.6007 87565	0.2553 62055	1
GO:0045766~positive regulation of angiogenesis	C3AR1, CYP1B1, LGALS3, HMOX1, HGF, AQP1, FGF2, VASH2	0.0241 3581	FGF2	0.1184 48677	-0.4929 64607	0.2720 34532	1
GO:0045766~positive regulation of angiogenesis	C3AR1, CYP1B1, LGALS3, HMOX1, HGF, AQP1, FGF2, VASH2	0.0241 3581	VASH 2	-0.9565 39427	-0.3966 09385	0.1046 61842	1
GO:0071372~cellular response to follicle-stimulating hormone stimulus	INHBA, HMGCS1, GCLM, POR	0.0305 19758	INHB A	-0.1654 08956	-0.4547 44251	-0.0602 09691	1
GO:0071372~cellular response to follicle-stimulating hormone stimulus	INHBA, HMGCS1, GCLM, POR	0.0305 19758	HMG CS1	-0.4876 11865	-0.1237 35082	-0.0813 60753	1
GO:0071372~cellular response to follicle-stimulating hormone stimulus	INHBA, HMGCS1, GCLM, POR	0.0305 19758	GCLM	-0.3772 03486	-0.5156 5766	0.0227 62576	1
GO:0071372~cellular response to follicle-stimulating hormone	INHBA, HMGCS1, GCLM, POR	0.0305 19758	POR	-0.8929 32008	-0.4659 14477	0.3617 43915	1

stimulus							
GO:0006979~response to oxidative stress	TXNIP, PTGS2, HMOX1, PTGS1, ABCC1, NQO1, GCLM, SRXN1	0.037548259	TXNIP	-0.488645629	-0.334661679	-0.072422834	1
GO:0006979~response to oxidative stress	TXNIP, PTGS2, HMOX1, PTGS1, ABCC1, NQO1, GCLM, SRXN1	0.037548259	PTGS2	-1.484870085	-1.695190956	0.286626058	1
GO:0006979~response to oxidative stress	TXNIP, PTGS2, HMOX1, PTGS1, ABCC1, NQO1, GCLM, SRXN1	0.037548259	HMOX1	-0.376862598	-0.987411621	-0.003174755	1
GO:0006979~response to oxidative stress	TXNIP, PTGS2, HMOX1, PTGS1, ABCC1, NQO1, GCLM, SRXN1	0.037548259	PTGS1	-0.662327693	-0.584740789	1.227936765	1
GO:0006979~response to oxidative stress	TXNIP, PTGS2, HMOX1, PTGS1, ABCC1, NQO1, GCLM, SRXN1	0.037548259	ABCC1	-0.428339319	-0.33270194	0.214136453	1
GO:0006979~response to oxidative stress	TXNIP, PTGS2, HMOX1, PTGS1, ABCC1, NQO1, GCLM, SRXN1	0.037548259	NQO1	-1.812058834	-1.769603856	0.426996977	1
GO:0006979~response to oxidative stress	TXNIP, PTGS2, HMOX1, PTGS1, ABCC1, NQO1, GCLM, SRXN1	0.037548259	GCLM	-0.377203486	-0.51565766	0.022762576	1
GO:0006979~response to oxidative stress	TXNIP, PTGS2, HMOX1, PTGS1, ABCC1, NQO1, GCLM, SRXN1	0.037548259	SRXN1	-0.3788882	-0.469575103	0.077091539	1
GO:0050731~positive regulation of peptidyl-tyrosine phosphorylation	CD44, ITGA5, PDGFRA, RIPK2, HGF, CD24A, HTR2A	0.047425342	CD44	-0.423537378	-0.583789719	-0.019520047	1
GO:0050731~positive regulation of peptidyl-tyrosine phosphorylation	CD44, ITGA5, PDGFRA, RIPK2, HGF, CD24A, HTR2A	0.047425342	ITGA5	-0.477172253	-0.17622396	0.050794061	1
GO:0050731~positive regulation of peptidyl-tyrosine phosphorylation	CD44, ITGA5, PDGFRA, RIPK2, HGF, CD24A, HTR2A	0.047425342	PDGFRA	-0.907253413	-0.396614293	0.1338055	1
GO:0050731~positive regulation of peptidyl-tyrosine phosphorylation	CD44, ITGA5, PDGFRA, RIPK2, HGF, CD24A, HTR2A	0.047425342	RIPK2	-0.557494782	-0.259886853	0.170159608	1
GO:0050731~po	CD44, ITGA5,	0.0474	HGF	-	-	1.2005	1

sitive regulation of peptidyl-tyrosine phosphorylation	PDGFRA, RIPK2, HGF, CD24A, HTR2A	25342		0.316537949	0.409370915	69685	
GO:0050731~positive regulation of peptidyl-tyrosine phosphorylation	CD44, ITGA5, PDGFRA, RIPK2, HGF, CD24A, HTR2A	0.047425342	CD24A	-2.012644425	-1.569299129	0.446804746	1
GO:0050731~positive regulation of peptidyl-tyrosine phosphorylation	CD44, ITGA5, PDGFRA, RIPK2, HGF, CD24A, HTR2A	0.047425342	HTR2A	-1.276006418	-0.973220171	0.138210845	1
GO:0071456~cellular response to hypoxia	SLC29A1, CLCA1, PTGS2, HMOX1, PTN, AQP1, KCNMB1	0.049772276	SLC29A1	-0.44954782	-0.094571409	0.009030914	1
GO:0071456~cellular response to hypoxia	SLC29A1, CLCA1, PTGS2, HMOX1, PTN, AQP1, KCNMB1	0.049772276	CLCA1	-0.700745803	-0.021713517	0.199482237	1
GO:0071456~cellular response to hypoxia	SLC29A1, CLCA1, PTGS2, HMOX1, PTN, AQP1, KCNMB1	0.049772276	PTGS2	-1.484870085	-1.695190956	0.286626058	1
GO:0071456~cellular response to hypoxia	SLC29A1, CLCA1, PTGS2, HMOX1, PTN, AQP1, KCNMB1	0.049772276	HMOX1	-0.376862598	-0.987411621	-0.003174755	1
GO:0071456~cellular response to hypoxia	SLC29A1, CLCA1, PTGS2, HMOX1, PTN, AQP1, KCNMB1	0.049772276	PTN	-1.07403337	-0.56582526	-0.617159513	1
GO:0071456~cellular response to hypoxia	SLC29A1, CLCA1, PTGS2, HMOX1, PTN, AQP1, KCNMB1	0.049772276	AQP1	-0.707154235	-0.600787565	0.255362055	1
GO:0071456~cellular response to hypoxia	SLC29A1, CLCA1, PTGS2, HMOX1, PTN, AQP1, KCNMB1	0.049772276	KCNMB1	-1.300462335	-0.60519212	-0.428584398	1
GO:0019233~sensory perception of pain	PTGS2, UCHL1, PTGS1, AQP1, NGF, HTR2A	0.079923715	PTGS2	-1.484870085	-1.695190956	0.286626058	1
GO:0019233~sensory perception of pain	PTGS2, UCHL1, PTGS1, AQP1, NGF, HTR2A	0.079923715	UCHL1	-0.385749886	-0.491597938	-0.319718934	1
GO:0019233~sensory perception of pain	PTGS2, UCHL1, PTGS1, AQP1, NGF, HTR2A	0.079923715	PTGS1	-0.662327693	-0.584740789	1.227936765	1
GO:0019233~sensory perception of pain	PTGS2, UCHL1, PTGS1, AQP1, NGF, HTR2A	0.079923715	AQP1	-0.707154235	-0.600787565	0.255362055	1

GO:0019233~sensory perception of pain	PTGS2, UCHL1, PTGS1, AQP1, NGF, HTR2A	0.079923715	NGF	-0.420443361	-0.352168505	0.059154538	1
GO:0019233~sensory perception of pain	PTGS2, UCHL1, PTGS1, AQP1, NGF, HTR2A	0.079923715	HTR2A	-1.276006418	-0.973220171	0.138210845	1
GO:0007613~memory	PTGS2, PLK2, ITGA5, PTGS1, NGF, HTR2A	0.104989066	PTGS2	-1.484870085	-1.695190956	0.286626058	1
GO:0007613~memory	PTGS2, PLK2, ITGA5, PTGS1, NGF, HTR2A	0.104989066	PLK2	-0.495731011	-0.689126971	0.007445328	1
GO:0007613~memory	PTGS2, PLK2, ITGA5, PTGS1, NGF, HTR2A	0.104989066	ITGA5	-0.477172253	-0.17622396	0.050794061	1
GO:0007613~memory	PTGS2, PLK2, ITGA5, PTGS1, NGF, HTR2A	0.104989066	PTGS1	-0.662327693	-0.584740789	1.227936765	1
GO:0007613~memory	PTGS2, PLK2, ITGA5, PTGS1, NGF, HTR2A	0.104989066	NGF	-0.420443361	-0.352168505	0.059154538	1
GO:0007613~memory	PTGS2, PLK2, ITGA5, PTGS1, NGF, HTR2A	0.104989066	HTR2A	-1.276006418	-0.973220171	0.138210845	1
GO:0010575~positive regulation of vascular endothelial growth factor production	C3AR1, CYP1B1, ADORA2B, PTGS2	0.109707276	C3AR1	-1.22676413	-0.927252235	0.584071632	1
GO:0010575~positive regulation of vascular endothelial growth factor production	C3AR1, CYP1B1, ADORA2B, PTGS2	0.109707276	CYP1B1	-1.010712986	-0.507932985	0.214850664	1
GO:0010575~positive regulation of vascular endothelial growth factor production	C3AR1, CYP1B1, ADORA2B, PTGS2	0.109707276	ADORA2B	-0.776534953	-0.553049483	0.262234282	1
GO:0010575~positive regulation of vascular endothelial growth factor production	C3AR1, CYP1B1, ADORA2B, PTGS2	0.109707276	PTGS2	-1.484870085	-1.695190956	0.286626058	1
GO:1902042~negative regulation of extrinsic apoptotic signaling pathway via	TNFRSF23, HMOX1, HGF, TNFAIP3	0.117825547	TNFRSF23	-0.511359765	-0.563707723	-0.05403322	1

death domain receptors							
GO:1902042~negative regulation of extrinsic apoptotic signaling pathway via death domain receptors	TNFRSF23, HMOX1, HGF, TNFAIP3	0.117825547	HMOX1	-0.376862598	-0.987411621	-0.003174755	1
GO:1902042~negative regulation of extrinsic apoptotic signaling pathway via death domain receptors	TNFRSF23, HMOX1, HGF, TNFAIP3	0.117825547	HGF	-0.316537949	-0.409370915	1.200569685	1
GO:1902042~negative regulation of extrinsic apoptotic signaling pathway via death domain receptors	TNFRSF23, HMOX1, HGF, TNFAIP3	0.117825547	TNFAIP3	-0.716278004	-0.42370585	-0.154737182	1
GO:0043065~positive regulation of apoptotic process	TXNIP, PLA2G4A, CYP1B1, PTGS2, HMOX1, PTN, RIPK2, UNC5C, HMGA2, DUSP6, NGF	0.14114097	TXNIP	-0.488645629	-0.334661679	-0.072422834	1
GO:0043065~positive regulation of apoptotic process	TXNIP, PLA2G4A, CYP1B1, PTGS2, HMOX1, PTN, RIPK2, UNC5C, HMGA2, DUSP6, NGF	0.14114097	PLA2G4A	-1.176823388	-1.093747275	0.162418202	1
GO:0043065~positive regulation of apoptotic process	TXNIP, PLA2G4A, CYP1B1, PTGS2, HMOX1, PTN, RIPK2, UNC5C, HMGA2, DUSP6, NGF	0.14114097	CYP1B1	-1.010712986	-0.507932985	0.214850664	1
GO:0043065~positive regulation of apoptotic process	TXNIP, PLA2G4A, CYP1B1, PTGS2, HMOX1, PTN, RIPK2, UNC5C, HMGA2, DUSP6, NGF	0.14114097	PTGS2	-1.484870085	-1.695190956	0.286626058	1
GO:0043065~positive regulation of apoptotic process	TXNIP, PLA2G4A, CYP1B1, PTGS2, HMOX1, PTN, RIPK2, UNC5C,	0.14114097	HMOX1	-0.376862598	-0.987411621	-0.003174755	1

	HMGA2, DUSP6, NGF						
GO:0043065~positive regulation of apoptotic process	TXNIP, PLA2G4A, CYP1B1, PTGS2, HMOX1, PTN, RIPK2, UNC5C, HMGA2, DUSP6, NGF	0.14114097	PTN	-1.07403337	-0.56582526	-0.617159513	1
GO:0043065~positive regulation of apoptotic process	TXNIP, PLA2G4A, CYP1B1, PTGS2, HMOX1, PTN, RIPK2, UNC5C, HMGA2, DUSP6, NGF	0.14114097	RIPK2	-0.557494782	-0.259886853	0.170159608	1
GO:0043065~positive regulation of apoptotic process	TXNIP, PLA2G4A, CYP1B1, PTGS2, HMOX1, PTN, RIPK2, UNC5C, HMGA2, DUSP6, NGF	0.14114097	UNC5C	-0.434834729	-0.336077616	-0.188855391	1
GO:0043065~positive regulation of apoptotic process	TXNIP, PLA2G4A, CYP1B1, PTGS2, HMOX1, PTN, RIPK2, UNC5C, HMGA2, DUSP6, NGF	0.14114097	HMGA2	-1.388611605	-0.995973927	0.422206229	1
GO:0043065~positive regulation of apoptotic process	TXNIP, PLA2G4A, CYP1B1, PTGS2, HMOX1, PTN, RIPK2, UNC5C, HMGA2, DUSP6, NGF	0.14114097	DUSP6	-0.636288799	-0.782141778	0.023999833	1
GO:0043065~positive regulation of apoptotic process	TXNIP, PLA2G4A, CYP1B1, PTGS2, HMOX1, PTN, RIPK2, UNC5C, HMGA2, DUSP6, NGF	0.14114097	NGF	-0.420443361	-0.352168505	0.059154538	1
GO:0032355~response to estradiol	TXNIP, CCND1, PTGS2, TFPI, PTN, NQO1	0.196772471	TXNIP	-0.488645629	-0.334661679	-0.072422834	1
GO:0032355~response to estradiol	TXNIP, CCND1, PTGS2, TFPI, PTN, NQO1	0.196772471	CCND1	-0.629935652	-0.102976531	0.210531411	1
GO:0032355~response to estradiol	TXNIP, CCND1, PTGS2, TFPI, PTN, NQO1	0.196772471	PTGS2	-1.484870085	-1.695190956	0.286626058	1
GO:0032355~response to estradiol	TXNIP, CCND1, PTGS2, TFPI, PTN, NQO1	0.196772471	TFPI	-0.539731062	-0.09941595	-0.248007761	1
GO:0032355~response to estradiol	TXNIP, CCND1, PTGS2, TFPI, PTN, NQO1	0.196772471	PTN	-1.07403337	-0.56582526	-0.617159513	1
GO:0032355~re	TXNIP, CCND1,	0.1967	NQO1	-	-	0.4269	1

sponse to estradiol	PTGS2, TFPI, PTN, NQO1	72471		1.812058834	1.769603856	96977	
GO:0098792~xenophagy	STOM, ATP1B1, PDK4, SNTG1, HIST2H3C2, HIST2H3C1	0.204722834	STOM	-0.405608644	-0.143002091	0.094698603	1
GO:0098792~xenophagy	STOM, ATP1B1, PDK4, SNTG1, HIST2H3C2, HIST2H3C1	0.204722834	ATP1B1	-0.788716332	-0.460856882	0.140741545	1
GO:0098792~xenophagy	STOM, ATP1B1, PDK4, SNTG1, HIST2H3C2, HIST2H3C1	0.204722834	PDK4	-0.708585422	-0.516986332	-0.149190265	1
GO:0098792~xenophagy	STOM, ATP1B1, PDK4, SNTG1, HIST2H3C2, HIST2H3C1	0.204722834	SNTG1	-0.475495705	-0.492163092	-0.451748787	1
GO:0098792~xenophagy	STOM, ATP1B1, PDK4, SNTG1, HIST2H3C2, HIST2H3C1	0.204722834	HIST2H3C2	-0.46085736	-0.104496009	0.150091546	1
GO:0098792~xenophagy	STOM, ATP1B1, PDK4, SNTG1, HIST2H3C2, HIST2H3C1	0.204722834	HIST2H3C1	-0.448130003	-0.10990776	0.133832752	1
GO:0007411~axon guidance	NRP2, FLRT2, EFNB2, UNC5C, SEMA3A, CD24A, FEZ1	0.208362627	NRP2	-0.519742916	-0.247671189	0.177469955	1
GO:0007411~axon guidance	NRP2, FLRT2, EFNB2, UNC5C, SEMA3A, CD24A, FEZ1	0.208362627	FLRT2	-0.753165786	-0.57372512	-0.133525535	1
GO:0007411~axon guidance	NRP2, FLRT2, EFNB2, UNC5C, SEMA3A, CD24A, FEZ1	0.208362627	EFNB2	-0.493942633	-0.527684043	0.158722493	1
GO:0007411~axon guidance	NRP2, FLRT2, EFNB2, UNC5C, SEMA3A, CD24A, FEZ1	0.208362627	UNC5C	-0.434834729	-0.336077616	-0.188855391	1
GO:0007411~axon guidance	NRP2, FLRT2, EFNB2, UNC5C, SEMA3A, CD24A, FEZ1	0.208362627	SEMA3A	-1.311258944	-0.731535817	0.24865124	1
GO:0007411~axon guidance	NRP2, FLRT2, EFNB2, UNC5C, SEMA3A, CD24A, FEZ1	0.208362627	CD24A	-2.012644425	-1.569299129	0.446804746	1
GO:0007411~axon guidance	NRP2, FLRT2, EFNB2, UNC5C, SEMA3A, CD24A, FEZ1	0.208362627	FEZ1	-0.493412513	-0.487482038	0.324862661	1

GO:0043066~negative regulation of apoptotic process	SGK1, LGALS3, HGF, AQP1, HMGA2, POR, PLAUR, PLAC8, PLK2, CD44, SERPINB2, NQO1, SLC40A1, SPP1	0.263816898	SGK1	-0.468271867	-0.625078522	0.186903987	1
GO:0043066~negative regulation of apoptotic process	SGK1, LGALS3, HGF, AQP1, HMGA2, POR, PLAUR, PLAC8, PLK2, CD44, SERPINB2, NQO1, SLC40A1, SPP1	0.263816898	LGALS3	-0.69840726	-0.41083659	0.108258074	1
GO:0043066~negative regulation of apoptotic process	SGK1, LGALS3, HGF, AQP1, HMGA2, POR, PLAUR, PLAC8, PLK2, CD44, SERPINB2, NQO1, SLC40A1, SPP1	0.263816898	HGF	-0.316537949	-0.409370915	1.200569685	1
GO:0043066~negative regulation of apoptotic process	SGK1, LGALS3, HGF, AQP1, HMGA2, POR, PLAUR, PLAC8, PLK2, CD44, SERPINB2, NQO1, SLC40A1, SPP1	0.263816898	AQP1	-0.707154235	-0.600787565	0.255362055	1
GO:0043066~negative regulation of apoptotic process	SGK1, LGALS3, HGF, AQP1, HMGA2, POR, PLAUR, PLAC8, PLK2, CD44, SERPINB2, NQO1, SLC40A1, SPP1	0.263816898	HMGA2	-1.388611605	-0.995973927	0.422206229	1
GO:0043066~negative regulation of apoptotic process	SGK1, LGALS3, HGF, AQP1, HMGA2, POR, PLAUR, PLAC8, PLK2, CD44, SERPINB2, NQO1, SLC40A1, SPP1	0.263816898	POR	-0.892932008	-0.465914477	0.361743915	1
GO:0043066~negative regulation of apoptotic process	SGK1, LGALS3, HGF, AQP1, HMGA2, POR, PLAUR, PLAC8, PLK2, CD44, SERPINB2, NQO1, SLC40A1, SPP1	0.263816898	PLAUR	-0.619618081	-0.796678173	0.126502551	1
GO:0043066~negative regulation of apoptotic process	SGK1, LGALS3, HGF, AQP1, HMGA2, POR, PLAUR, PLAC8, PLK2, CD44,	0.263816898	PLAC8	-1.68715324	-0.811324009	-0.105281737	1

	SERPINB2, NQO1, SLC40A1, SPP1						
GO:0043066~negative regulation of apoptotic process	SGK1, LGALS3, HGF, AQP1, HMGA2, POR, PLAUR, PLAC8, PLK2, CD44, SERPINB2, NQO1, SLC40A1, SPP1	0.263816898	PLK2	-0.495731011	-0.689126971	0.007445328	1
GO:0043066~negative regulation of apoptotic process	SGK1, LGALS3, HGF, AQP1, HMGA2, POR, PLAUR, PLAC8, PLK2, CD44, SERPINB2, NQO1, SLC40A1, SPP1	0.263816898	CD44	-0.423537378	-0.583789719	-0.019520047	1
GO:0043066~negative regulation of apoptotic process	SGK1, LGALS3, HGF, AQP1, HMGA2, POR, PLAUR, PLAC8, PLK2, CD44, SERPINB2, NQO1, SLC40A1, SPP1	0.263816898	SERPINB2	-1.019283474	-0.975679133	0.76628434	1
GO:0043066~negative regulation of apoptotic process	SGK1, LGALS3, HGF, AQP1, HMGA2, POR, PLAUR, PLAC8, PLK2, CD44, SERPINB2, NQO1, SLC40A1, SPP1	0.263816898	NQO1	-1.812058834	-1.769603856	0.426996977	1
GO:0043066~negative regulation of apoptotic process	SGK1, LGALS3, HGF, AQP1, HMGA2, POR, PLAUR, PLAC8, PLK2, CD44, SERPINB2, NQO1, SLC40A1, SPP1	0.263816898	SLC40A1	-1.105683598	-0.789931301	0.287961235	1
GO:0043066~negative regulation of apoptotic process	SGK1, LGALS3, HGF, AQP1, HMGA2, POR, PLAUR, PLAC8, PLK2, CD44, SERPINB2, NQO1, SLC40A1, SPP1	0.263816898	SPP1	-0.868611397	-0.831046522	1.004219144	1
GO:0030198~extracellular matrix organization	LGALS3, NPNT, OLFML2B, PDGFRA, NID1, VIT	0.270058878	LGALS3	-0.69840726	-0.41083659	0.108258074	1
GO:0030198~extracellular matrix organization	LGALS3, NPNT, OLFML2B, PDGFRA, NID1, VIT	0.270058878	NPNT	-0.447168282	-0.651735773	0.029240619	1
GO:0030198~extracellular matrix organization	LGALS3, NPNT, OLFML2B, PDGFRA, NID1, VIT	0.270058878	OLFML2B	-0.484127011	-0.005433381	0.221158768	1
GO:0030198~ex	LGALS3, NPNT,	0.2700	PDGF	-	-	0.1338	1

tracellular matrix organization	OLFML2B, PDGFRA, NID1, VIT	58878	RA	0.907253413	0.396614293	055	
GO:0030198~extracellular matrix organization	LGALS3, NPNT, OLFML2B, PDGFRA, NID1, VIT	0.270058878	NID1	-0.631400618	-0.23562376	0.21415057	1
GO:0030198~extracellular matrix organization	LGALS3, NPNT, OLFML2B, PDGFRA, NID1, VIT	0.270058878	VIT	-0.620399314	-0.471265041	-0.283586966	1
GO:0008285~negative regulation of cell proliferation	INHBA, CD9, CYP1B1, EREG, ADORA2B, PTGS2, HMOX1, RIAN, FGF2, HIST1H2AO, TES	0.270347473	INHBA	-0.165408956	-0.454744251	-0.060209691	1
GO:0008285~negative regulation of cell proliferation	INHBA, CD9, CYP1B1, EREG, ADORA2B, PTGS2, HMOX1, RIAN, FGF2, HIST1H2AO, TES	0.270347473	CD9	-0.354138468	0.029541306	-0.1053562	1
GO:0008285~negative regulation of cell proliferation	INHBA, CD9, CYP1B1, EREG, ADORA2B, PTGS2, HMOX1, RIAN, FGF2, HIST1H2AO, TES	0.270347473	CYP1B1	-1.010712986	-0.507932985	0.214850664	1
GO:0008285~negative regulation of cell proliferation	INHBA, CD9, CYP1B1, EREG, ADORA2B, PTGS2, HMOX1, RIAN, FGF2, HIST1H2AO, TES	0.270347473	EREG	0.021918492	-0.496740145	-0.086555927	1
GO:0008285~negative regulation of cell proliferation	INHBA, CD9, CYP1B1, EREG, ADORA2B, PTGS2, HMOX1, RIAN, FGF2, HIST1H2AO, TES	0.270347473	ADORA2B	-0.776534953	-0.553049483	0.262234282	1
GO:0008285~negative regulation of cell proliferation	INHBA, CD9, CYP1B1, EREG, ADORA2B, PTGS2, HMOX1, RIAN, FGF2, HIST1H2AO, TES	0.270347473	PTGS2	-1.484870085	-1.695190956	0.286626058	1
GO:0008285~negative regulation of cell proliferation	INHBA, CD9, CYP1B1, EREG, ADORA2B, PTGS2, HMOX1, RIAN, FGF2, HIST1H2AO, TES	0.270347473	HMOX1	-0.376862598	-0.987411621	-0.003174755	1
GO:0008285~negative regulation of cell proliferation	INHBA, CD9, CYP1B1, EREG, ADORA2B, PTGS2, HMOX1, RIAN,	0.270347473	RIAN	-0.67289361	-0.144533537	-0.112589638	1

	FGF2, HIST1H2AO, TES						
GO:0008285~negative regulation of cell proliferation	INHBA, CD9, CYP1B1, EREG, ADORA2B, PTGS2, HMOX1, RIAN, FGF2, HIST1H2AO, TES	0.270347473	FGF2	0.118448677	-0.492964607	0.272034532	1
GO:0008285~negative regulation of cell proliferation	INHBA, CD9, CYP1B1, EREG, ADORA2B, PTGS2, HMOX1, RIAN, FGF2, HIST1H2AO, TES	0.270347473	HIST1H2AO	-0.556865375	-0.193375003	0.088933559	1
GO:0008285~negative regulation of cell proliferation	INHBA, CD9, CYP1B1, EREG, ADORA2B, PTGS2, HMOX1, RIAN, FGF2, HIST1H2AO, TES	0.270347473	TES	-1.214608125	-0.837870916	0.128590607	1
GO:0043627~response to estrogen	CCND1, HMOX1, AQP1, PTPRN, CD24A	0.285561787	CCND1	-0.629935652	-0.102976531	0.210531411	1
GO:0043627~response to estrogen	CCND1, HMOX1, AQP1, PTPRN, CD24A	0.285561787	HMOX1	-0.376862598	-0.987411621	-0.003174755	1
GO:0043627~response to estrogen	CCND1, HMOX1, AQP1, PTPRN, CD24A	0.285561787	AQP1	-0.707154235	-0.600787565	0.255362055	1
GO:0043627~response to estrogen	CCND1, HMOX1, AQP1, PTPRN, CD24A	0.285561787	PTPRN	-0.525514127	-0.251573901	0.468803	1
GO:0043627~response to estrogen	CCND1, HMOX1, AQP1, PTPRN, CD24A	0.285561787	CD24A	-2.012644425	-1.569299129	0.446804746	1
GO:0002230~positive regulation of defense response to virus by host	STOM, ATP1B1, PDK4, SNTG1, HIST2H3C2, HIST2H3C1	0.314413999	STOM	-0.405608644	-0.143002091	0.094698603	1
GO:0002230~positive regulation of defense response to virus by host	STOM, ATP1B1, PDK4, SNTG1, HIST2H3C2, HIST2H3C1	0.314413999	ATP1B1	-0.788716332	-0.460856882	0.140741545	1
GO:0002230~positive regulation of defense response to virus by host	STOM, ATP1B1, PDK4, SNTG1, HIST2H3C2, HIST2H3C1	0.314413999	PDK4	-0.708585422	-0.516986332	-0.149190265	1
GO:0002230~positive regulation of defense response to	STOM, ATP1B1, PDK4, SNTG1, HIST2H3C2, HIST2H3C1	0.314413999	SNTG1	-0.475495705	-0.492163092	-0.451748787	1

virus by host							
GO:0002230~positive regulation of defense response to virus by host	STOM, ATP1B1, PDK4, SNTG1, HIST2H3C2, HIST2H3C1	0.314413999	HIST2H3C2	-0.46085736	-0.104496009	0.150091546	1
GO:0002230~positive regulation of defense response to virus by host	STOM, ATP1B1, PDK4, SNTG1, HIST2H3C2, HIST2H3C1	0.314413999	HIST2H3C1	-0.448130003	-0.10990776	0.133832752	1
GO:0048661~positive regulation of smooth muscle cell proliferation	C3AR1, EREG, PTGS2, HMOX1, FGF2	0.326544842	C3AR1	-1.22676413	-0.927252235	0.584071632	1
GO:0048661~positive regulation of smooth muscle cell proliferation	C3AR1, EREG, PTGS2, HMOX1, FGF2	0.326544842	EREG	0.021918492	-0.496740145	-0.086555927	1
GO:0048661~positive regulation of smooth muscle cell proliferation	C3AR1, EREG, PTGS2, HMOX1, FGF2	0.326544842	PTGS2	-1.484870085	-1.695190956	0.286626058	1
GO:0048661~positive regulation of smooth muscle cell proliferation	C3AR1, EREG, PTGS2, HMOX1, FGF2	0.326544842	HMOX1	-0.376862598	-0.987411621	-0.003174755	1
GO:0048661~positive regulation of smooth muscle cell proliferation	C3AR1, EREG, PTGS2, HMOX1, FGF2	0.326544842	FGF2	0.118448677	-0.492964607	0.272034532	1
GO:0000188~inactivation of MAPK activity	DUSP4, DUSP10, DUSP6	0.335819467	DUSP4	-0.517842476	-0.225987074	0.110928674	1
GO:0000188~inactivation of MAPK activity	DUSP4, DUSP10, DUSP6	0.335819467	DUSP10	-0.103303255	-0.489526837	0.021464395	1
GO:0000188~inactivation of MAPK activity	DUSP4, DUSP10, DUSP6	0.335819467	DUSP6	-0.636288799	-0.782141778	0.023999833	1
GO:0070374~positive regulation of ERK1 and ERK2 cascade	CD44, NPNT, PDGFRA, RIPK2, GPNMB, FGF2, HTR2A	0.41557517	CD44	-0.423537378	-0.583789719	-0.019520047	1
GO:0070374~positive regulation of ERK1 and ERK2 cascade	CD44, NPNT, PDGFRA, RIPK2, GPNMB, FGF2, HTR2A	0.41557517	NPNT	-0.447168282	-0.651735773	0.029240619	1
GO:0070374~po	CD44, NPNT,	0.4155	PDGF	-	-	0.1338	1

sitive regulation of ERK1 and ERK2 cascade	PDGFRA, RIPK2, GPNMB, FGF2, HTR2A	7517	RA	0.907253413	0.396614293	055	
GO:0070374~positive regulation of ERK1 and ERK2 cascade	CD44, NPNT, PDGFRA, RIPK2, GPNMB, FGF2, HTR2A	0.41557517	RIPK2	-0.557494782	-0.259886853	0.170159608	1
GO:0070374~positive regulation of ERK1 and ERK2 cascade	CD44, NPNT, PDGFRA, RIPK2, GPNMB, FGF2, HTR2A	0.41557517	GPNMB	-0.447514067	0.009257219	0.313147954	1
GO:0070374~positive regulation of ERK1 and ERK2 cascade	CD44, NPNT, PDGFRA, RIPK2, GPNMB, FGF2, HTR2A	0.41557517	FGF2	0.118448677	-0.492964607	0.272034532	1
GO:0070374~positive regulation of ERK1 and ERK2 cascade	CD44, NPNT, PDGFRA, RIPK2, GPNMB, FGF2, HTR2A	0.41557517	HTR2A	-1.276006418	-0.973220171	0.138210845	1
GO:2000573~positive regulation of DNA biosynthetic process	C3AR1, CYP1B1, HGF	0.424776975	C3AR1	-1.22676413	-0.927252235	0.584071632	1
GO:2000573~positive regulation of DNA biosynthetic process	C3AR1, CYP1B1, HGF	0.424776975	CYP1B1	-1.010712986	-0.507932985	0.214850664	1
GO:2000573~positive regulation of DNA biosynthetic process	C3AR1, CYP1B1, HGF	0.424776975	HGF	-0.316537949	-0.409370915	1.200569685	1
GO:0042060~wound healing	PDGFRA, SERPINB2, AQP1, FGF2, PLAU	0.456842036	PDGFRA	-0.907253413	-0.396614293	0.1338055	1
GO:0042060~wound healing	PDGFRA, SERPINB2, AQP1, FGF2, PLAU	0.456842036	SERPINB2	-1.019283474	-0.975679133	0.76628434	1
GO:0042060~wound healing	PDGFRA, SERPINB2, AQP1, FGF2, PLAU	0.456842036	AQP1	-0.707154235	-0.600787565	0.255362055	1
GO:0042060~wound healing	PDGFRA, SERPINB2, AQP1, FGF2, PLAU	0.456842036	FGF2	0.118448677	-0.492964607	0.272034532	1
GO:0042060~wound healing	PDGFRA, SERPINB2, AQP1, FGF2, PLAU	0.456842036	PLAU	-1.028169119	-0.534422078	0.207035543	1
GO:0002227~innate immune response in mucosa	HIST1H2BN, HIST1H2BK, HIST2H2BE	0.506583225	HIST1H2BN	-0.645313402	-0.203264947	0.181669073	1
GO:0002227~in	HIST1H2BN,	0.5065	HIST1	-	-	0.1338	1

nate immune response in mucosa	HIST1H2BK, HIST2H2BE	83225	H2BK	0.509820734	0.204682195	36776	
GO:0002227~innate immune response in mucosa	HIST1H2BN, HIST1H2BK, HIST2H2BE	0.506583225	HIST2H2BE	-0.526938534	-0.323547959	-0.192197457	1
GO:0030178~negative regulation of Wnt signaling pathway	DKK2, CCND1, HMGA2, TSKU	0.509027291	DKK2	-1.537331255	-0.740024196	0.581012453	1
GO:0030178~negative regulation of Wnt signaling pathway	DKK2, CCND1, HMGA2, TSKU	0.509027291	CCND1	-0.629935652	-0.102976531	0.210531411	1
GO:0030178~negative regulation of Wnt signaling pathway	DKK2, CCND1, HMGA2, TSKU	0.509027291	HMGA2	-1.388611605	-0.995973927	0.422206229	1
GO:0030178~negative regulation of Wnt signaling pathway	DKK2, CCND1, HMGA2, TSKU	0.509027291	TSKU	-0.356486796	-0.637008958	0.110641426	1
GO:0045987~positive regulation of smooth muscle contraction	PTGS2, NPNT, PTGS1	0.579699983	PTGS2	-1.484870085	-1.695190956	0.286626058	1
GO:0045987~positive regulation of smooth muscle contraction	PTGS2, NPNT, PTGS1	0.579699983	NPNT	-0.447168282	-0.651735773	0.029240619	1
GO:0045987~positive regulation of smooth muscle contraction	PTGS2, NPNT, PTGS1	0.579699983	PTGS1	-0.662327693	-0.584740789	1.227936765	1
GO:2000377~regulation of reactive oxygen species metabolic process	CYP1B1, RIPK3, PRCP	0.581648286	CYP1B1	-1.010712986	-0.507932985	0.214850664	1
GO:2000377~regulation of reactive oxygen species metabolic process	CYP1B1, RIPK3, PRCP	0.581648286	RIPK3	-0.761759161	-0.519699955	0.172958663	1
GO:2000377~regulation of reactive oxygen species	CYP1B1, RIPK3, PRCP	0.581648286	PRCP	-0.463904038	-0.113779079	-0.1765 2095	1

metabolic process							
GO:0016311~dephosphorylation	PTPRB, DUSP4, DUSP10, PTPRN, DUSP6	0.583448299	PTPRB	-1.272295565	-0.682530654	0.079615522	1
GO:0016311~dephosphorylation	PTPRB, DUSP4, DUSP10, PTPRN, DUSP6	0.583448299	DUSP4	-0.517842476	-0.225987074	0.110928674	1
GO:0016311~dephosphorylation	PTPRB, DUSP4, DUSP10, PTPRN, DUSP6	0.583448299	DUSP10	-0.103303255	-0.489526837	0.021464395	1
GO:0016311~dephosphorylation	PTPRB, DUSP4, DUSP10, PTPRN, DUSP6	0.583448299	PTPRN	-0.525514127	-0.251573901	0.468803	1
GO:0016311~dephosphorylation	PTPRB, DUSP4, DUSP10, PTPRN, DUSP6	0.583448299	DUSP6	-0.636288799	-0.782141778	0.023999833	1
GO:0006935~chemotaxis	C3AR1, ECSCR, PDGFRA, CMTM4, CXCL12	0.584684637	C3AR1	-1.22676413	-0.927252235	0.584071632	1
GO:0006935~chemotaxis	C3AR1, ECSCR, PDGFRA, CMTM4, CXCL12	0.584684637	ECSCR	-0.485332782	-0.215438307	-0.274351718	1
GO:0006935~chemotaxis	C3AR1, ECSCR, PDGFRA, CMTM4, CXCL12	0.584684637	PDGFRA	-0.907253413	-0.396614293	0.1338055	1
GO:0006935~chemotaxis	C3AR1, ECSCR, PDGFRA, CMTM4, CXCL12	0.584684637	CMTM4	-0.398283961	-0.259145138	-0.118026339	1
GO:0006935~chemotaxis	C3AR1, ECSCR, PDGFRA, CMTM4, CXCL12	0.584684637	CXCL12	-1.096137743	-0.485286992	0.577416667	1
GO:0008217~regulation of blood pressure	C3AR1, PTGS2, HMOX1, PTGS1	0.5874736	C3AR1	-1.22676413	-0.927252235	0.584071632	1
GO:0008217~regulation of blood pressure	C3AR1, PTGS2, HMOX1, PTGS1	0.5874736	PTGS2	-1.484870085	-1.695190956	0.286626058	1
GO:0008217~regulation of blood pressure	C3AR1, PTGS2, HMOX1, PTGS1	0.5874736	HMOX1	-0.376862598	-0.987411621	-0.003174755	1
GO:0008217~regulation of blood pressure	C3AR1, PTGS2, HMOX1, PTGS1	0.5874736	PTGS1	-0.662327693	-0.584740789	1.227936765	1
GO:0045765~regulation of angiogenesis	ADORA2B, ITGA5, VASH2	0.590469407	ADORA2B	-0.776534953	-0.553049483	0.262234282	1
GO:0045765~regulation of angiogenesis	ADORA2B, ITGA5, VASH2	0.590469407	ITGA5	-0.477172253	-0.17622396	0.050794061	1
GO:0045765~regulation of angiogenesis	ADORA2B, ITGA5, VASH2	0.590469407	VASH2	-0.956539427	-0.396609385	0.104661842	1
GO:0007568~ag	ENO3, NQO1, FGF2,	0.5914	ENO3	-	-	0.3502	1

ing	GCLM, KCNMB1, HTR2A	63918		0.829485548	0.443803637	74932	
GO:0007568~aging	ENO3, NQO1, FGF2, GCLM, KCNMB1, HTR2A	0.591463918	NQO1	-1.812058834	-1.769603856	0.426996977	1
GO:0007568~aging	ENO3, NQO1, FGF2, GCLM, KCNMB1, HTR2A	0.591463918	FGF2	0.118448677	-0.492964607	0.272034532	1
GO:0007568~aging	ENO3, NQO1, FGF2, GCLM, KCNMB1, HTR2A	0.591463918	GCLM	-0.377203486	-0.51565766	0.022762576	1
GO:0007568~aging	ENO3, NQO1, FGF2, GCLM, KCNMB1, HTR2A	0.591463918	KCNMB1	-1.300462335	-0.60519212	-0.428584398	1
GO:0007568~aging	ENO3, NQO1, FGF2, GCLM, KCNMB1, HTR2A	0.591463918	HTR2A	-1.276006418	-0.973220171	0.138210845	1
GO:0035987~endodermal cell differentiation	INHBA, ITGA5, HMGA2	0.594687929	INHBA	-0.165408956	-0.454744251	-0.060209691	1
GO:0035987~endodermal cell differentiation	INHBA, ITGA5, HMGA2	0.594687929	ITGA5	-0.477172253	-0.17622396	0.050794061	1
GO:0035987~endodermal cell differentiation	INHBA, ITGA5, HMGA2	0.594687929	HMGA2	-1.388611605	-0.995973927	0.422206229	1
GO:0051592~response to calcium ion	TXNIP, PLA2G4A, CCND1, KCNMB1	0.59556189	TXNIP	-0.488645629	-0.334661679	-0.072422834	1
GO:0051592~response to calcium ion	TXNIP, PLA2G4A, CCND1, KCNMB1	0.59556189	PLA2G4A	-1.176823388	-1.093747275	0.162418202	1
GO:0051592~response to calcium ion	TXNIP, PLA2G4A, CCND1, KCNMB1	0.59556189	CCND1	-0.629935652	-0.102976531	0.210531411	1
GO:0051592~response to calcium ion	TXNIP, PLA2G4A, CCND1, KCNMB1	0.59556189	KCNMB1	-1.300462335	-0.60519212	-0.428584398	1
GO:0043154~negative regulation of cysteine-type endopeptidase activity involved in apoptotic process	CD44, HGF, AQP1, POR	0.596183036	CD44	-0.423537378	-0.583789719	-0.019520047	1
GO:0043154~negative regulation of cysteine-type endopeptidase activity involved in apoptotic process	CD44, HGF, AQP1, POR	0.596183036	HGF	-0.316537949	-0.409370915	1.200569685	1
GO:0043154~negative regulation	CD44, HGF, AQP1, POR	0.596183036	AQP1	-0.7071	-0.6007	0.255362055	1

of cysteine-type endopeptidase activity involved in apoptotic process				54235	87565		
GO:0043154~negative regulation of cysteine-type endopeptidase activity involved in apoptotic process	CD44, HGF, AQP1, POR	0.596183036	POR	-0.892932008	-0.465914477	0.361743915	1
GO:0030154~cell differentiation	NRP2, LGALS3, NPNT, FHL1, EFNB2, MGP, EREG, ECSCR, SEMA3E, SEMA3A, TNFAIP2, FGF2, SYT17, TLL1, DUSP6	0.597861821	NRP2	-0.519742916	-0.247671189	0.177469955	1
GO:0030154~cell differentiation	NRP2, LGALS3, NPNT, FHL1, EFNB2, MGP, EREG, ECSCR, SEMA3E, SEMA3A, TNFAIP2, FGF2, SYT17, TLL1, DUSP6	0.597861821	LGALS3	-0.6984 0726	-0.4108 3659	0.108258074	1
GO:0030154~cell differentiation	NRP2, LGALS3, NPNT, FHL1, EFNB2, MGP, EREG, ECSCR, SEMA3E, SEMA3A, TNFAIP2, FGF2, SYT17, TLL1, DUSP6	0.597861821	NPNT	-0.447168282	-0.651735773	0.029240619	1
GO:0030154~cell differentiation	NRP2, LGALS3, NPNT, FHL1, EFNB2, MGP, EREG, ECSCR, SEMA3E, SEMA3A, TNFAIP2, FGF2, SYT17, TLL1, DUSP6	0.597861821	FHL1	-0.637474645	-0.318185774	-0.182333407	1
GO:0030154~cell differentiation	NRP2, LGALS3, NPNT, FHL1, EFNB2, MGP, EREG, ECSCR, SEMA3E, SEMA3A, TNFAIP2, FGF2, SYT17, TLL1, DUSP6	0.597861821	EFNB2	-0.493942633	-0.527684043	0.158722493	1
GO:0030154~cell differentiation	NRP2, LGALS3, NPNT, FHL1,	0.597861821	MGP	-0.8164	-0.8195	1.300353362	1

	EFNB2, MGP, EREG, ECSCR, SEMA3E, SEMA3A, TNFAIP2, FGF2, SYT17, TLL1, DUSP6			41763	60688		
GO:0030154~cell differentiation	NRP2, LGALS3, NPNT, FHL1, EFNB2, MGP, EREG, ECSCR, SEMA3E, SEMA3A, TNFAIP2, FGF2, SYT17, TLL1, DUSP6	0.597861821	EREG	0.021918492	-0.496740145	-0.086555927	1
GO:0030154~cell differentiation	NRP2, LGALS3, NPNT, FHL1, EFNB2, MGP, EREG, ECSCR, SEMA3E, SEMA3A, TNFAIP2, FGF2, SYT17, TLL1, DUSP6	0.597861821	ECSCR	-0.485332782	-0.215438307	-0.274351718	1
GO:0030154~cell differentiation	NRP2, LGALS3, NPNT, FHL1, EFNB2, MGP, EREG, ECSCR, SEMA3E, SEMA3A, TNFAIP2, FGF2, SYT17, TLL1, DUSP6	0.597861821	SEMA3E	-0.742357249	-0.665614674	-0.167255282	1
GO:0030154~cell differentiation	NRP2, LGALS3, NPNT, FHL1, EFNB2, MGP, EREG, ECSCR, SEMA3E, SEMA3A, TNFAIP2, FGF2, SYT17, TLL1, DUSP6	0.597861821	SEMA3A	-1.311258944	-0.731535817	0.24865124	1
GO:0030154~cell differentiation	NRP2, LGALS3, NPNT, FHL1, EFNB2, MGP, EREG, ECSCR, SEMA3E, SEMA3A, TNFAIP2, FGF2, SYT17, TLL1, DUSP6	0.597861821	TNFAIP2	-0.881017093	-0.692657286	0.21556035	1
GO:0030154~cell differentiation	NRP2, LGALS3, NPNT, FHL1, EFNB2, MGP, EREG, ECSCR, SEMA3E, SEMA3A, TNFAIP2, FGF2, SYT17, TLL1, DUSP6	0.597861821	FGF2	0.118448677	-0.492964607	0.272034532	1

GO:0030154~cell differentiation	NRP2, LGALS3, NPNT, FHL1, EFNB2, MGP, EREG, ECSCR, SEMA3E, SEMA3A, TNFAIP2, FGF2, SYT17, TLL1, DUSP6	0.597861821	SYT17	-0.994271007	-0.609316329	0.029736669	1
GO:0030154~cell differentiation	NRP2, LGALS3, NPNT, FHL1, EFNB2, MGP, EREG, ECSCR, SEMA3E, SEMA3A, TNFAIP2, FGF2, SYT17, TLL1, DUSP6	0.597861821	TLL1	-1.55117389	-0.963629225	-0.30123344	1
GO:0030154~cell differentiation	NRP2, LGALS3, NPNT, FHL1, EFNB2, MGP, EREG, ECSCR, SEMA3E, SEMA3A, TNFAIP2, FGF2, SYT17, TLL1, DUSP6	0.597861821	DUSP6	-0.636288799	-0.782141778	0.023999833	1
GO:0042127~regulation of cell proliferation	TXNIP, PLA2G4A, SGK1, PTGS2, PTGS1, PLAU, TES	0.599535425	TXNIP	-0.488645629	-0.334661679	-0.072422834	1
GO:0042127~regulation of cell proliferation	TXNIP, PLA2G4A, SGK1, PTGS2, PTGS1, PLAU, TES	0.599535425	PLA2G4A	-1.176823388	-1.093747275	0.162418202	1
GO:0042127~regulation of cell proliferation	TXNIP, PLA2G4A, SGK1, PTGS2, PTGS1, PLAU, TES	0.599535425	SGK1	-0.468271867	-0.625078522	0.186903987	1
GO:0042127~regulation of cell proliferation	TXNIP, PLA2G4A, SGK1, PTGS2, PTGS1, PLAU, TES	0.599535425	PTGS2	-1.484870085	-1.695190956	0.286626058	1
GO:0042127~regulation of cell proliferation	TXNIP, PLA2G4A, SGK1, PTGS2, PTGS1, PLAU, TES	0.599535425	PTGS1	-0.662327693	-0.584740789	1.227936765	1
GO:0042127~regulation of cell proliferation	TXNIP, PLA2G4A, SGK1, PTGS2, PTGS1, PLAU, TES	0.599535425	PLAU	-1.028169119	-0.534422078	0.207035543	1
GO:0042127~regulation of cell proliferation	TXNIP, PLA2G4A, SGK1, PTGS2, PTGS1, PLAU, TES	0.599535425	TES	-1.214608125	-0.837870916	0.128590607	1
GO:0050919~negative chemotaxis	NRP2, SEMA3E, SEMA3A	0.600433704	NRP2	-0.519742916	-0.247671189	0.177469955	1
GO:0050919~negative chemotaxis	NRP2, SEMA3E, SEMA3A	0.600433704	SEMA3E	-0.742357249	-0.665614674	-0.167255282	1
GO:0050919~negative chemotaxis	NRP2, SEMA3E, SEMA3A	0.600433704	SEMA3A	-1.311258944	-0.731535817	0.24865124	1

GO:0007612~learning	PRKAR2B, PTGS2, PTGS1, PTN	0.605053197	PRKAR2B	-1.497545677	-0.912519394	0.757271011	1
GO:0007612~learning	PRKAR2B, PTGS2, PTGS1, PTN	0.605053197	PTGS2	-1.484870085	-1.695190956	0.286626058	1
GO:0007612~learning	PRKAR2B, PTGS2, PTGS1, PTN	0.605053197	PTGS1	-0.662327693	-0.584740789	1.227936765	1
GO:0007612~learning	PRKAR2B, PTGS2, PTGS1, PTN	0.605053197	PTN	-1.07403337	-0.56582526	-0.617159513	1
GO:0002246~wound healing involved in inflammatory response	CD44, HMOX1	0.606911258	CD44	-0.423537378	-0.583789719	-0.019520047	1
GO:0002246~wound healing involved in inflammatory response	CD44, HMOX1	0.606911258	HMOX1	-0.376862598	-0.987411621	-0.003174755	1
GO:0021828~gonadotrophin-releasing hormone neuronal migration to the hypothalamus	NRP2, SEMA3A	0.606911258	NRP2	-0.519742916	-0.247671189	0.177469955	1
GO:0021828~gonadotrophin-releasing hormone neuronal migration to the hypothalamus	NRP2, SEMA3A	0.606911258	SEMA3A	-1.311258944	-0.731535817	0.24865124	1
GO:1903375~facioacoustic ganglion development	NRP2, SEMA3A	0.606911258	NRP2	-0.519742916	-0.247671189	0.177469955	1
GO:1903375~facioacoustic ganglion development	NRP2, SEMA3A	0.606911258	SEMA3A	-1.311258944	-0.731535817	0.24865124	1
GO:0034395~regulation of transcription from RNA polymerase II promoter in response to iron	HMOX1, SLC40A1	0.606911258	HMOX1	-0.376862598	-0.987411621	-0.003174755	1
GO:0034395~regulation of transcription	HMOX1, SLC40A1	0.606911258	SLC40A1	-1.105683598	-0.789931301	0.287961235	1

from RNA polymerase II promoter in response to iron							
GO:0032570~response to progesterone	TXNIP, PTN, FOSB	0.617345718	TXNIP	-0.488645629	-0.334661679	-0.072422834	1
GO:0032570~response to progesterone	TXNIP, PTN, FOSB	0.617345718	PTN	-1.07403337	-0.56582526	-0.617159513	1
GO:0032570~response to progesterone	TXNIP, PTN, FOSB	0.617345718	FOSB	-0.72242176	-0.839750518	-0.874927267	1
GO:2000379~positive regulation of reactive oxygen species metabolic process	CYP1B1, RIPK3, PLAU	0.620322805	CYP1B1	-1.010712986	-0.507932985	0.214850664	1
GO:2000379~positive regulation of reactive oxygen species metabolic process	CYP1B1, RIPK3, PLAU	0.620322805	RIPK3	-0.761759161	-0.519699955	0.172958663	1
GO:2000379~positive regulation of reactive oxygen species metabolic process	CYP1B1, RIPK3, PLAU	0.620322805	PLAU	-1.028169119	-0.534422078	0.207035543	1
GO:0036486~ventral trunk neural crest cell migration	NRP2, SEMA3A	0.62577212	NRP2	-0.519742916	-0.247671189	0.177469955	1
GO:0036486~ventral trunk neural crest cell migration	NRP2, SEMA3A	0.62577212	SEMA3A	-1.311258944	-0.731535817	0.24865124	1
GO:0035633~maintenance of blood-brain barrier	PTGS2, PTGS1	0.62577212	PTGS2	-1.484870085	-1.695190956	0.286626058	1
GO:0035633~maintenance of blood-brain barrier	PTGS2, PTGS1	0.62577212	PTGS1	-0.662327693	-0.584740789	1.227936765	1
GO:0051409~response to nitrosative stress	GCLM, DUSP6	0.62577212	GCLM	-0.377203486	-0.51565766	0.022762576	1
GO:0051409~response to nitrosative stress	GCLM, DUSP6	0.62577212	DUSP6	-0.636288799	-0.782141778	0.023999833	1
GO:0097490~sy	NRP2, SEMA3A	0.6257	NRP2	-	-	0.1774	1

mpathetic neuron projection extension		7212		0.519742916	0.247671189	69955	
GO:0097490~sympathetic neuron projection extension	NRP2, SEMA3A	0.62577212	SEMA3A	-1.311258944	-0.731535817	0.24865124	1
GO:0097491~sympathetic neuron projection guidance	NRP2, SEMA3A	0.62577212	NRP2	-0.519742916	-0.247671189	0.177469955	1
GO:0097491~sympathetic neuron projection guidance	NRP2, SEMA3A	0.62577212	SEMA3A	-1.311258944	-0.731535817	0.24865124	1
GO:0060279~positive regulation of ovulation	INHBA, PLAU	0.62577212	INHBA	-0.165408956	-0.454744251	-0.060209691	1
GO:0060279~positive regulation of ovulation	INHBA, PLAU	0.62577212	PLAU	-1.028169119	-0.534422078	0.207035543	1
GO:1902285~semaphorin-plexin signaling pathway involved in neuron projection guidance	NRP2, SEMA3A	0.62577212	NRP2	-0.519742916	-0.247671189	0.177469955	1
GO:1902285~semaphorin-plexin signaling pathway involved in neuron projection guidance	NRP2, SEMA3A	0.62577212	SEMA3A	-1.311258944	-0.731535817	0.24865124	1
GO:0007584~response to nutrient	GATM, NQO1, GCLM, POR	0.628108248	GATM	-0.75452638	-0.378834856	0.190616924	1
GO:0007584~response to nutrient	GATM, NQO1, GCLM, POR	0.628108248	NQO1	-1.812058834	-1.769603856	0.426996977	1
GO:0007584~response to nutrient	GATM, NQO1, GCLM, POR	0.628108248	GCLM	-0.377203486	-0.51565766	0.022762576	1
GO:0007584~response to nutrient	GATM, NQO1, GCLM, POR	0.628108248	POR	-0.892932008	-0.465914477	0.361743915	1
GO:0006813~po	ATP1B1, KCND3,	0.6310	ATP1	-	-	0.1407	1

tassium ion transport	KCNAB1, AQP1, KCNMB1	07545	B1	0.7887 16332	0.4608 56882	41545	
GO:0006813~po tassium ion transport	ATP1B1, KCND3, KCNAB1, AQP1, KCNMB1	0.6310 07545	KCND 3	-0.5976 21842	-0.4025 05976	-0.3253 02873	1
GO:0006813~po tassium ion transport	ATP1B1, KCND3, KCNAB1, AQP1, KCNMB1	0.6310 07545	KCNA B1	-0.4945 95642	-0.1634 61587	-0.5902 86177	1
GO:0006813~po tassium ion transport	ATP1B1, KCND3, KCNAB1, AQP1, KCNMB1	0.6310 07545	AQP1	-0.7071 54235	-0.6007 87565	0.2553 62055	1
GO:0006813~po tassium ion transport	ATP1B1, KCND3, KCNAB1, AQP1, KCNMB1	0.6310 07545	KCN MB1	-1.3004 62335	-0.6051 9212	-0.4285 84398	1
GO:0001934~po sitive regulation of protein phosphorylation	CCND1, PELI2, GPNMB, FGF2, PLAUR, NGF	0.6347 91449	CCND 1	-0.6299 35652	-0.1029 76531	0.2105 31411	1
GO:0001934~po sitive regulation of protein phosphorylation	CCND1, PELI2, GPNMB, FGF2, PLAUR, NGF	0.6347 91449	PELI2	-0.6538 79818	-0.3404 95225	0.0899 86551	1
GO:0001934~po sitive regulation of protein phosphorylation	CCND1, PELI2, GPNMB, FGF2, PLAUR, NGF	0.6347 91449	GPN MB	-0.4475 14067	0.0092 57219	0.3131 47954	1
GO:0001934~po sitive regulation of protein phosphorylation	CCND1, PELI2, GPNMB, FGF2, PLAUR, NGF	0.6347 91449	FGF2	0.1184 48677	-0.4929 64607	0.2720 34532	1
GO:0001934~po sitive regulation of protein phosphorylation	CCND1, PELI2, GPNMB, FGF2, PLAUR, NGF	0.6347 91449	PLAU R	-0.6196 18081	-0.7966 78173	0.1265 02551	1
GO:0001934~po sitive regulation of protein phosphorylation	CCND1, PELI2, GPNMB, FGF2, PLAUR, NGF	0.6347 91449	NGF	-0.4204 43361	-0.3521 68505	0.0591 54538	1
GO:0019731~an tibacterial humoral response	HIST1H2BN, HIST1H2BK, HIST2H2BE	0.6445 13818	HIST1 H2BN	-0.6453 13402	-0.2032 64947	0.1816 69073	1
GO:0019731~an tibacterial humoral response	HIST1H2BN, HIST1H2BK, HIST2H2BE	0.6445 13818	HIST1 H2BK	-0.5098 20734	-0.2046 82195	0.1338 36776	1
GO:0019731~an tibacterial humoral response	HIST1H2BN, HIST1H2BK, HIST2H2BE	0.6445 13818	HIST2 H2BE	-0.5269 38534	-0.3235 47959	-0.1921 97457	1
GO:0098609~cel l-cell adhesion	SNX9, PDLIM5, HIST2H3C2, HIST2H3C1, CXCL12, TES	0.6486 36935	SNX9	-0.5114 46344	-0.3738 7703	0.0697 02091	1

GO:0098609~cell-cell adhesion	SNX9, PDLIM5, HIST2H3C2, HIST2H3C1, CXCL12, TES	0.648636935	PDLIM5	-0.396974891	-0.416075997	-0.105928494	1
GO:0098609~cell-cell adhesion	SNX9, PDLIM5, HIST2H3C2, HIST2H3C1, CXCL12, TES	0.648636935	HIST2H3C2	-0.46085736	-0.104496009	0.150091546	1
GO:0098609~cell-cell adhesion	SNX9, PDLIM5, HIST2H3C2, HIST2H3C1, CXCL12, TES	0.648636935	HIST2H3C1	-0.448130003	-0.10990776	0.133832752	1
GO:0098609~cell-cell adhesion	SNX9, PDLIM5, HIST2H3C2, HIST2H3C1, CXCL12, TES	0.648636935	CXCL12	-1.096137743	-0.485286992	0.577416667	1
GO:0098609~cell-cell adhesion	SNX9, PDLIM5, HIST2H3C2, HIST2H3C1, CXCL12, TES	0.648636935	TES	-1.214608125	-0.837870916	0.128590607	1
GO:0060326~cell chemotaxis	PDGFRA, ABCC1, HGF, CXCL12	0.652489571	PDGFRA	-0.907253413	-0.396614293	0.1338055	1
GO:0060326~cell chemotaxis	PDGFRA, ABCC1, HGF, CXCL12	0.652489571	ABCC1	-0.428339319	-0.33270194	0.214136453	1
GO:0060326~cell chemotaxis	PDGFRA, ABCC1, HGF, CXCL12	0.652489571	HGF	-0.316537949	-0.409370915	1.200569685	1
GO:0060326~cell chemotaxis	PDGFRA, ABCC1, HGF, CXCL12	0.652489571	CXCL12	-1.096137743	-0.485286992	0.577416667	1
GO:0030282~bone mineralization	PTGS2, PTN, GPNMB	0.661126848	PTGS2	-1.484870085	-1.695190956	0.286626058	1
GO:0030282~bone mineralization	PTGS2, PTN, GPNMB	0.661126848	PTN	-1.07403337	-0.56582526	-0.617159513	1
GO:0030282~bone mineralization	PTGS2, PTN, GPNMB	0.661126848	GPNMB	-0.447514067	0.009257219	0.313147954	1
GO:0061551~trigeminal ganglion development	NRP2, SEMA3A	0.665214026	NRP2	-0.519742916	-0.247671189	0.177469955	1
GO:0061551~trigeminal ganglion development	NRP2, SEMA3A	0.665214026	SEMA3A	-1.311258944	-0.731535817	0.24865124	1
GO:0019371~cyclooxygenase pathway	PTGS2, PTGS1	0.665214026	PTGS2	-1.484870085	-1.695190956	0.286626058	1
GO:0019371~cyclooxygenase pathway	PTGS2, PTGS1	0.665214026	PTGS1	-0.662327693	-0.584740789	1.227936765	1
GO:0050920~re	EFNB2, PDGFRA	0.6652	EFNB	-	-	0.1587	1

gulation of chemotaxis		14026	2	0.493942633	0.527684043	22493	
GO:0050920~regulation of chemotaxis	EFNB2, PDGFRA	0.665214026	PDGFRA	-0.907253413	-0.396614293	0.1338055	1
GO:0033631~cell-cell adhesion mediated by integrin	ITGA5, NPNT	0.665214026	ITGA5	-0.477172253	-0.17622396	0.050794061	1
GO:0033631~cell-cell adhesion mediated by integrin	ITGA5, NPNT	0.665214026	NPNT	-0.447168282	-0.651735773	0.029240619	1
GO:0051260~protein homooligomerization	STOM, KCTD10, KCND3, HMOX1, RIPK3, DPYSL3	0.680799555	STOM	-0.405608644	-0.143002091	0.094698603	1
GO:0051260~protein homooligomerization	STOM, KCTD10, KCND3, HMOX1, RIPK3, DPYSL3	0.680799555	KCTD10	-0.365810604	-0.150696958	-0.111066922	1
GO:0051260~protein homooligomerization	STOM, KCTD10, KCND3, HMOX1, RIPK3, DPYSL3	0.680799555	KCND3	-0.597621842	-0.402505976	-0.325302873	1
GO:0051260~protein homooligomerization	STOM, KCTD10, KCND3, HMOX1, RIPK3, DPYSL3	0.680799555	HMOX1	-0.376862598	-0.987411621	-0.003174755	1
GO:0051260~protein homooligomerization	STOM, KCTD10, KCND3, HMOX1, RIPK3, DPYSL3	0.680799555	RIPK3	-0.761759161	-0.519699955	0.172958663	1
GO:0051260~protein homooligomerization	STOM, KCTD10, KCND3, HMOX1, RIPK3, DPYSL3	0.680799555	DPYSL3	-0.533480784	-0.248636084	-0.066900888	1
GO:0010976~positive regulation of neuron projection development	PTN, DPYSL3, CD24A, FEZ1, NGF	0.684618034	PTN	-1.07403337	-0.56582526	-0.617159513	1
GO:0010976~positive regulation of neuron projection development	PTN, DPYSL3, CD24A, FEZ1, NGF	0.684618034	DPYSL3	-0.533480784	-0.248636084	-0.066900888	1
GO:0010976~positive regulation of neuron projection development	PTN, DPYSL3, CD24A, FEZ1, NGF	0.684618034	CD24A	-2.012644425	-1.569299129	0.446804746	1
GO:0010976~positive regulation	PTN, DPYSL3, CD24A, FEZ1, NGF	0.684618034	FEZ1	-0.4934	-0.4874	0.324862661	1

of neuron projection development				12513	82038		
GO:0010976~positive regulation of neuron projection development	PTN, DPYSL3, CD24A, FEZ1, NGF	0.684618034	NGF	-0.420443361	-0.352168505	0.059154538	1
GO:0006470~protein dephosphorylation	PTPRB, DUSP4, DUSP10, PTPRN, DUSP6	0.684618034	PTPRB	-1.272295565	-0.682530654	0.079615522	1
GO:0006470~protein dephosphorylation	PTPRB, DUSP4, DUSP10, PTPRN, DUSP6	0.684618034	DUSP4	-0.517842476	-0.225987074	0.110928674	1
GO:0006470~protein dephosphorylation	PTPRB, DUSP4, DUSP10, PTPRN, DUSP6	0.684618034	DUSP10	-0.103303255	-0.489526837	0.021464395	1
GO:0006470~protein dephosphorylation	PTPRB, DUSP4, DUSP10, PTPRN, DUSP6	0.684618034	PTPRN	-0.525514127	-0.251573901	0.468803	1
GO:0006470~protein dephosphorylation	PTPRB, DUSP4, DUSP10, PTPRN, DUSP6	0.684618034	DUSP6	-0.636288799	-0.782141778	0.023999833	1
GO:0008202~steroid metabolic process	SULT4A1, CYP1B1, CH25H, HMGCS1	0.686617379	SULT4A1	-0.629262769	-0.406739446	-0.018723102	1
GO:0008202~steroid metabolic process	SULT4A1, CYP1B1, CH25H, HMGCS1	0.686617379	CYP1B1	-1.010712986	-0.507932985	0.214850664	1
GO:0008202~steroid metabolic process	SULT4A1, CYP1B1, CH25H, HMGCS1	0.686617379	CH25H	-1.055673771	-1.436741974	0.602829466	1
GO:0008202~steroid metabolic process	SULT4A1, CYP1B1, CH25H, HMGCS1	0.686617379	HMGCS1	-0.487611865	-0.123735082	-0.081360753	1
GO:0030216~keratinocyte differentiation	TXNIP, CRCT1, PTGS2, PTGS1	0.691999538	TXNIP	-0.488645629	-0.334661679	-0.072422834	1
GO:0030216~keratinocyte differentiation	TXNIP, CRCT1, PTGS2, PTGS1	0.691999538	CRCT1	-0.211707381	-0.859622077	-0.237719825	1
GO:0030216~keratinocyte differentiation	TXNIP, CRCT1, PTGS2, PTGS1	0.691999538	PTGS2	-1.484870085	-1.695190956	0.286626058	1
GO:0030216~keratinocyte differentiation	TXNIP, CRCT1, PTGS2, PTGS1	0.691999538	PTGS1	-0.662327693	-0.584740789	1.227936765	1
GO:0002819~regulation of	RIPK3, DUSP10	0.698985586	RIPK3	-0.7617	-0.5196	0.172958663	1

adaptive immune response				59161	99955		
GO:0002819~regulation of adaptive immune response	RIPK3, DUSP10	0.698985586	DUSP10	-0.103303255	-0.489526837	0.021464395	1
GO:0021637~trigeminal nerve structural organization	NRP2, SEMA3A	0.698985586	NRP2	-0.519742916	-0.247671189	0.177469955	1
GO:0021637~trigeminal nerve structural organization	NRP2, SEMA3A	0.698985586	SEMA3A	-1.311258944	-0.731535817	0.24865124	1
GO:0055072~iron ion homeostasis	HMOX1, STEAP2, SLC40A1	0.734526415	HMOX1	-0.376862598	-0.987411621	-0.003174755	1
GO:0055072~iron ion homeostasis	HMOX1, STEAP2, SLC40A1	0.734526415	STEAP2	-0.494842601	-0.476352959	-0.037316428	1
GO:0055072~iron ion homeostasis	HMOX1, STEAP2, SLC40A1	0.734526415	SLC40A1	-1.105683598	-0.789931301	0.287961235	1
GO:0006954~inflammatory response	C3AR1, S1PR3, PTGS2, TSPAN2, PTGS1, TNFAIP3, CXCL12, SPP1	0.737553009	C3AR1	-1.22676413	-0.927252235	0.584071632	1
GO:0006954~inflammatory response	C3AR1, S1PR3, PTGS2, TSPAN2, PTGS1, TNFAIP3, CXCL12, SPP1	0.737553009	S1PR3	-1.743204937	-1.123069709	0.657009845	1
GO:0006954~inflammatory response	C3AR1, S1PR3, PTGS2, TSPAN2, PTGS1, TNFAIP3, CXCL12, SPP1	0.737553009	PTGS2	-1.484870085	-1.695190956	0.286626058	1
GO:0006954~inflammatory response	C3AR1, S1PR3, PTGS2, TSPAN2, PTGS1, TNFAIP3, CXCL12, SPP1	0.737553009	TSPAN2	-0.563493032	-0.291606064	-0.39920472	1
GO:0006954~inflammatory response	C3AR1, S1PR3, PTGS2, TSPAN2, PTGS1, TNFAIP3, CXCL12, SPP1	0.737553009	PTGS1	-0.662327693	-0.584740789	1.227936765	1
GO:0006954~inflammatory response	C3AR1, S1PR3, PTGS2, TSPAN2, PTGS1, TNFAIP3, CXCL12, SPP1	0.737553009	TNFAIP3	-0.716278004	-0.42370585	-0.154737182	1
GO:0006954~inflammatory response	C3AR1, S1PR3, PTGS2, TSPAN2, PTGS1, TNFAIP3, CXCL12, SPP1	0.737553009	CXCL12	-1.096137743	-0.485286992	0.577416667	1
GO:0006954~infl	C3AR1, S1PR3,	0.7375	SPP1	-	-	1.0042	1

ammatory response	PTGS2, TSPAN2, PTGS1, TNFAIP3, CXCL12, SPP1	53009		0.868611397	0.831046522	19144	
GO:1903672~positive regulation of sprouting angiogenesis	ITGA5, FGF2	0.73898336	ITGA5	-0.477172253	-0.17622396	0.050794061	1
GO:1903672~positive regulation of sprouting angiogenesis	ITGA5, FGF2	0.73898336	FGF2	0.118448677	-0.492964607	0.272034532	1
GO:0030214~hyaluronan catabolic process	CD44, FGF2	0.73898336	CD44	-0.423537378	-0.583789719	-0.019520047	1
GO:0030214~hyaluronan catabolic process	CD44, FGF2	0.73898336	FGF2	0.118448677	-0.492964607	0.272034532	1
GO:2000347~positive regulation of hepatocyte proliferation	PTN, TNFAIP3	0.73898336	PTN	-1.07403337	-0.56582526	-0.617159513	1
GO:2000347~positive regulation of hepatocyte proliferation	PTN, TNFAIP3	0.73898336	TNFAIP3	-0.716278004	-0.42370585	-0.154737182	1
GO:1904706~negative regulation of vascular smooth muscle cell proliferation	HMOX1, CNN1	0.73898336	HMOX1	-0.376862598	-0.987411621	-0.003174755	1
GO:1904706~negative regulation of vascular smooth muscle cell proliferation	HMOX1, CNN1	0.73898336	CNN1	-0.702429824	-0.200476479	-0.406097108	1
GO:1901166~neural crest cell migration involved in autonomic nervous system development	NRP2, SEMA3A	0.73898336	NRP2	-0.519742916	-0.247671189	0.177469955	1
GO:1901166~neural crest cell migration involved in autonomic nervous system development	NRP2, SEMA3A	0.73898336	SEMA3A	-1.311258944	-0.731535817	0.24865124	1
GO:1901016~regulation of potassium ion	KCNAB1, FHL1	0.73898336	KCNAB1	-0.494595642	-0.163461587	-0.590286177	1

transmembrane transporter activity							
GO:1901016~regulation of potassium ion transmembrane transporter activity	KCNAB1, FHL1	0.73898336	FHL1	-0.637474645	-0.318185774	-0.182333407	1
GO:0050830~defense response to Gram-positive bacterium	HIST1H2BN, HIST1H2BK, HIST2H2BE, RIPK2	0.74128135	HIST1H2BN	-0.645313402	-0.203264947	0.181669073	1
GO:0050830~defense response to Gram-positive bacterium	HIST1H2BN, HIST1H2BK, HIST2H2BE, RIPK2	0.74128135	HIST1H2BK	-0.509820734	-0.204682195	0.133836776	1
GO:0050830~defense response to Gram-positive bacterium	HIST1H2BN, HIST1H2BK, HIST2H2BE, RIPK2	0.74128135	HIST2H2BE	-0.526938534	-0.323547959	-0.192197457	1
GO:0050830~defense response to Gram-positive bacterium	HIST1H2BN, HIST1H2BK, HIST2H2BE, RIPK2	0.74128135	RIPK2	-0.557494782	-0.259886853	0.170159608	1
GO:0007275~multicellular organism development	NRP2, FLRT2, NPNT, FHL1, EFNB2, PRRX1, MGP, DKK2, EREG, SEMA3E, ECSCR, PDGFRA, UNC5C, SEMA3A, TNFAIP2, FGF2, TLL1	0.743009082	NRP2	-0.519742916	-0.247671189	0.177469955	1
GO:0007275~multicellular organism development	NRP2, FLRT2, NPNT, FHL1, EFNB2, PRRX1, MGP, DKK2, EREG, SEMA3E, ECSCR, PDGFRA, UNC5C, SEMA3A, TNFAIP2, FGF2, TLL1	0.743009082	FLRT2	-0.753165786	-0.57372512	-0.133525535	1
GO:0007275~multicellular organism development	NRP2, FLRT2, NPNT, FHL1, EFNB2, PRRX1, MGP, DKK2, EREG, SEMA3E, ECSCR, PDGFRA, UNC5C, SEMA3A, TNFAIP2, FGF2, TLL1	0.743009082	NPNT	-0.447168282	-0.651735773	0.029240619	1
GO:0007275~multicellular organism development	NRP2, FLRT2, NPNT, FHL1, EFNB2, PRRX1, MGP, DKK2, EREG, SEMA3E, ECSCR,	0.743009082	FHL1	-0.637474645	-0.318185774	-0.182333407	1

	PDGFRA, UNC5C, SEMA3A, TNFAIP2, FGF2, TLL1						
GO:0007275~multicellular organism development	NRP2, FLRT2, NPNT, FHL1, EFNB2, PRRX1, MGP, DKK2, EREG, SEMA3E, ECSCR, PDGFRA, UNC5C, SEMA3A, TNFAIP2, FGF2, TLL1	0.743009082	EFNB2	-0.493942633	-0.527684043	0.158722493	1
GO:0007275~multicellular organism development	NRP2, FLRT2, NPNT, FHL1, EFNB2, PRRX1, MGP, DKK2, EREG, SEMA3E, ECSCR, PDGFRA, UNC5C, SEMA3A, TNFAIP2, FGF2, TLL1	0.743009082	PRRX1	-0.417412586	-0.308124359	0.67951328	1
GO:0007275~multicellular organism development	NRP2, FLRT2, NPNT, FHL1, EFNB2, PRRX1, MGP, DKK2, EREG, SEMA3E, ECSCR, PDGFRA, UNC5C, SEMA3A, TNFAIP2, FGF2, TLL1	0.743009082	MGP	-0.816441763	-0.819560688	1.300353362	1
GO:0007275~multicellular organism development	NRP2, FLRT2, NPNT, FHL1, EFNB2, PRRX1, MGP, DKK2, EREG, SEMA3E, ECSCR, PDGFRA, UNC5C, SEMA3A, TNFAIP2, FGF2, TLL1	0.743009082	DKK2	-1.537331255	-0.740024196	0.581012453	1
GO:0007275~multicellular organism development	NRP2, FLRT2, NPNT, FHL1, EFNB2, PRRX1, MGP, DKK2, EREG, SEMA3E, ECSCR, PDGFRA, UNC5C, SEMA3A, TNFAIP2, FGF2, TLL1	0.743009082	EREG	-0.021918492	-0.496740145	-0.086555927	1
GO:0007275~multicellular organism development	NRP2, FLRT2, NPNT, FHL1, EFNB2, PRRX1, MGP, DKK2, EREG, SEMA3E, ECSCR, PDGFRA, UNC5C, SEMA3A, TNFAIP2, FGF2, TLL1	0.743009082	SEMA3E	-0.742357249	-0.665614674	-0.167255282	1
GO:0007275~multicellular organism	NRP2, FLRT2, NPNT, FHL1, EFNB2, PRRX1,	0.743009082	ECSCR	-0.485332782	-0.215438307	-0.274351718	1

development	MGP, DKK2, EREG, SEMA3E, ECSCR, PDGFRA, UNC5C, SEMA3A, TNFAIP2, FGF2, TLL1						
GO:0007275~multicellular organism development	NRP2, FLRT2, NPNT, FHL1, EFNB2, PRRX1, MGP, DKK2, EREG, SEMA3E, ECSCR, PDGFRA, UNC5C, SEMA3A, TNFAIP2, FGF2, TLL1	0.743009082	PDGFRA	-0.907253413	-0.396614293	0.1338055	1
GO:0007275~multicellular organism development	NRP2, FLRT2, NPNT, FHL1, EFNB2, PRRX1, MGP, DKK2, EREG, SEMA3E, ECSCR, PDGFRA, UNC5C, SEMA3A, TNFAIP2, FGF2, TLL1	0.743009082	UNC5C	-0.434834729	-0.336077616	-0.188855391	1
GO:0007275~multicellular organism development	NRP2, FLRT2, NPNT, FHL1, EFNB2, PRRX1, MGP, DKK2, EREG, SEMA3E, ECSCR, PDGFRA, UNC5C, SEMA3A, TNFAIP2, FGF2, TLL1	0.743009082	SEMA3A	-1.311258944	-0.731535817	0.24865124	1
GO:0007275~multicellular organism development	NRP2, FLRT2, NPNT, FHL1, EFNB2, PRRX1, MGP, DKK2, EREG, SEMA3E, ECSCR, PDGFRA, UNC5C, SEMA3A, TNFAIP2, FGF2, TLL1	0.743009082	TNFAIP2	-0.881017093	-0.692657286	0.21556035	1
GO:0007275~multicellular organism development	NRP2, FLRT2, NPNT, FHL1, EFNB2, PRRX1, MGP, DKK2, EREG, SEMA3E, ECSCR, PDGFRA, UNC5C, SEMA3A, TNFAIP2, FGF2, TLL1	0.743009082	FGF2	0.118448677	-0.492964607	0.272034532	1
GO:0007275~multicellular organism development	NRP2, FLRT2, NPNT, FHL1, EFNB2, PRRX1, MGP, DKK2, EREG, SEMA3E, ECSCR, PDGFRA, UNC5C, SEMA3A, TNFAIP2, FGF2, TLL1	0.743009082	TLL1	-1.55117389	-0.963629225	-0.30123344	1
GO:0007420~br	CD9, TSPAN2,	0.7486	CD9	-	0.0295	-	1

ain development	KCNAB1, HMGCS1, UNC5C, CXCL12	22508		0.354138468	41306	0.1053562	
GO:0007420~brain development	CD9, TSPAN2, KCNAB1, HMGCS1, UNC5C, CXCL12	0.748622508	TSPAN2	-0.563493032	-0.291606064	-0.39920472	1
GO:0007420~brain development	CD9, TSPAN2, KCNAB1, HMGCS1, UNC5C, CXCL12	0.748622508	KCNAB1	-0.494595642	-0.163461587	-0.590286177	1
GO:0007420~brain development	CD9, TSPAN2, KCNAB1, HMGCS1, UNC5C, CXCL12	0.748622508	HMGCS1	-0.487611865	-0.123735082	-0.081360753	1
GO:0007420~brain development	CD9, TSPAN2, KCNAB1, HMGCS1, UNC5C, CXCL12	0.748622508	UNC5C	-0.434834729	-0.336077616	-0.188855391	1
GO:0007420~brain development	CD9, TSPAN2, KCNAB1, HMGCS1, UNC5C, CXCL12	0.748622508	CXCL12	-1.096137743	-0.485286992	0.577416667	1
GO:0001889~liver development	CCND1, HMGCS1, PTN, HGF	0.750162131	CCND1	-0.629935652	-0.102976531	0.210531411	1
GO:0001889~liver development	CCND1, HMGCS1, PTN, HGF	0.750162131	HMGCS1	-0.487611865	-0.123735082	-0.081360753	1
GO:0001889~liver development	CCND1, HMGCS1, PTN, HGF	0.750162131	PTN	-1.07403337	-0.56582526	-0.617159513	1
GO:0001889~liver development	CCND1, HMGCS1, PTN, HGF	0.750162131	HGF	-0.316537949	-0.409370915	1.200569685	1
GO:2000107~negative regulation of leukocyte apoptotic process	MERTK, CXCL12	0.757924561	MERTK	-0.468191533	-0.843402232	0.012440032	1
GO:2000107~negative regulation of leukocyte apoptotic process	MERTK, CXCL12	0.757924561	CXCL12	-1.096137743	-0.485286992	0.577416667	1
GO:0010863~positive regulation of phospholipase C activity	PDGFRA, FGF2	0.757924561	PDGFRA	-0.907253413	-0.396614293	0.1338055	1
GO:0010863~positive regulation of phospholipase C activity	PDGFRA, FGF2	0.757924561	FGF2	-0.118448677	-0.492964607	0.272034532	1
GO:0086009~membrane repolarization	ATP1B1, KCND3	0.757924561	ATP1B1	-0.788716332	-0.460856882	0.140741545	1
GO:0086009~membrane repolarization	ATP1B1, KCND3	0.757924561	KCND3	-0.597621842	-0.402505976	-0.325302873	1
GO:0045907~po	PTGS2, PTGS1,	0.7594	PTGS	-	-	0.2866	1

sitive regulation of vasoconstriction	HTR2A	94234	2	1.484870085	1.695190956	26058	
GO:0045907~positive regulation of vasoconstriction	PTGS2, PTGS1, HTR2A	0.759494234	PTGS1	-0.662327693	-0.584740789	1.227936765	1
GO:0045907~positive regulation of vasoconstriction	PTGS2, PTGS1, HTR2A	0.759494234	HTR2A	-1.276006418	-0.973220171	0.138210845	1
GO:0051781~positive regulation of cell division	EREG, PTN, FGF2	0.759494234	EREG	-0.021918492	-0.496740145	-0.086555927	1
GO:0051781~positive regulation of cell division	EREG, PTN, FGF2	0.759494234	PTN	-1.07403337	-0.56582526	-0.617159513	1
GO:0051781~positive regulation of cell division	EREG, PTN, FGF2	0.759494234	FGF2	0.118448677	-0.492964607	0.272034532	1
GO:0034644~cellular response to UV	PTGS2, PTN, AQP1	0.764329051	PTGS2	-1.484870085	-1.695190956	0.286626058	1
GO:0034644~cellular response to UV	PTGS2, PTN, AQP1	0.764329051	PTN	-1.07403337	-0.56582526	-0.617159513	1
GO:0034644~cellular response to UV	PTGS2, PTN, AQP1	0.764329051	AQP1	-0.707154235	-0.600787565	0.255362055	1
GO:0043524~negative regulation of neuron apoptotic process	CLCF1, HMOX1, ITSN1, GCLM, NGF	0.773769436	CLCF1	-0.44127015	-0.24742057	-0.046635788	1
GO:0043524~negative regulation of neuron apoptotic process	CLCF1, HMOX1, ITSN1, GCLM, NGF	0.773769436	HMOX1	-0.376862598	-0.987411621	-0.003174755	1
GO:0043524~negative regulation of neuron apoptotic process	CLCF1, HMOX1, ITSN1, GCLM, NGF	0.773769436	ITSN1	-0.621287116	-0.404618118	0.036293357	1
GO:0043524~negative regulation of neuron apoptotic process	CLCF1, HMOX1, ITSN1, GCLM, NGF	0.773769436	GCLM	-0.377203486	-0.51565766	0.022762576	1
GO:0043524~negative regulation of neuron apoptotic process	CLCF1, HMOX1, ITSN1, GCLM, NGF	0.773769436	NGF	-0.420443361	-0.352168505	0.059154538	1

GO:0071243~cellular response to arsenic-containing substance	HMOX1, GSTO2	0.781059307	HMOX1	-0.376862598	-0.987411621	-0.003174755	1
GO:0071243~cellular response to arsenic-containing substance	HMOX1, GSTO2	0.781059307	GSTO2	-1.155190218	-0.961546063	0.103929947	1
GO:0003094~glomerular filtration	AQP1, MCAM	0.781059307	AQP1	-0.707154235	-0.600787565	0.255362055	1
GO:0003094~glomerular filtration	AQP1, MCAM	0.781059307	MCAM	-1.417441084	-0.587348783	-0.299371592	1
GO:0061549~sympathetic ganglion development	NRP2, SEMA3A	0.781059307	NRP2	-0.519742916	-0.247671189	0.177469955	1
GO:0061549~sympathetic ganglion development	NRP2, SEMA3A	0.781059307	SEMA3A	-1.311258944	-0.731535817	0.24865124	1
GO:0001658~branching involved in ureteric bud morphogenesis	CD44, NPNT, FGF2	0.78165156	CD44	-0.423537378	-0.583789719	-0.019520047	1
GO:0001658~branching involved in ureteric bud morphogenesis	CD44, NPNT, FGF2	0.78165156	NPNT	-0.447168282	-0.651735773	0.029240619	1
GO:0001658~branching involved in ureteric bud morphogenesis	CD44, NPNT, FGF2	0.78165156	FGF2	0.118448677	-0.492964607	0.272034532	1
GO:0045666~positive regulation of neuron differentiation	MMD, CXCL12, FEZ1, NGF	0.786687703	MMD	-0.653208853	-0.734388451	0.278023894	1
GO:0045666~positive regulation of neuron differentiation	MMD, CXCL12, FEZ1, NGF	0.786687703	CXCL12	-1.096137743	-0.485286992	0.577416667	1
GO:0045666~positive regulation of neuron differentiation	MMD, CXCL12, FEZ1, NGF	0.786687703	FEZ1	-0.493412513	-0.487482038	0.324862661	1
GO:0045666~positive regulation of neuron differentiation	MMD, CXCL12, FEZ1, NGF	0.786687703	NGF	-0.420443361	-0.352168505	0.059154538	1
GO:0055114~oxidation-reduction	CYP1B1, PTGS2, KCNAB1, CH25H,	0.794013295	CYP1B1	-1.0107	-0.5079	0.214850664	1

process	HMOX1, PTGS1, UGDH, GSTO2, NQO1, STEAP2, POR, SRXN1			12986	32985		
GO:0055114~oxidation-reduction process	CYP1B1, PTGS2, KCNAB1, CH25H, HMOX1, PTGS1, UGDH, GSTO2, NQO1, STEAP2, POR, SRXN1	0.794013295	PTGS2	-1.484870085	-1.695190956	0.286626058	1
GO:0055114~oxidation-reduction process	CYP1B1, PTGS2, KCNAB1, CH25H, HMOX1, PTGS1, UGDH, GSTO2, NQO1, STEAP2, POR, SRXN1	0.794013295	KCNAB1	-0.494595642	-0.163461587	-0.590286177	1
GO:0055114~oxidation-reduction process	CYP1B1, PTGS2, KCNAB1, CH25H, HMOX1, PTGS1, UGDH, GSTO2, NQO1, STEAP2, POR, SRXN1	0.794013295	CH25H	-1.055673771	-1.436741974	0.602829466	1
GO:0055114~oxidation-reduction process	CYP1B1, PTGS2, KCNAB1, CH25H, HMOX1, PTGS1, UGDH, GSTO2, NQO1, STEAP2, POR, SRXN1	0.794013295	HMOX1	-0.376862598	-0.987411621	-0.003174755	1
GO:0055114~oxidation-reduction process	CYP1B1, PTGS2, KCNAB1, CH25H, HMOX1, PTGS1, UGDH, GSTO2, NQO1, STEAP2, POR, SRXN1	0.794013295	PTGS1	-0.662327693	-0.584740789	1.227936765	1
GO:0055114~oxidation-reduction process	CYP1B1, PTGS2, KCNAB1, CH25H, HMOX1, PTGS1, UGDH, GSTO2, NQO1, STEAP2, POR, SRXN1	0.794013295	UGDH	-0.19130914	-0.417899075	0.081098168	1
GO:0055114~oxidation-reduction process	CYP1B1, PTGS2, KCNAB1, CH25H, HMOX1, PTGS1, UGDH, GSTO2, NQO1, STEAP2, POR, SRXN1	0.794013295	GSTO2	-1.155190218	-0.961546063	0.103929947	1
GO:0055114~oxidation-reduction process	CYP1B1, PTGS2, KCNAB1, CH25H, HMOX1, PTGS1, UGDH, GSTO2, NQO1, STEAP2, POR, SRXN1	0.794013295	NQO1	-1.812058834	-1.769603856	0.426996977	1
GO:0055114~oxidation-reduction	CYP1B1, PTGS2, KCNAB1, CH25H,	0.794013295	STEAP2	-0.4948	-0.4763	-0.0373	1

process	HMOX1, PTGS1, UGDH, GSTO2, NQO1, STEAP2, POR, SRXN1			42601	52959	16428	
GO:0055114~oxidation-reduction process	CYP1B1, PTGS2, KCNAB1, CH25H, HMOX1, PTGS1, UGDH, GSTO2, NQO1, STEAP2, POR, SRXN1	0.794013295	POR	-0.892932008	-0.465914477	0.361743915	1
GO:0055114~oxidation-reduction process	CYP1B1, PTGS2, KCNAB1, CH25H, HMOX1, PTGS1, UGDH, GSTO2, NQO1, STEAP2, POR, SRXN1	0.794013295	SRXN1	-0.3788882	-0.469575103	0.077091539	1
GO:0021612~facial nerve structural organization	NRP2, SEMA3A	0.803854432	NRP2	-0.519742916	-0.247671189	0.177469955	1
GO:0021612~facial nerve structural organization	NRP2, SEMA3A	0.803854432	SEMA3A	-1.311258944	-0.731535817	0.24865124	1
GO:0048846~axon extension involved in axon guidance	NRP2, SEMA3A	0.803854432	NRP2	-0.519742916	-0.247671189	0.177469955	1
GO:0048846~axon extension involved in axon guidance	NRP2, SEMA3A	0.803854432	SEMA3A	-1.311258944	-0.731535817	0.24865124	1